Mechanical Engineering Graduate Theses & Dissertations

Mechanical Engineering

Spring 1-1-2016

Smart Surface Wrinkling Enabled by Shape Memory Polymers

Yu Wang
University of Colorado Boulder, yuwang0318@gmail.com

SMART SURFACE WRINKLING ENABLED BY SHAPE MEMORY POLYMERS

by

YU WANG

B.S., Xi'an University of Technology, 2008

M.S., Northwestern Polytechnical University, 2011

A thesis submitted to the

Faculty of the Graduate School of the

University of Colorado in partial fulfillment

of the requirements for the degree of

Doctor of Philosophy

Department of Mechanical Engineering

2016

This thesis entitled:
SMART SURFACE WRINKLING ENABLED BY SHAPE MEMORY POLYMERS
written by YU WANG
has been approved for the Department of Mechanical Engineering

_____
Prof. Jianliang Xiao

_____
Prof. Yifu Ding

_____
Prof. Yung-Cheng Lee

_____
Prof. Jae-Woong Jeong

_____
Prof. Rong Long

Date _____

The final copy of this thesis has been examined by the signatories, and we find that both the content and the form meet acceptable presentation standards of scholarly work in the above mentioned discipline.

WANG, YU (Ph.D., Mechanical Engineering)

SMART SURFACE WRINKLING ENABLED BY SHAPE MEMORY POLYMERS

Thesis directed by Prof. Jianliang Xiao

In this dissertation, we demonstrate self-assembly fabrication methods for programmable global and localized surface wrinkling by utilizing the shape memory effects of shape memory polymers (SMPs). Heat responsive SMPs, due to their capability of memorizing and recovering different shapes, can provide unique opportunities to realize smart surface wrinkling, and therefore were used as smart substrates or films. To build the bilayer film-substrate system, thin films, such as Si ribbons and aluminum films, were transferred or deposited on the surface of programmed SMP substrates. In the Si ribbon-SMP system, time and temperature dependent wrinkling formation and evolution were observed and systematically studied. For the localized heating cases, such as line and point heating, aluminum thin films were deposited on the programmed SMP substrates and heating wires were used to achieve heating the samples locally. The wrinkling patterns by line heating showed good sinusoidal profiles, with wavelength and amplitude decreasing gradually with the distance from the heating source. The area of wrinkling can also be tuned with large range. For the systems heated by point heat sources, hierarchical wrinkling patterns were achieved. Two distinct wrinkling patterns, spoke and ring patterns, formed in a circular area around the heat source. Spoke patterns appeared around the point heat sources due to the free boundary conditions in the radial direction, and ring patterns appeared at the periphery due to the constraint from the outside SMP. We have also demonstrated the method to reversibly control the formation and disappearance of the wrinkling through SMP film-elastomer substrate system. In addition, fabrication of three-dimensional hierarchical structures through sequential wrinkling is presented. These results in this dissertation offer simple methods to fabricate different types of programmable surface wrinkling pattern, with potential applications in stretchable electronics, optical gratings, surface engineering, advanced manufacturing, and other demanding applications.

Dedication

To my family.

Acknowledgements

Firstly, I would like to express my gratitude to my advisor Prof. Jianliang Xiao for the guidance and support in my Ph.D. study and research. During the beginning of my Ph.D. study, he is patient to give me sufficient time to learn new knowledge and technology. In the research, he has given me the freedom to pursue various projects and encouraged me to solve the problem independently. His immense knowledge and insightful comments helped me throughout my research. I appreciate the help forever.

I thank Prof. Jerry Qi for the assistance in the first year. I would like to thank Prof. Yifu Ding, Prof. Rong Long, Prof. Jae-Woong Jeong, Prof. Franck Vernerey, and Dr. Frank Delrio for the brilliant comments and suggestions in my comprehensive exam. I am grateful for Prof. Yung-Cheng Lee for serving as my committee member.

I would like to thank my labmates Zhengwei Li, Zhanan Zou, and Andres Villada for the fruitful discussion and generous support. I appreciate the experimental assistance from Kai Yu, Qi Ge, Liang Wang, Xiaoming Mu, Lewis Cox, Sajjad Maruf, Blake Wiehe, Tzu-min Ou, Ryan Brow, Yao Zhai, Sabrina David, and Jacob Carson.

I thank my parents, parents in law, sister, and brother for supporting me all the time. I would like to express my special appreciation to my wife, Meng Jiang, for her unconditional love and encouragement through my ups and downs. I am so lucky to have found my best friend and soulmate, who loves and respects me, and sticks by my side. I'd like to thank my daughter Amelia, who was born in last October. I enjoy the happiness she brings to me and the family.

Contents

Chapter

Figures

Figure

Chapter 1

Introduction

1.1   Background

Thin film materials have many advantages over their bulk counterparts, in terms of properties, applications and economical considerations. One example is mechanical flexibility, i.e. bendability, when they are in freestanding forms or integrated with other thin film materials. Mechanics theory indicates that the strain in the thin film caused by bending is proportional to its thickness and the bending curvature [1]. For example, when a 100 nm thick Si thin film is integrated with a 20 μm thick plastic substrate and bended to a radius of curvature 10 mm, the maximum strain in the Si film is only 0.1%, which is 10 times smaller than its fracture strain ($\sim$ 1%) [2,3]. This type of mechanical robustness has enabled many applications, such as flexible electronics, and micro/nanoelectromechanical systems (M/NEMS) [4,5].

However, the mechanical flexibility provided by thin film materials cannot meet the much more critical challenges posed by novel applications that require very large stretchability [6,7]. Examples range from stretchable electronics and tunable optical gratings, to biomedical implants and stretchable energy harvesting and storage devices [8–13]. These applications require thin films to be extremely soft and stretchable, like a rubber band. The mechanical strains introduced in these applications can be as large as 100%, way beyond the failure strains of most thin film materials (typically $\sim$ 1%) [3]. To conquer this challenge, a lot of research efforts have been invested in the last two and half decades. Different strategies have been utilized to realize mechanically stretchable thin films without affecting their intrinsic functionalities, such as semiconducting properties, elec-

trical conductance and piezoelectricity [7, 14–19]. All these strategies take advantage of nonlinear mechanics associated with novel geometrical patterns and layouts to enable huge stretchabilities in otherwise inextensible thin film materials [1, 14–19]. One feasible way to realize stretchable thin films is by transforming thin film materials into wavy structure through nonlinear buckling of thin films on soft substrates. The underlying mechanism is analogous to a spring, an extensible structure made of inextensible material. Film wrinkling is a common phenomenon in nature world, such as these on aging human skin [20]. For the first time, Bowden and co-workers obtained highly ordered wrinkling patterns with distinctive features in laboratory in 1998 [21]. Since then, wrinkled, wavy patterns have been realized on various thin film materials, such as metals [8, 21], semiconductor materials [18, 19, 22], and polymers [23, 24].

The purpose of this chapter is to review fabrication, application and mechanics of thin film wrinkling. Different fabrication methods and processes to induce thin film wrinkling and realize mechanically stretchable thin film materials will be introduced. Interesting and novel applications enabled by thin film wrinkling will be summarized, such as stretchable and tunable optical gratings, precision metrology, tunable surface properties, and stretchable electronics. The underlying mechanics of thin film wrinkling will also be discussed.

1.2   Fabrication of surface wrinkling

Different strategies have been utilized to induce buckling in thin films on soft substrates, such as thermal mismatch, mechanical strain, surface treatment by Ultraviolet/Ozone (UVO), and focused ion beam [21,25–34]. Although these strategies are convenient and effective in making wavy, stretchable thin films, they share some common drawbacks. The wavy structures of the thin films, which determine the stretchability, are defined by the material and geometric properties of the thin films and the substrates [35]. This gives little freedom in designing the wavy structures once the thin films and substrates are specified. Two different methods were then introduced to resolve this issue: controlled buckling and prefabricated wavy thin films [18, 35]. On the other hand, mesh layouts that combine rigid islands and stretchable interconnectors were also widely used in stretchable

electronics. This strategy leaves the functional electronic elements in their flat, microscale formats, but transforms the metal interconnectors into wavy, stretchable forms, in order to comply with the established manufacturing processes in semiconductor industry [1, 3, 4, 6, 12–16, 36–46].

1.2.1   Wrinkles through thermal mismatch

This method was first introduced by Bowden et al. in 1998 [21]. In this study, a thin layer of gold film is deposited onto polydimethylsiloxane (PDMS) by electron beam evaporation, as shown in Fig. 1.1 [21]. In the film deposition process, PDMS is heated by metal source, which leads to its volume expansion. Because the coefficient of thermal expansion of PDMS is much larger than that of gold, after the film-substrate system cools down, the film is compressed by the substrate, leading to wrinkled, wavy pattern on the surface. Figures 1.1b and c show wrinkling patterns induced by this method. Many other researchers have also realized wrinkling of different metal films, such as nickel, aluminum, titanium and chromium, by adopting similar approaches [21, 31].

Surface treatment using plasma or ozone is also a common approach to form stiff thin films on PDMS substrates for creating wrinkle patterns [25, 28–33]. It leads to substitution of carbon atoms by oxygen atoms at the surface of PDMS, which produces a thin and stiff silica-like layer [28–30, 47]. When the system cools down, thermal mismatch introduces compression into the stiff thin film, leading to thin film wrinkling at the surface.

The wrinkle patterns on the surface is also controllable. When a continuous, uniform stiff thin film is deposited, and the substrate is also heated uniformly, equi-biaxial thermal mismatch strain induces 2D, herringbone wrinkle patterns (Fig. 1.1b) [21]. When ridges are introduced with appropriate spacing, guided 1D sinusoidal wrinkle patterns can be realized (Fig. 1.1c) [21]. When very narrow thin films are deposited on the surface, the transfer of shear strain at the interface between thin films and substrate is only effective along the length direction, and hence only 1D sinusoidal wrinkle patterns show up [48]. Similar phenomenon can also be seen at the edges of 2D herringbone patterns [49].
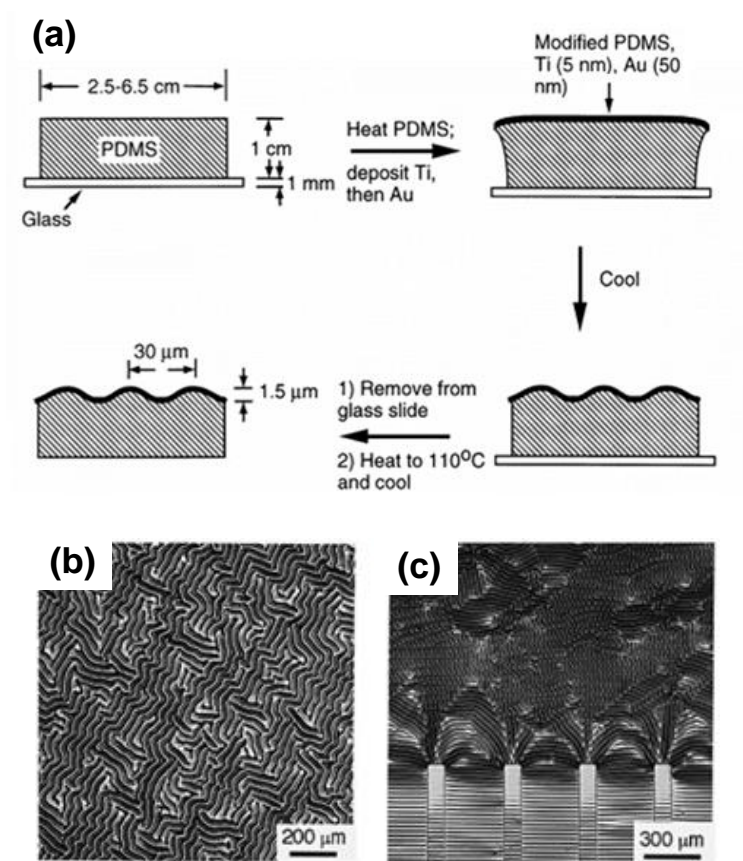
Figure 1.1: Wrinkling of metal thin film by thermal strain mismatch. (a) Fabrication processes of wrinkling of metal thin film on PDMS substrate via thermal strain mismatch, (b) and (c) Optical microscope images of wrinkling patterns produced from (a). (Reproduced with permission from Ref. [21], © Macmillan Publishers Ltd)

1.2.2   Wrinkles through mechanical strain mismatch

In thermal mismatch induced wrinkling as discussed above, the strain and its rate is difficult to control and the wrinkling pattern is usually anisotropic, except when the substrate surfaces are fabricated with steps [21, 30]. Especially, when large strain mismatch is desired, thermal mismatch is not a viable approach. By applying mechanical strains to the substrates, strain mismatch between the thin film and substrate can be applied with precise control and with desired rate [32]. Mechanical strains can be applied on either substrate only or the bilayer system. For example, tensile strain can be applied to the compliant substrate, then the thin film is introduced to the substrate surface. Releasing the strain in the substrate leads to wrinkling of the thin film if the compressive strain exceeds a critical value. Compressive strain can also be applied to the bilayer system directly to induce surface wrinkling [50]. However, this method may induce global system buckling instead of thin film wrinkling on the surface, depending on the material properties of the film and substrate, and the ratio of their thicknesses [51].

Uniaxial and biaxial mechanical strains induce 1D and 2D wrinkling patterns, respectively. Figure 1.2a shows the fabrication processes of 1D wrinkling by uniaxial mechanical strain mismatch [19]. In this example, thin Si ribbons are fabricated from silicon on insulator (SOI) wafer by photolithography and etching processes. After etching away the bonding layer of SiO_2, Si ribbons are supported by, but not bonded to the mother wafer. Then Si ribbons are transferred to prestretched PDMS substrate. Releasing the prestretch in the PDMS substrate induces 1D wrinkling of the Si ribbons. As shown in Fig. 1.2b, wrinkled Si ribbons show uniform wavy patterns. Inspired by this method, researchers fabricated stretchable electronics and curvilinear electronics systems [8, 22, 38–45, 52].

Similar to the processes of realizing 1D Si ribbon wrinkling patterns in Fig. 1.2a, Choi et al. produced 2D wrinkling in Si nanomembranes on PDMS substrates to provide biaxial stretchability for the electronics [53]. Fabrication processes are shown in Fig. 1.2c [49,53]. The difference from 1D wrinkling is that the PDMS substrate is biaxially stretched before transferring Si nanomembranes.
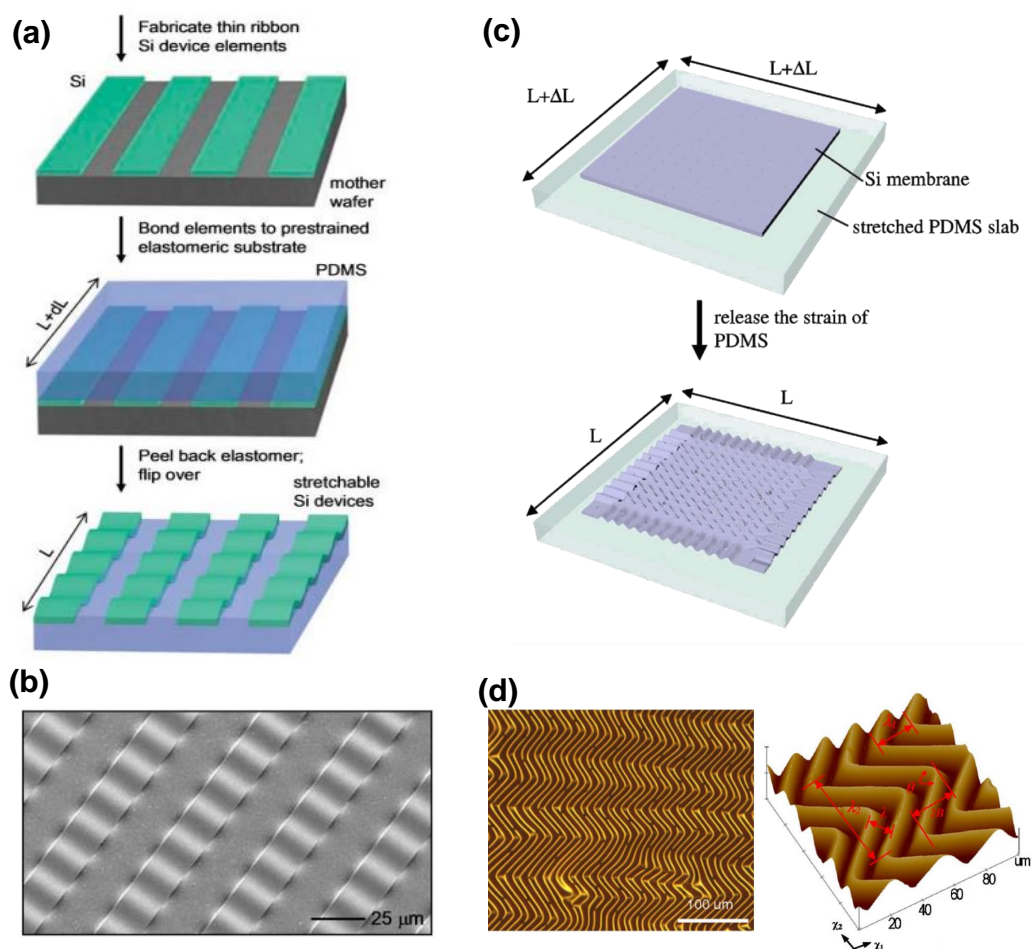
Figure 1.2: 1D and 2D surface wrinkling by mechanial strain. (a) Processes to fabricate stretchable single crystalline Si ribbons on elastomeric substrates, (b) Scanning electron microscope image of wrinkled Si ribbons on PDMS substrate, (Reproduced with permission from Ref. [19], © American Association for the Advancement of Science) (c) Schematic illustration of the fabrication processes for two-dimensional wavy Si nanomembranes on PDMS substrate, (d) Optical microscope image (left) and AFM image (right) of wrinkled Si nanomembrane. (Reproduced with permission from Ref. [49], © 2008 American Institute of Physics)

Optical and AFM images are shown in the left and right frames of Fig. 1.2d, respectively. At different locations, the wrinkling shows different patterns. For example, 1D wrinkling is observed at the edges, and 2D herringbone patterns are present at the inner region.

2D wrinkling can also be obtained on PDMS substrates with surfaces treated by plasma or UV [29–33]. Lin et al. used a square-shaped PDMS strip, clamped and stretched equally in both directions [32]. Plasma treatment is performed on the surface of the stretched sample. Highly ordered zigzag herringbone patterns are observed when the strain in X direction is released before strain release in Y direction. They also observed disordered zigzag herringbone patterns form when the sample is stretched and released simultaneously in both directions with equal strains.

1.2.3   Wrinkles through other methods

In the previous discussion, wrinkling forms in the whole film simultaneously. Meanwhile, some researchers have used different methods, such as focused ion beam or laser treatment, to modify the surface of substrate or the film in designed paths to induce surface wrinkling in desired areas [34,54]. The material used here is a flat PDMS sheet. Upon exposing the surface to a focused ion beam (FIB) of Ga+ ions, wrinkling forms in desired paths. The resolution of this method is high and can produce complex wrinkling patterns with various widths by controlling movement of the sample.

Ohzono and coworkers combined lithography and self-organization to fabricate micro-wrinkle structures [55]. In this approach, wrinkling patterns strongly depend on the sizes of the microspheres. Swelling is another approach to introduce strain mismatch and thus to induce surface wrinkling in bilayer systems [56]. When UVO treated PDMS is exposed to ethanol, the stiff top layer swells much more than the substrate [56]. This mismatch leads to an anisotropic stress field in the film and induces the formation of surface wrinkling patterns. With the same approach, Chung and coworkers fabricated diffusion-controlled and self-organized symmetric wrinkling patterns on UVO treated polystyrene (PS) film [24]. The exposure time is critical for the surface morphologies. Different exposure time leads to different patterns, including spoke and target patterns. A possible

mechanism for the symmetric patterns is the defects in the film.

The approaches discussed above demonstrated effective methods to create ordered wrinkling patterns in bilayer systems, however, it is difficult to control the geometries of the patterns directly once the thin films and substrates are selected, which limits the freedom in designing the wavy structures for applications. More recently, Xu and coworkers extended this method to assemble the micro/nanomaterials, including device-grade silicon, into three-dimensional architectures by mechanical compressive bulking [40]. 2D planar filamentary serpentine silicon ribbons are treated by UV light to create precisely controlled patterns of surface hydroxyl terminations at desired locations. This method offers many possibilities for the fabrication of complicated 3D electronics and devices.

Prefabricated wavy patterns can also provide an effective method to fabricate wavy thin films with controlled geometries. To fabricate a wavy substrate, a series of molding and smoothing processes from a rigid silicon template are involved [35]. The thin film obtained through this method offers both high stretchability and compressibility for the thin films because of the initial wavy shape. Furthermore, the surface wavy geometries can be easily controlled by designing different surface relief features.

Mesh layouts that combine rigid islands and stretchable interconnectors offers extremely high compressibility and stretchability, and therefore are widely used in stretchable electronics [15, 39, 41, 44, 46]. When the system is compressed or stretched, noncoplanar movement of the bridges absorbs most of the strains, due to their narrow and thin geometries that can easily bend and twist. This form of circuit can be stretched or compressed to strain level as high as 100%. More advanced designs utilize serpentine interconnectors and fractal designs, to offer improved compressibility and stretchability to the system [57].

1.3   Application of thin film wrinkling

Thin film wrinkles on soft substrate have many potential applications. For example, optical grating based on thin film wrinkling, as shown in Fig. 1.3a [9]. Prestretched PDMS is treated by

oxygen plasma and then an ultrathin gold and palladium film is sputtered on top of the surface. When the strain in PDMS is released, sinusoidal wrinkling forms with submicron period, which can provide grating effect to light, as shown in Fig. 1.3b. As the system is stretched, the period of the sinusoidal wrinkles increases, leading to the shift of the peak wavelength. Stretch of the system also causes decrease of the amplitude of the wrinkles, resulting in decrease of the diffraction intensity (Fig. 1.3c). This optical grating based on thin film buckling has also been used to amplify small strain signals to orders of magnitude larger signals of change in diffraction angles, for measurement of very small strains [58].

Thin film wrinkling has shown applications in precision metrology, for example, measurement of elastic moduli of polymeric thin film and micro-strain sensing, due to the strong correlation between the wrinkle formation and the mechanical properties of the bilayer system [23]. Stafford and coworkers developed an efficient method for the measurement of moduli of nanoscale polymer films (Fig. 1.3d) [23, 59]. In this method, thin polymer films wrinkle on PDMS substrate with wavy, sinusoidal profiles (Fig. 1.3e). According to thin film bulking theory, the modulus of the film can be precisely determined once the wavelength of the wrinkling, the thickness of the film and the modulus of the substrate are known.

Surface roughness and chemistry determine the adhesion between two surfaces [33, 60, 61]. Lin et al. developed a new method to regulate adhesion by varying the strain applied to the wrinkled film, which leads to the change of the surface roughness [33]. Wrinkle pattern is produced on UV treated PDMS sample by releasing tensile prestrain and completely disappears after the system is stretched to the same magnitude of prestrain. Surface roughness increases as wrinkle amplitude increases due to the increase of applied prestrain, which leads to monotonic decrease of adhesion. The pull-off force drops by more than 10 times from flat surface to a wrinkled surface due to applied prestrain of 22.4%. Another study, however, demonstrated that wrinkled surface could lead to increase in adhesion, due to increasing contact perimeters [62]. The wrinkle pattern shows 2D, short features in this study. When in contact with a flat test probe, the interface forms small enclosed perimeters, which is different with that in Lin et al.'s study.
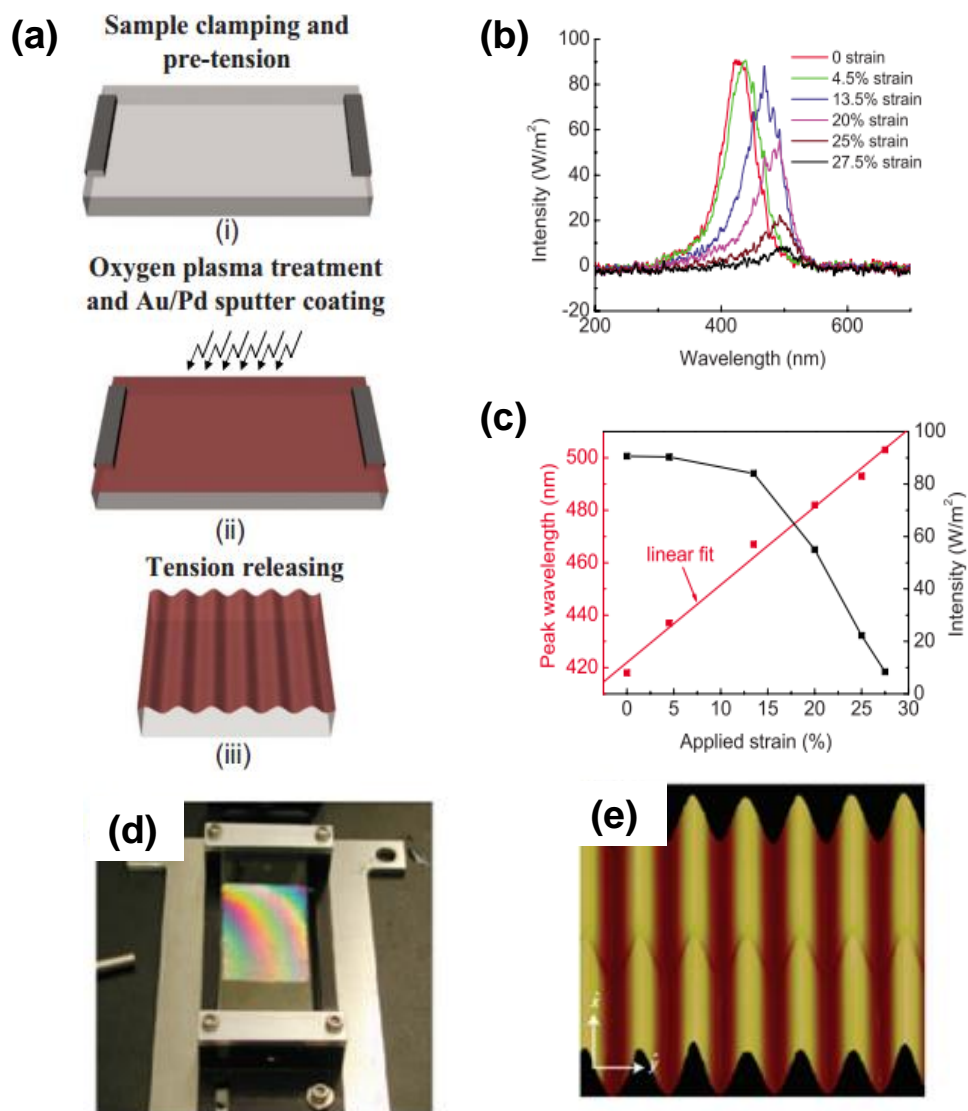
Figure 1.3: Tunable optical grating and metrology enabled by thin films wrinkling. (a) Schematic illustration of the fabrication of tunable optical gratings, (b) Light wavelength shift with the change of the prestrain, (c) Peak wavelength and intensity as a function of applied strain. (Reprinted with permission from Ref. [9], © 2007 American Institute of Physics) (d) Experimental setup for measuring elastic modulus of thin films via buckling, (e) AFM image of buckled thin film. (Reprinted with permission from Ref. [23], © 2004 Nature Publishing Group)

In addition to the previous applications, thin film winkling induced by strain mismatch is a promising way to realize stretchable thin films that can be used in stretchable electronics and optoelectronic systems. The approach of mechanical strain mismatch allows application of desired strain levels to the bilayer system to induce desired surface patterns. Wrinkled nanoribbons and nanomembranes on PDMS offers stretchibility to the brittle, inextensible semiconductor materials. Based on this method, stretchable electronics and optoelectronic systems are realized [6, 16, 18, 19, 38–45, 52, 63–70]. For example, silicon based integrated circuit that is stretchable, twistable and foldable, as shown in Fig. 1.4a [16]. In this study, a thin layer of silicon circuit covered by PI film is transferred onto PDMS substrate to form wrinkled, wavy structures of logic gates, ring oscillators and differential amplifiers. This form of silicon circuit offers good strechibility and foldability.

To further improve strechibility, serpentine and self-similar designs of interconnects were also developed. An epidermal electronic system (EES) that can be mounted on human skin is developed based on such design [11], as shown in Fig. 1.4d and e. This system works well even under large deformation, such as compression and stretching.

1.4   Mechanics of wrinkled thin films

The pattern of thin film wrinkling is determined by the material properties of the thin film and the substrate, as well as the thickness of the film. Long wavelength is preferred for the stiff film, while substrate favors short wavelength [20]. Formation of wrinkling is the process to balance the bending energy of the film and the deformation energy of the substrate [71]. Total system energy is minimized in the form of wrinkling with specific wavelength and amplitude [71].

In this section, mechanics of 1D wrinkling, including small deformation and finite deformation theory are briefly reviewed.

1.4.1   Small deformation theory

Based on plane strain, small deformation theory, energy method was used to determine the buckling geometry of the thin film with 1D sinusoidal profile [19, 49, 72]. In a bilayer system, a stiff
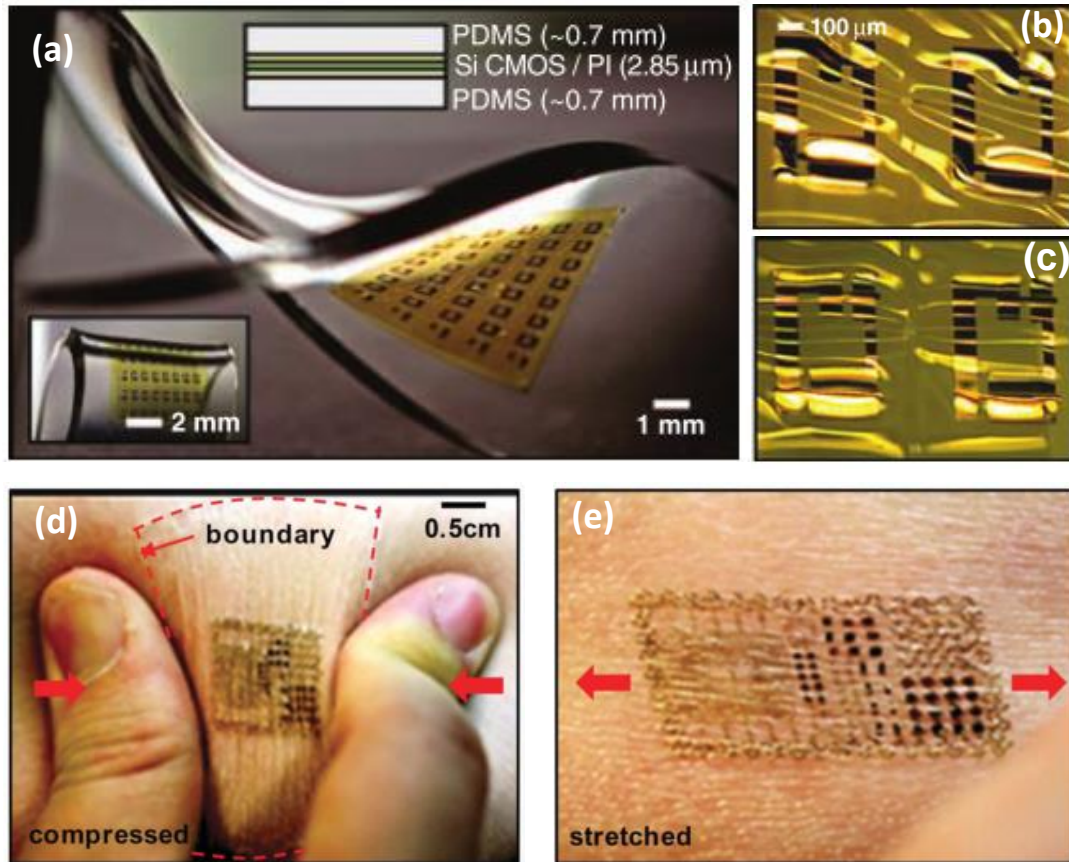
Figure 1.4: Strechable electronics based on thin film wrinkling. (a) Si-CMOS circuit under twisting and bending (bottom inset), Optical microscope images of functional units at the center (b) and edge (c) of the circuit sample in the twisted configuration. (Reprinted with permission from Ref. [16], ©️ American Association for the Advancement of Science) Epidermal electronics under (d) compressed and (e) stretched status. (Reprinted with permission from Ref. [11], ©️ American Association for the Advancement of Science)

thin film with thickness h_f, Poisson's ratio ν_f and elastic modulus E_f is attached to a prestretched thick compliant substrate with Young's modulus E_s, and Poisson's ratio ν_s. The substrate is assumed to be much more compliant than the thin film, thus $E_s \ll E_f$. Upon release of the prestrain ε_{pre}, the thin film wrinkles with wavelength λ_0 and amplitude A_0. Figure 1.5a shows an optical microscope image of wrinkled Si nanoribbons on PDMS [19]. The wrinkle profile can be fitted very well by a sinusoidal function, as demonstrated in Fig. 1.5b [19]. The out-of-plane displacement of the wrinkled film can be expressed as

$$w = A_0 \cos(kx_1) = A_0 \cos(\frac{2\pi x_1}{\lambda_0}), \tag{1.1}$$

where x_1 is the coordinate along the film length direction. The total energy per unit length of the film-substrate system consists of three parts, the membrane energy U_m and bending energy U_b in the thin film, and the strain energy U_s in the substrate, and is obtained as

$$U_{tot} = U_b + U_m + U_s = \frac{\pi^4 \bar{E}_f h_f^3 A_0^2}{3\lambda_0^4} + \frac{1}{2}\bar{E}_f h_f \left(\frac{\pi^2 A_0^2}{\lambda_0^2} - \varepsilon_{pre}\right)^2 + \frac{\pi}{4\lambda_0}\bar{E}_s A_0^2, \tag{1.2}$$

where $\bar{E}_f = E_f / \left(1 - \nu_f^2\right)$ and $\bar{E}_s = E_s / \left(1 - \nu_s^2\right)$ are the plane strain moduli of the film and substrate, respectively. Minimizing the total energy with respect to buckling amplitude and wavelength, i.e. $\partial U_{tot}/\partial A_0 = \partial U_{tot}/\partial \lambda_0 = 0$, gives buckling wavelength λ_0 and amplitude A_0 as [72]

$$\lambda_0 = 2\pi h_f \left(\frac{\bar{E}_f}{3\bar{E}_s}\right)^{1/3}, A_0 = h_f \sqrt{\frac{\varepsilon_{pre}}{\varepsilon_c} - 1}, \tag{1.3}$$

where $\varepsilon_c = \frac{1}{4}\left(\frac{3\bar{E}_s}{\bar{E}_f}\right)^{2/3}$ is the critical buckling strain. If the prestrain applied to the substrate is smaller than ε_c , buckling doesn't occur. The buckling amplitude and wavelength of a Si thin film given by Eq. 1.3 versus Si film thickness are presented in the top and bottom frames of Fig. 1.5c, respectively [19]. Both show good agreement with experiment.

For small deformation buckling theory, the membrane strain $\varepsilon_m = -\varepsilon_c$ and bending strain $\varepsilon_b = 2\pi^2 A h_f / \lambda^2$ keeps constant after buckling, and the maximum bending strain increases with the deformation of the system. When the film is much stiffer than the substrate ($E_f \gg E_s$), the membrane strain (i.e. the critical buckling strain) is negligibly small. Then the peak strain in the
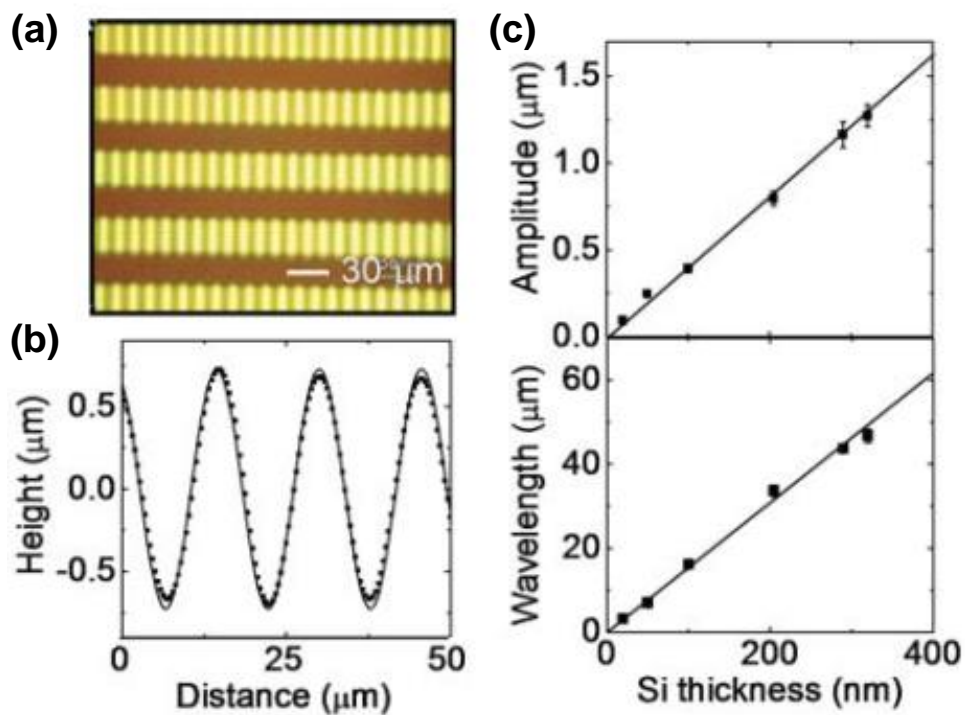
Figure 1.5: Mechanics of thin film wrinkling based on small deformation theory. (a) Optical image of wrinkled Si ribbons on PDMS, (b) The profile of a wrinkled Si ribbon in (a), (c) Wrinkling wavelength and amplitude versus Si ribbon thickness. (Reprinted with permission from Ref. [19], © American Association for the Advancement of Science)

thin film is approximately obtained as

$$\varepsilon_{peak} \approx 2\sqrt{\varepsilon_{pre}\varepsilon_c}. \tag{1.4}$$

For a Si film-PDMS substrate system, with material properties E_f=130 GPa, E_s= 1.8 MPa, $\nu_f = 0.27$, and $\nu_s = 0.48$ [73], the critical buckling strain is 0.034%. The prestrain can be as high as 23.8% before the peak strain in Si film reaches the fracture value 1.8% [74]. This means the stretchability of the bilayer system can reach 25.6%, which is 14.2 times of the fracture strain of Si.

The small deformation theory of thin film wrinkling has also been extended to study buckling of carbon nanotubes and nanowires on elastomeric substrates [75–78]. These studies are helpful for understanding of the mechanical behaviors of nanowires and nanotubes, and can provide theoretical basis for designing nanowire/nanotube-based stretchable devices. To account for the viscoelastic behavior of the elastomeric substrate, Huang and Suo have also studied wrinkling mechanics of thin films on viscos and viscoelastic substrates [79–82]. The kinetics of the wrinkle formation and growth are illustrated.

1.4.2   Finite deformation theory

In the above theoretical model based on small deformation theory, buckling wavelength is independent of the prestrain. However, when large strains are applied, experiments show that the wavelength decreases with the prestrain [83, 84], as shown in Fig. 1.5b. To understand this phenomenon, a finite deformation thin film wrinkling theory was established [83, 84]. By using energy method, the buckling wavelength and amplitude can be obtained as

$$\lambda = \frac{\lambda_0}{(1 + \varepsilon_{pre})(1 + \xi)^{1/3}}, A = \frac{A_0}{\sqrt{1 + \varepsilon_{pre}}(1 + \xi)^{1/3}}, \tag{1.5}$$

where λ_0 and A_0 are the wavelength and amplitude in Eq. 1.3, and $\xi = 5\varepsilon_{pre}(1 + \varepsilon_{pre})/32$. As shown in Fig. 1.6b, both amplitude and wavelength show good agreement with experimental results [83]. For a very stiff thin film on a compliant substrate, the membrane strain is negligibly
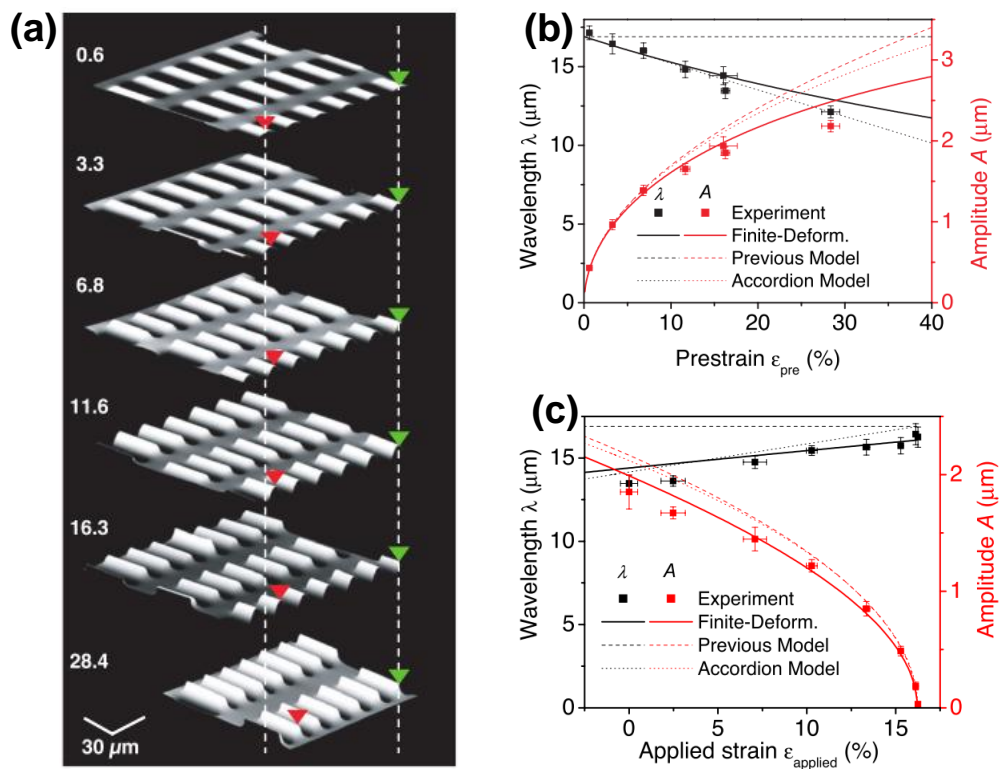
Figure 1.6: Mechanics of thin film wrinkling based on finite deformation theory. (a) AFM images of wrinkled Si ribbons induced by different prestrains, green and red triangle mark the change of wavelength, (b) Wavelength and amplitude of buckled Si ribbons with 100 nm thickness on PDMS substrate versus the prestrain, (c) Wavelength and amplitude of the same system to (b) as a function of the applied strain. (Reprinted with permission from Ref. [83].)

small [83]. The peak strain in the thin film can be approximate obtained as

$$\varepsilon_{peak} \approx 2\sqrt{\varepsilon_{pre}\varepsilon_c}\frac{(1+\xi)^{1/3}}{\sqrt{1+\varepsilon_{pre}}}. \tag{1.6}$$

When an external strain $\varepsilon_{applied}$ is applied to the wrinkled system, the wavelength and amplitude becomes

$$\lambda = \frac{\lambda_0(1+\varepsilon_{applied})}{(1+\varepsilon_{pre})(1+\varepsilon_{applied}+\zeta)^{1/3}}, A = \frac{h\sqrt{(\varepsilon_{pre}-\varepsilon_{applied})/\varepsilon_c-1}}{\sqrt{1+\varepsilon_{pre}}(1+\varepsilon_{applied}+\zeta)^{1/3}}, \tag{1.7}$$

where $\zeta = 5(\varepsilon_{pre}-\varepsilon_{applied})(1+\varepsilon_{pre})/32$. The peak strain of the film is

$$\varepsilon_{peak} = 2\sqrt{(\varepsilon_{pre}-\varepsilon_{applied})\varepsilon_c}\frac{(1+\varepsilon_{applied}+\zeta)^{1/3}}{\sqrt{1+\varepsilon_{pre}}}. \tag{1.8}$$

Figure 1.6c shows that the theoretically predicted wavelength and amplitude agree very well with experiment, for a wrinkled Si thin film on PDMS substrate with prestrain 16.2% [83].

When 2D strain mismatch is introduced to the bilayer system, stiff thin films wrinkle with 2D patterns, which are much more complex than the 1D sinusoidal patterns observed in 1D wrinkling. Typically, three types of surface morphological patterns can show up, i.e. 1D sinusoidal wavy pattern, checkerboard pattern and herringbone pattern. To study 2D wrinkling of stiff thin films on compliant substrates, Huang et al. adopted spectral method and demonstrated that the surface morphology shows checkerboard pattern when the prestrain is slightly above the critical buckling strain, and evolves to herringbone pattern as the prestrain increases [85]. Chen and Hutchinson developed a finite element model to study energetics of 2D wrinkling, and the results showed that the herringbone pattern has the lowest energy [86, 87]. Using energy method, Song et al. systematically investigated the 1D, checkerboard and herringbone buckling modes for 2D wrinkling [49, 53]. Analytical solutions for all three modes were obtained for biaxial prestrains ε_{11}^{pre} and ε_{22}^{pre}.

1.5   Conclusions

We have reviewed fabrication, application and mechanics of thin film wrinkling on compliant substrates. Different approaches and strategies can be utilized, including wrinkling induced by thermal strain, mechanical strain and swelling, controlled buckling. Thin film wrinkling has been

shown to have promising applications in optical gratings, precision metrology, smart adhesion, and stretchable electronics. Mechanics has been playing a central role in the development of thin film wrinkling. Results from mechanics analyses provide important information to relate the wavy morphologies and stretchability to the material and geometrical properties of the system. These results offer important tools for guiding system prediction, design and optimization.

Chapter 2

Time and temperature dependent wrinkling of stiff thin films on shape memory polymers

2.1   Research statement

In recent years, shape memory polymers (SMPs) become attractive for using as substrate in surface wrinkling fabrication because of their shape memory effect (SME), low cost, and convenience in processing [88–92]. As a kind of smart material, SMPs can fully recover its original shape after a severe deformation in the presence of the right stimuli [93], such as temperature, light, magnetic or humidity [94–98]. The recoverable strain of SMPs is on the order of 100%, while the recovery stress is low [99]. Thermal triggered SMPs (the stimulus for triggering the shape recovery is heat) is the most widely studied class in literature [100] and it is also used in present study. For such class SMPs, there are two steps in a shape memory cycle: programming step and recover step [100]. In programming step, the SMPs reqiured to be deformed at temperature above its glass transition temperature (T_g) and then cooled down to temperature below T_g to fix the deformed shape without constraint. Shape recovery is achieved in recovery step by heating the sample to temperature above T_g. When SMPs is used as substrate, shape recovery support a way to compress thin film without external force, which leads to wrinkling occurs automatically.

In this chapter, using SME of SMPs, we present a method to build wrinkling of single-crystal silicon thin film atop SMPs and investigate the evolution of wavelength and amplitude with time and temperature in substrate recovery process. This form of Si ribbon have potential application in stretchable and smart electronics.

2.2   Methods and materials

Si ribbons were obtained from Si-on-insulator (SOI) wafer by photolithography and etching process (Fig. 2.1). The top silicon layer of the SOI wafer is < 100 >, N-type with thickness 2.5 μm and is attached to the substrate silicon layer by a 1 μm thick silicon dioxide layer. The first step is to define a resist layer of ribbon array pattern on a SOI wafer by photolithography. And then the exposed part of top Si was etched. Cleaning the wafer with acetone to remove the resist layer and then etching the buried silicon dioxide layer with concentrated hydrofluoric acid (49%). Cleaning the wafer with de-ionized (DI) water after the silicon dioxide layer was etched completely. To prevent the ribbons from washing away in the etching and washing process, the ends of them were connected with the wafer [19]. After these process, Si ribbons were released and supported by the substrate Si layer, as shown in Fig. 2.1. The thickness of Si ribbon is determined by the thickness of top Si layer of SOI wafer, which is 2.5 μm in present study. And the size of the ribbon (20 $mm\times$50 μm) was defined by the resist pattern on the mask.

To synthesize SMP, the monomer tert-butyl acrylate (tBA) and crosslinker poly(ethylene glycol) dimethacrylate (PEGDMA) were mixed with a ratio 4:1 in weight, and 2, 2-dimethoxy-2-phenylacetophenone was added as the photoinitiator. The polymer solution was injected into a mold, which was made by glass slides. The mold with polymer solution was then placed under UV lamp for 5 minutes for polymerization and then placed into oven for 1 hour at 80 ℃ for post-curing [101, 102]. Upon the completion of synthesis, the SMP materials was demolded and cut into rectangular shapes with the dimension of 25$\times$8$\times$2 mm. For SMP material used in present study, T_g=42 ℃.

Uniaxial stretching of SMP samples were conducted at 60 ℃ ($>T_g$) using Dynamic Mechanical Analysis (DMA) tester (TA Instruments, DMA Q800). To fix the deformation strain, SMP samples were quenched to 25 ℃ with constraint. After these procedures, the constraint was removed and SMP samples with temporary shape were ready to be used as substrate of film-substrate system.

In the next step, Si ribbons were transfered on top of SMP substrate (Fig. 2.2). Strain
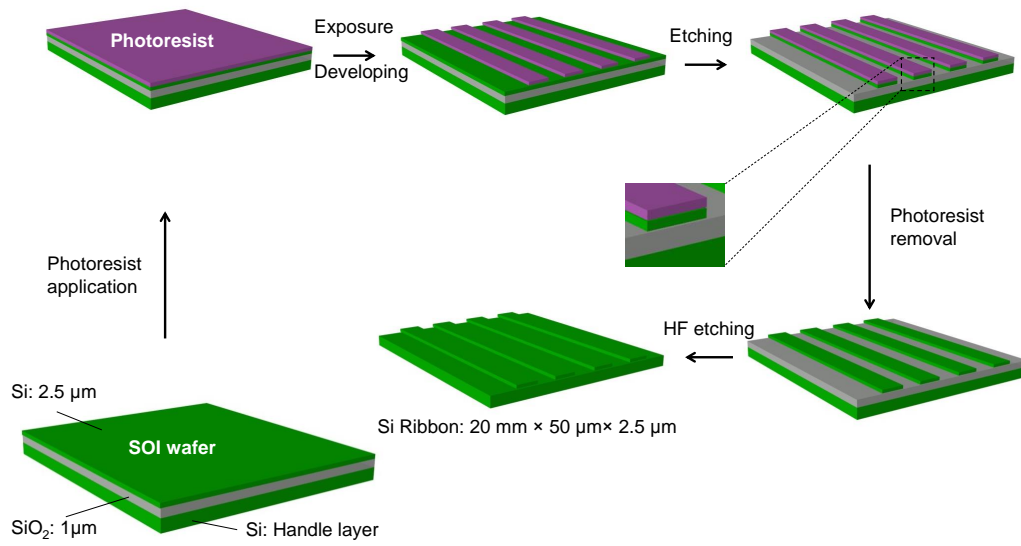
Figure 2.1: Fabrication of Si ribbon from SOI wafer by photolithography and etching process.

recovery of the Si-SMP system was conducted in an oven at different temperature under constraint free condition. According to the difference of strain recovery temperature, Si-SMP samples were divided into three types: (i) 60 ℃ sample: recovering Si-SMP samples at 60 ℃ for 5 minutes and then they were quenched to 25 ℃; (ii) 40 ℃ sample: recovering Si-SMP samples at 40 ℃ for 5 minutes and then they were quenched to 25 ℃; (iii) 25 ℃ sample: Si-SMP samples were kept in a water tank at constant temperature 25 ℃. After 60 ℃ and 40 ℃ sample were cooled down, both of them were kept in the tank at constant temperature 25 ℃ too. Upon recovery of the SMP substrate, wrinkling formed on the Si ribbon due to compression from substrate (Fig. 2.2, Bottom).

2.3 Results and discussions

Fig. 2.3 shows the images and profiles of Si ribbon wrinkling on SMP substrate of 60 ℃ sample. These images and profile were taken after the sample was cooled to 25 ℃. Fig. 2.3a and b are optical microscope and scanning electron microscope (SEM) images, respectively. It is clearly from these images that the uniform waves were formed due to the deformation from recovering the strain of the substrate. The direction of the waves is perpendicular to that of the prestrain (Fig. 2.3b). Black solid line in Fig. 2.4 is the profile of buckled Si ribbon in the experiment and red dot line is sinusoidal fit. The sinusoidal wave matches the profile very well, which demonstrates that the profile of the buckled Si ribbon surface is sinusoidal with wavelength 211.5 μm and amplitude 4.7 μm. It is clear that over a long range both of wavelengths and amplitudes are uniform.

The wrinkling of thin film occurs when the stiff film supported by soft substrate is compressed beyond a critical strain [89]. According to classic linear elastic buckling theory (Eq. 1.3), critical strain is only determined by the moduli ratio of the substrate and film [59]. In our experiment, when the Si film-SMP substrate sample was heated to 60 ℃, prestrain on SMP substrate fully recovered in a short time and the compression strain on the film reaches critical value of the system, which leads to Si ribbon wrinkles on the surface of SMP substrate. Both the wavelength and amplitude are uniform, due to the isotropic properties of the substrate.

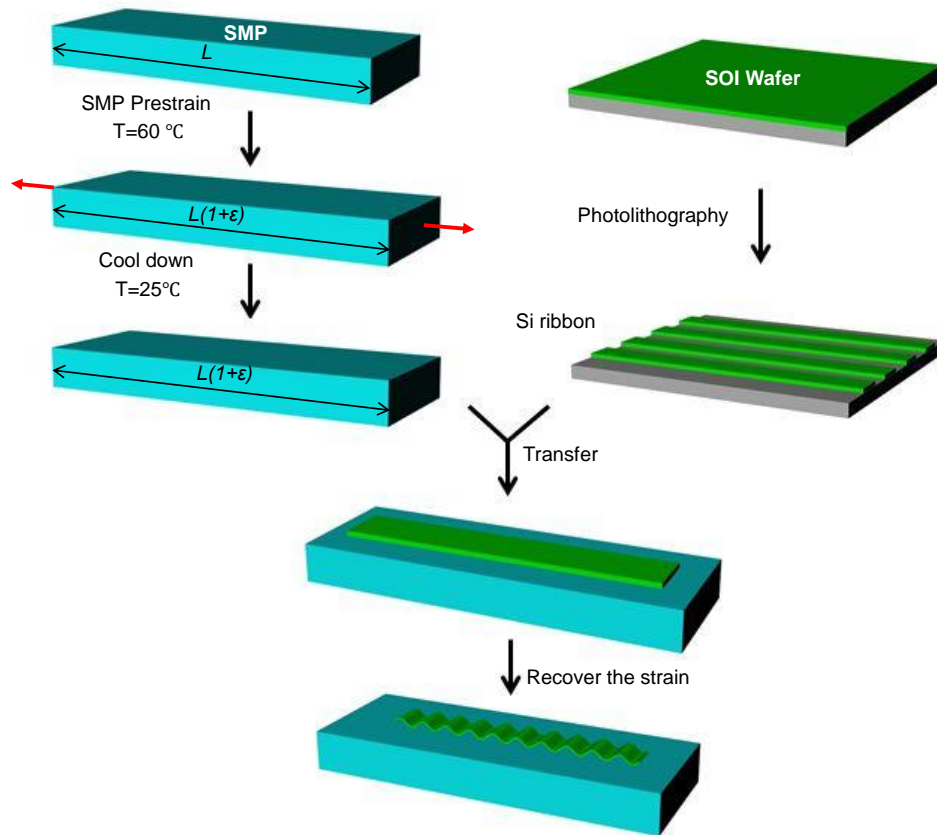The wrinkling profiles of 40 ℃ and 25 ℃ samples at different time are shown in Fig. 2.5. For

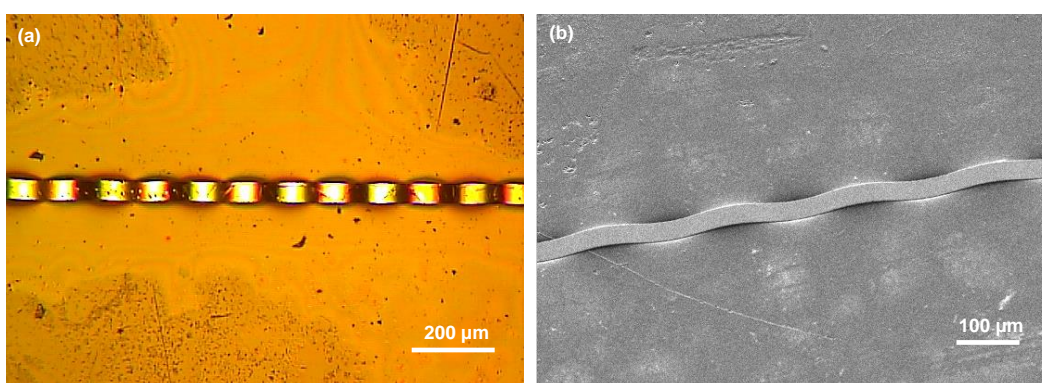Figure 2.2: Process for fabricating the wave form of Si ribbon on SMP substrate.

Figure 2.3: Images of Si ribbon wrinkling on SMP substrate. (a) Optical microscope and (b) SEM image of Si ribbon wrinkling on SMP (Recovering the strain in the SMP at 60 ℃).
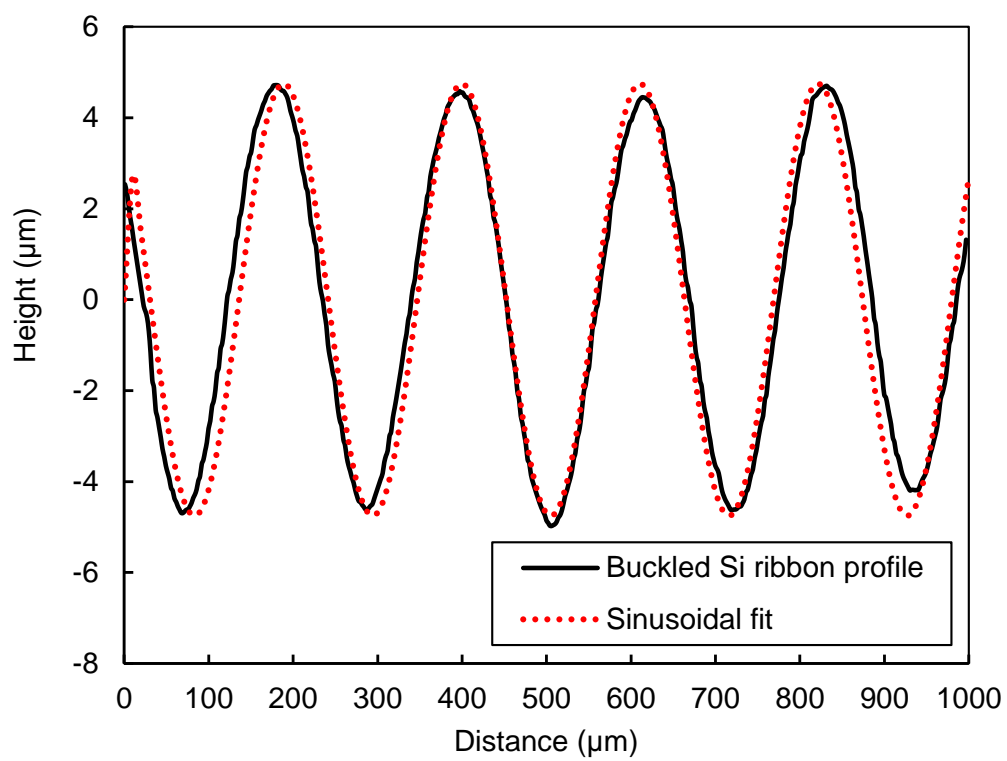
Figure 2.4: Profiles of buckled Si ribbon (Recovering the strain in the SMP at 60 ℃).

40 ℃ sample, timing began at the sample was heated up to 40 ℃ and for 25 ℃ sample, it began at the sample was kept in a water tank at constant temperature 25 ℃. The wavelengths, as well as the amplitudes, of two samples increase with time. For 25 ℃ sample, the wavelength increases from 128 μm at t=2.4 h to 168 μm at t=70 h. While for 40 ℃ sample, it increases from 145 μm at t=2.5 h to 170 μm at t=9.6 h. Fig. 2.5a and d are the first measurements of 25 ℃ and 40 ℃ sample, respectively. The time of this measurements are almost the same (with 360 s difference). Clearly, the wavelength of 40 ℃ sample is larger than that of 25 ℃ one at the same time point.

Simulation was also performed using finite element software package ABAQUS (Simulia, Providence, RI) in present study. Both procedure and sample size in the simulation are the same as that in the experiment. To describe the mechanical behaviors of SMP substrate, the constitutive model in the literature [100] was implemented in ABAQUS as a user material subroutine (UMAT). The paremeters in the constitutive model is the same as that in the literature [100]. Young's modulus and Poisson's ratio of Si are E_{Si}=130 GPa and ν=0.27, respectively [74].

Fig. 2.6 presents the wavelengths comparison between experiment and simulation results of each sample. Simulation results show good consistency with the experiment data. The results reveal that the higher temperature for SMP substrate recovery, the earlier the wave forms. And at the same time point, the wavelength of the sample with higher recovering temperature is larger than that of the sample with lower one. In the substrate recovery process, the difference of wavelegths between each type of samples decrease with time. In the simulation, the wavelengths of each sample converge to approximate 212 μm after the substrate was completely recovered. The experiment results also shown the same trend (Fig. 2.6).

Linear buckling theory shows that the wavelength is independent with the prestrain and amplitude increase nonlinearly with prestrain (Eqs. 1.1, 1.2, and 1.3). According to finite deformation theory, wavelength decreases with prestrain and amplitude increase with prestrain. However, in current study, with the prestrain recovery of the SMP substrate, both wavelength and amplitude increase. This phenomenon is due to the viscoelasticity of SMP substrate. For material with viscoelasticity, the stress needed to hold a fixed strain decreases with time. Equivalently, the effective
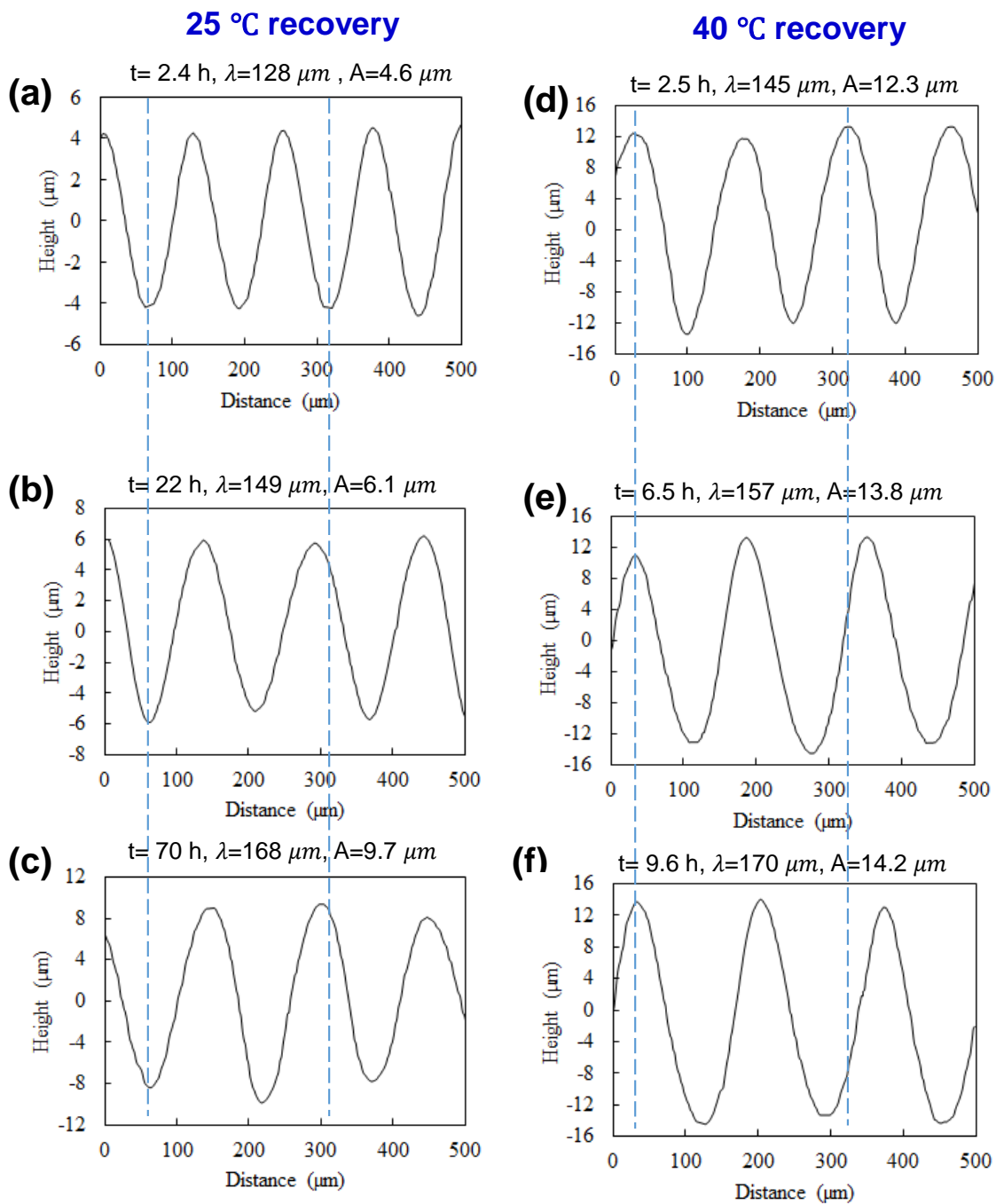
Figure 2.5: Time sequence of wrinkling profiles of 25 ℃ and 40 ℃ samples.
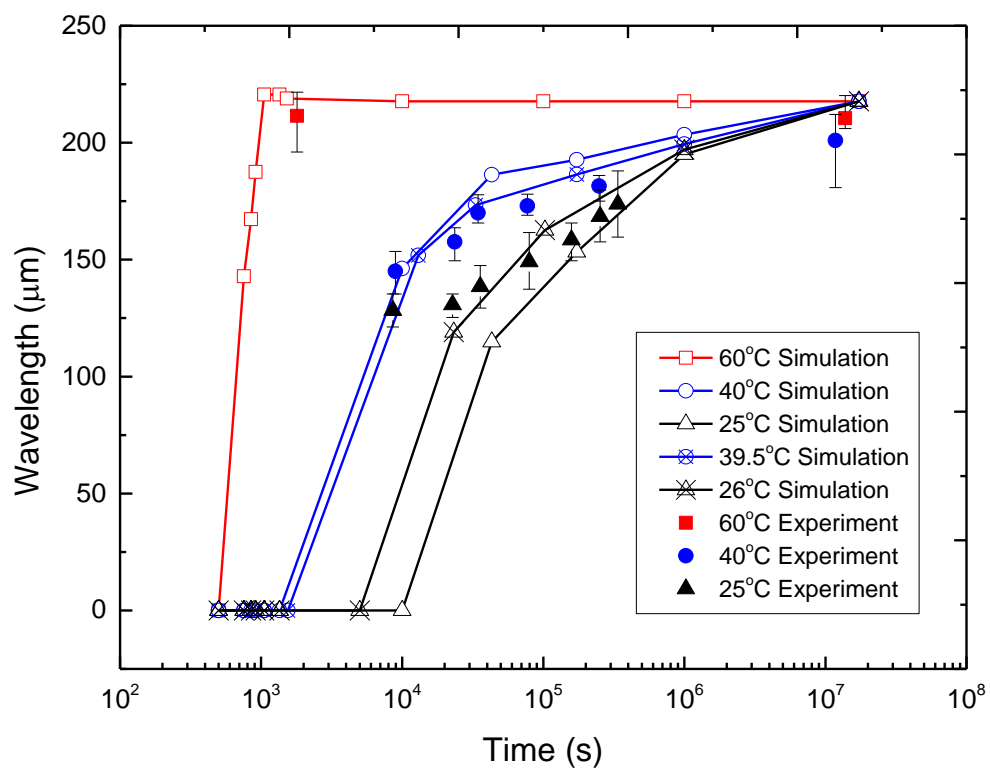
Figure 2.6: Wavelengths comparison between experiment and simulation results.
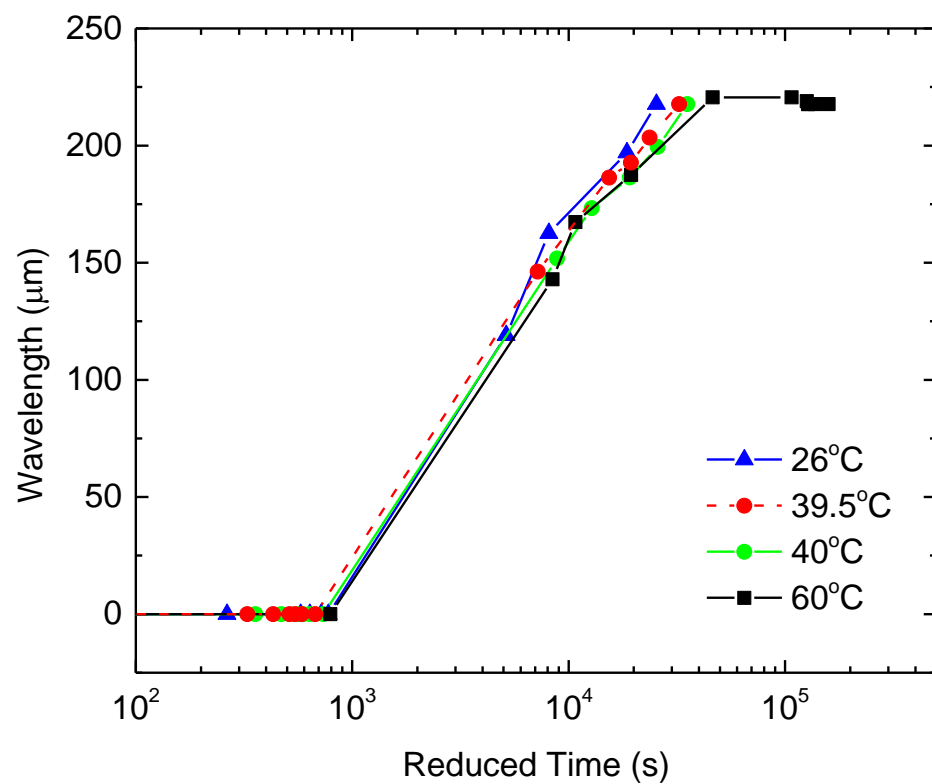
Figure 2.7: Shift of evolution of the wavelength by time-temperature superposition principle (TTSP).

modulus decreases. Decreased modulus leads to increasing of both wavelength and amplitude.

The evolution of each sample will not stop until the system reaches equilibrium state, which is completion of recovering prestrain of substrate. Recovery of SMP strongly depends on recovery temperature [100]. The higher the recovery temperature, the shorter the process. As recovery temperature changes, the recovery time scale changes significantly. The time for completing recovery for 25 ℃, 40 ℃, and 60 ℃ samples decrease gradually. Before reaching the equilibrium state, both wavelength and amplitude keep increasing. With the highest recovery temperature, 60 ℃ sample complete the process in the shortest time ($\sim$500 s) and its wavelength reached equilibrium state in this time and then kept for this state. Wavelength of the sample with high recovery temperature is larger than that of the sample with low recovery temperature at the same time point. Finally they all converge to the value in equilibrium state. These results reveal the wrinkling of stiff thin films on thermal triggered SMP substrate is time and temperature dependent.

According to Time-Temperature Superposition Principle (TTSP), polymer behaviors between short-time range at high temperature is equivalent to long-time range at low temperature. Thus, the wavelength evaluation in different temperature can be shifted to the reference one. As shown in Fig. 2.7, the experiment results are shifted to the results of 40 ℃ sample. The results show good agreement. Once the evolution process at any temperature is known, the process at different temperature can be obtained according to TTSP.

2.4   Conclusions

Using SME of SMPs, time and temperature dependent wrinkling of stiff thin films on such substrate was investigated. By applying prestrain on SMP substrate, a compressive stress field was created in the thin film when the film-substrate system was heated. And as a result, uniform sinusoidal wave was formed on the surface of the substrate. Experiments on samples with different recovery temperature shows the wavelengths and amplitudes of each sample increase with time before the substrate is fully recovered. And the higher temperature for strain recover, the larger of the wavelength at the same time point. The simulation results shows good agreement with

experiment results and it reveals the wavelengths of each sample converge to approximate 212 μm after the completion of recovery. Both results indicate both wavelength and amplitudes of such wrinkling atop SMP substrate is time and temperature dependent.

Chapter 3

Reversible surface wrinkling of shape memory polymer thin film atop elastomeric substrate

3.1   Research statement

In the previous chapter, programmable Si film-SMP substrate system was built to investigate the evolution of thin film wrinkling. When SMP is used as thin film on top of elastomeric substrate, its shape memory effect with mechanical strain makes the formation of wrinkling controllable, programmable, and reversible. Such system has potential applications in tunable optical gratings, surface engineering, and stretchable electronics.

The system are fabricated by using thermal responsive SMP as thin film and polydimethylsiloxane (PDMS) as substrate. Typical wavy wrinkling pattern with good sinusoidal shape formed spontaneously when prestrain of the substrate is recovered. Both wrinkling amplitude and wavelength increase linearly with the film thickness. Amplitude increase nonlinearly with the prestrain and wavelength shows weak dependence with the prestrain. When the system is heated above glass transition temperature (T_g) of SMP, the film recovers to its original length, which leads to disappearance of the wrinkling. By adjusting the prestrain recovery of the substrate and system temperature, formation and disappearance of the wrinkling pattern can be controlled. Present study is expected to give a simple way to fabricate unidirectional wavy pattern and control its formation and disappearance. In this chapter, three types of reversible wrinkling cycles were investigated, which are general wrinkling cycle (wrinkling cycle I), wrinkling cycle with two prestrain recovery steps (wrinkling cycle II), and wrinkling cycle with prestrain and compression (wrinkling

cycle III).

3.2   Methods and materials

PDMS substrate was made from Sylgard 184 elastomer kit (Dow Corning) using a 20: 1 prepolymer-crosslinker ratio by weight. Degassing the mixture for 2 hours to allow air bubbles to escape. Then the mixture was placed in oven at 80 ℃ for 2 hours for curing. Slabs were cut from the cured PDMS sheet with dimension $20\times10\times5\ mm$.

The method to synthesize SMPs is the same as that in chapter 2, the monomer tert-butyl acrylate (tBA) and crosslinker poly(ethylene glycol) dimethacrylate (PEGDMA) were mixed with a ratio 4:1 in weight, and 2, 2-dimethoxy-2-phenylacetophenone was added as the photoinitiator. Polymer solution was injected into a mold, which was made by two glass slides with shims between them. Thickness of SMP thin film was determined by the shim. The mold with polymer solution was then placed under UV lamp for 5 minutes for polymerization followed by post-curing in oven at 80 ℃ for 1 hour [101, 102]. And then SMP sheet was demolded and cut into rectangular shapes with dimension of $15\times5\ mm$. Film thickness is $5\sim15\ \mu m$. The last step before proceeding wrinkling cycle was to transfer SMP films on top of PDMS slabs in room temperature. Thickness of SMP films were measured by profilemeter before transfer.

Wrinkling cycle I Process of this wrinkling cycle is illustrated in Fig. 3.1. It started from permanent shape in room temperature. Film-substrate system was heated to 60 ℃ firstly, which is higher than T_g of SMP. And then PDMS substrate was stretched with desired strain. SMP film was stretched with the same prestrain simultaneously due to the bonding between the film and substrate. To keep this shape, system with constraint was cooled to room temperature. At this time, temporary shape of SMP film can be kept even it is not supported by the substrate. After the strain in PDMS was recovered in room temperature, SMP film wrinkled on top of the PDMS substrate. When the system was heated again, strain in SMP film was recovered and the wrinkling disappeared. Both film and substrate backed to original shape eventually and were ready for new cycle. This wrinkling cycle can be repeated for many times.
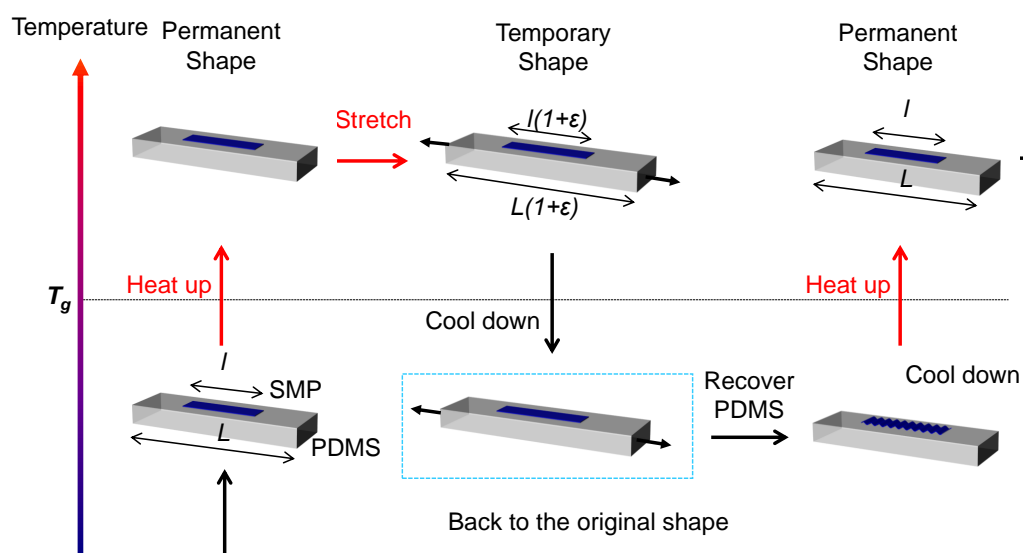
Figure 3.1: Thermomechanical history of general wrinkling cycle (wrinkling cycle I).
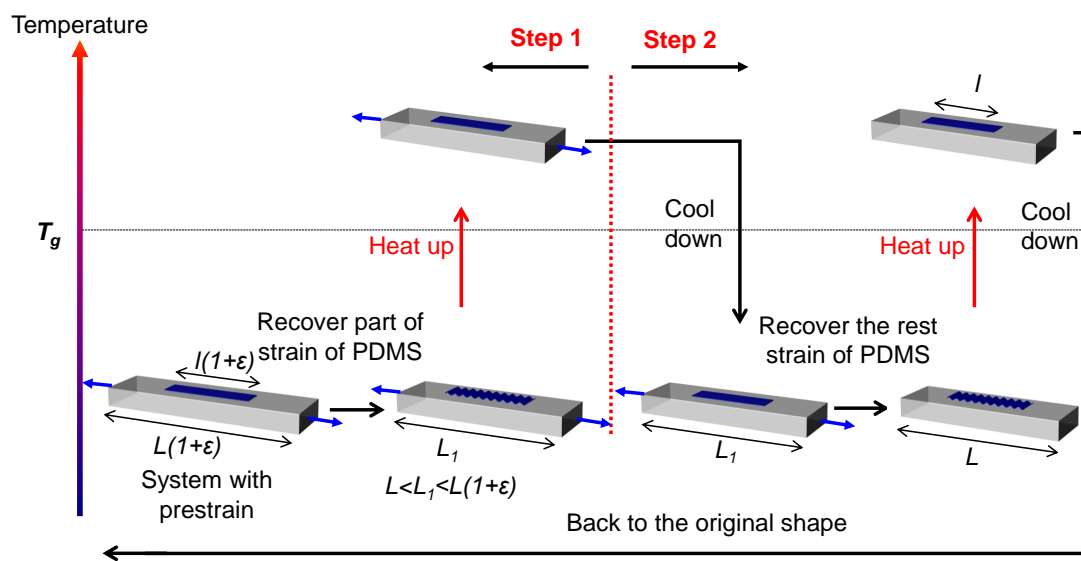
Figure 3.2: Thermomechanical history of wrinkling cycle with two prestrain recovery steps (wrinkling cycle II).
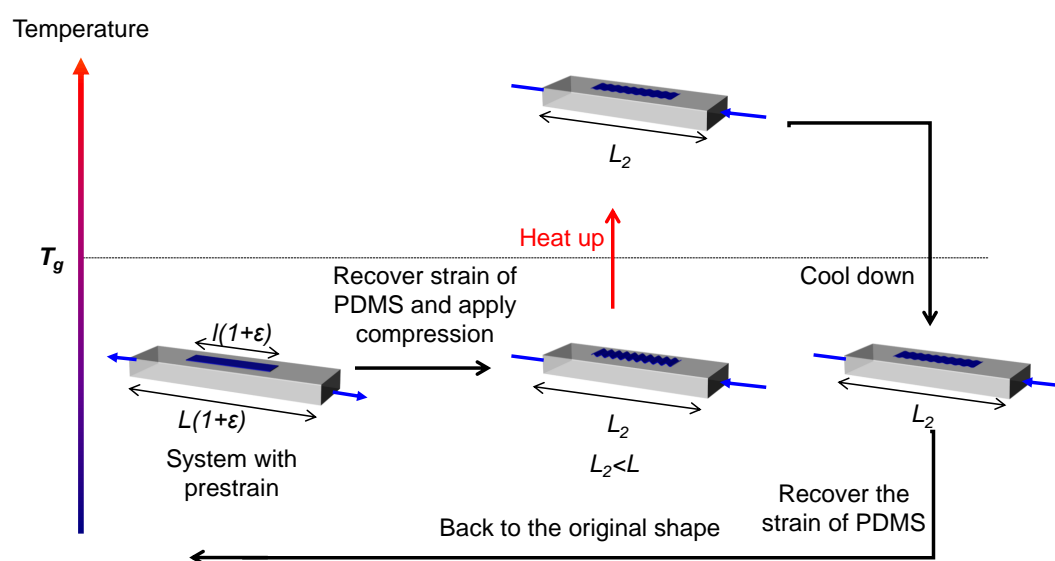
Figure 3.3: Thermomechanical history of wrinkling cycle with prestrain recover and compression (wrinkling cycle III).

Both following two types of wrinkling cycles started from the stretched system, as shown in the dashed box in Fig. 3.1. The stretching procedure is the same as that in wrinkling cycle I (Fig. 3.1). At this point, film and substrate have the same prestrain.

Wrinkling cycle II In this cycle, strain in PDMS was recovered in two steps, which made film wrinkling forms and disappears twice. Procedure of this cycle is shown in Fig. 3.2. In room temperature, when partial prestrain of PDMS substrate was recovered, SMP film wrinkled for the first time (step 1 in Fig. 3.2). Wrinkling disappeared when system was heated to temperature above T_g due to strain recovery of the film. At this time, strain of the film equals to that of the substrate. After the system was cooled and rest strain of PDMS substrate was recovered, the film wrinkled again (step 2 in Fig. 3.2). Subsequently, the system was heated above T_g, the wrinkling disappeared and both film and substrate backed to their original length and were ready for next wrinkling cycle. This wrinkling cycle is repeatable too. Inspired by two times wrinkling in this cycle, we could obtain wrinkling multiple times by recovering prestrain in multiple steps.

Wrinkling cycle III Different from the previous two cycles, in this wrinkling cycle, compression was applied to PDMS after prestrain was recovered. Fig. 3.3 shows procedure of this cycle. The thickness of PDMS substrate is about 10 mm. Wrinkling before heating was produced by prestrain and compression strain in PDMS. After the system was heated, amplitude of wrinkling decreased instead of disappearing due to the film was still under compression, even the prestrain in the film was totally recovered. When the system was cooled, the wrinkling was still there and it disappeared after compression strain was removed. This wrinkling cycle is also repeatable.

3.3   Results and discussions

Fig. 3.4 shows optical microscope images and profiles of film surface in wrinkling cycle I. In this case, film thickness is 5.1 μm and prestrain is 10%. Fig. 3.4a represents the typical morphology of the patterns in three types of wrinkling cycles. Bright lines in this figure are peak or valley of the wrinkled wavy pattern. Profiles of such pattern is shown in Fig. 3.5 in blue line. Red dot line in this figure is sinusoidal fitting. As we can see the wrinkling pattern shows good sinusoidal shape

with wavelength λ=303.7 μm (min. 286.8 μm, max. 315.1 μm) and amplitude =27.1 μm (min. 25.5 μm, max. 29.7 μm). After the system was heated above T_g, the film became flat. Fig. 3.4 shows optical microscope image of SMP film after heating and its profile is shown in Fig. 3.5 in red solid line. The profile of the film after heating is close to a straight line, which reveals the surface is almost flat after heating.

In the beginning of this wrinkling cycle, SMP was stretched with PDMS in temperature above T_g due to the adhesion between two layers. The temporary shape of the film was kept after the system was cooled. Upon lateral compression strain of the system beyond a critical value, wrinkling formed. According to the linear elastic buckling theory, the critical strain (ε_c), wavelength λ, and amplitude A of the wrinkling pattern are commonly derived as Eqs. 1.1, 1.2, and 1.3. In room temperature, Young's modulus of SMP is $\sim$2 GPa and that of PDMS is $\sim$1 MPa. With ν_f=0.4 and ν_s=0.49, the critical strain of this system can be calculated to be 0.0035, which is very small compare to the prestrain in the experiment. The film wrinkles once applied strain beyond this critical value.

Quantitative correlations in this system were also investigated. A group of samples with same film thickness (7 μm) were applied different prestrain. The results show that amplitude increase with prestrain nonlinearly (Fig. 3.6a) and no significant relationship is found between wavelength and prestrain (Fig. 3.6b), which are consistent with the prediction from Eq. 1.2 and 1.3. Equation 1.2 implies that constant wavelength is independent on the prestrain in small deformation range. The experiment results of SMP-PDMS system show the same independent relationship. In metal-SMP system, there is no significant relationship between wavelength and prestrain either (small deformation range) [92]. With considering influence of the prestrain, Jiang et al. updated the elastic theory based on single-crystal silicon film and elastomer substrate system [83]. They predicted that wavelength decrease with the prestrain in a large strain range (0-30%), which showed very good agreement with their experiment data. However, this theory may not validate in the system due to the special material property of the SMP [92]. We believe a model taking account of thermal mechanical property of SMP film-PDMS substrate system needs to be developed to characterize the
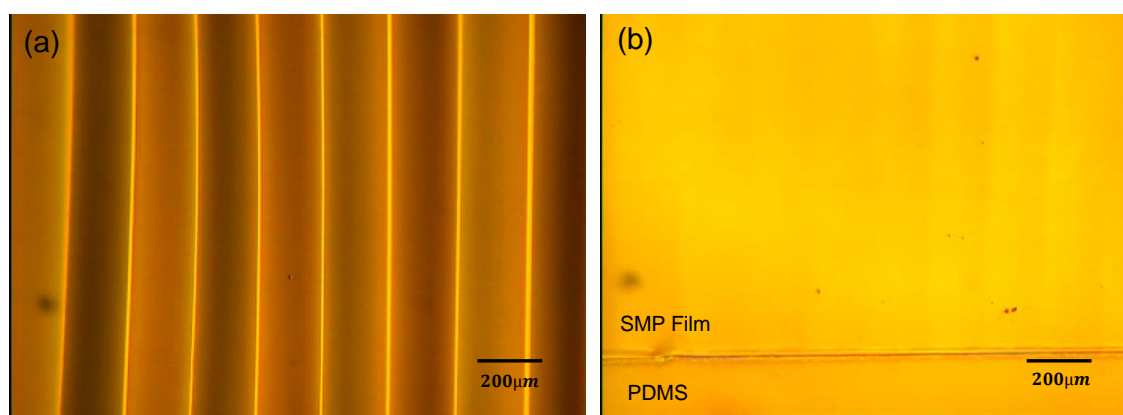
Figure 3.4: Optical microscope images of SMP thin film in wrinkling cycle I. (a) Microscope image of wrinkling after prestrain recover, (b) Microscope image of the sample after heating.
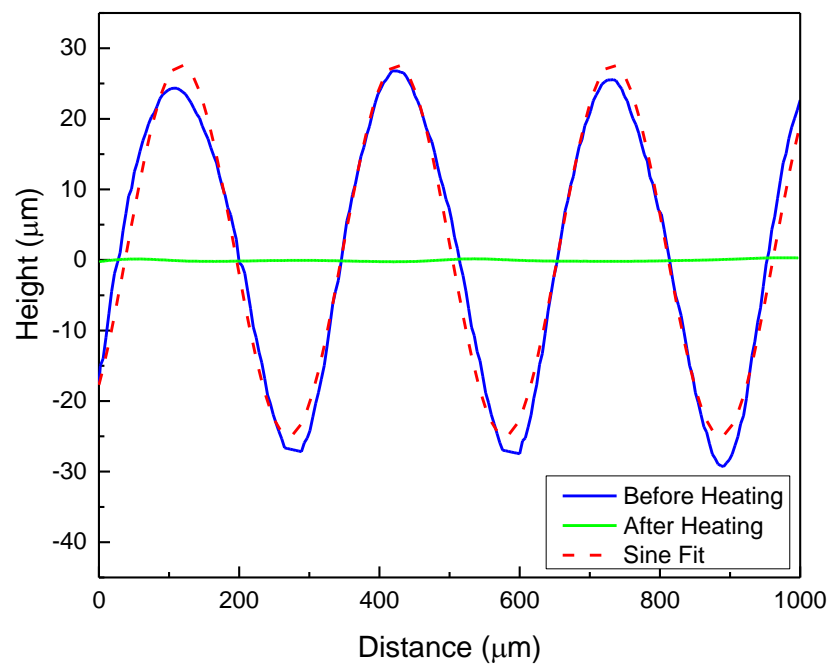
Figure 3.5: Profiles of SMP thin film in Fig. 3.4.

quantitative correlations in such system. This model should be validate to predict amplitude and wavelength of the wrinkling pattern over a large prestrain range. Once the quantitative correlations are predicted, the wavelength can be tuned by film thickness, as well as the prestrain, which is significant when the system is used as tunable optical diffraction grating [9] and other demanding applications.

The other group of samples with different film thickness were applied same prestrain (∼4.7%). Wavelength and amplitude versus film thickness are plotted in Fig. 3.6c and d, respectively. Experiment results show wavelength and amplitude increase linearly with film thickness, which is consistent with the trend from the theory. However, there is some variance between experiment data and theory calculation. Since thermal responsive SMP cannot be simply treated as elastic material. Some variance may be introduced by using the elastic theory to predict the quantitative correlations of the system with SMP. Both experiment and theory indicate that with constant prestrain, wavelength and amplitude can be tuned by thickness of the film. When a SMP thin film with gradient thickness is transferred on top of PDMS substrate, surface pattern with gradient wavelength and amplitude will be produced. This pattern can be used to separate polydisperse particles into aligned monodisperse ones [25].

Profiles of wrinkling pattern in wrinkling cycle II (Fig. 3.2) are plotted in Fig. 3.7. In this case, film thickness is 11.2 μm. In the first step, ∼3.7% prestrain was recovered and that for step 2 was ∼1.7%, which led to different amplitude. Wavelength of the pattern in different steps changes little. After part of the prestrain in PDMS was recovered in room temperature in step 1, the strain stored in the SMP film was not recovered yet. So the film was compressed by the substrate which induced the wrinkling spontaneously. After the system was heated, the mismatched strain in the film was recovered and the system reached to an equivalent strain state. In this heating process, the amplitude decreased with the strain recover in SMP and made surface became flat. At this time, rest strain in the film and substrate were equal. If the rest strain in the substrate was recovered in temperature above T_g, due to property of SMP, the film will be recovered simultaneously and no wrinkling will be observed. In order to make the surface wrinkle again, the rest strain in the PDMS

Figure 3.6: Parameter study: Relationship between (a) amplitude and prestrain, (b) wavelength and prestrain, (c) wavelength and thickness, (d) amplitude and thickness.
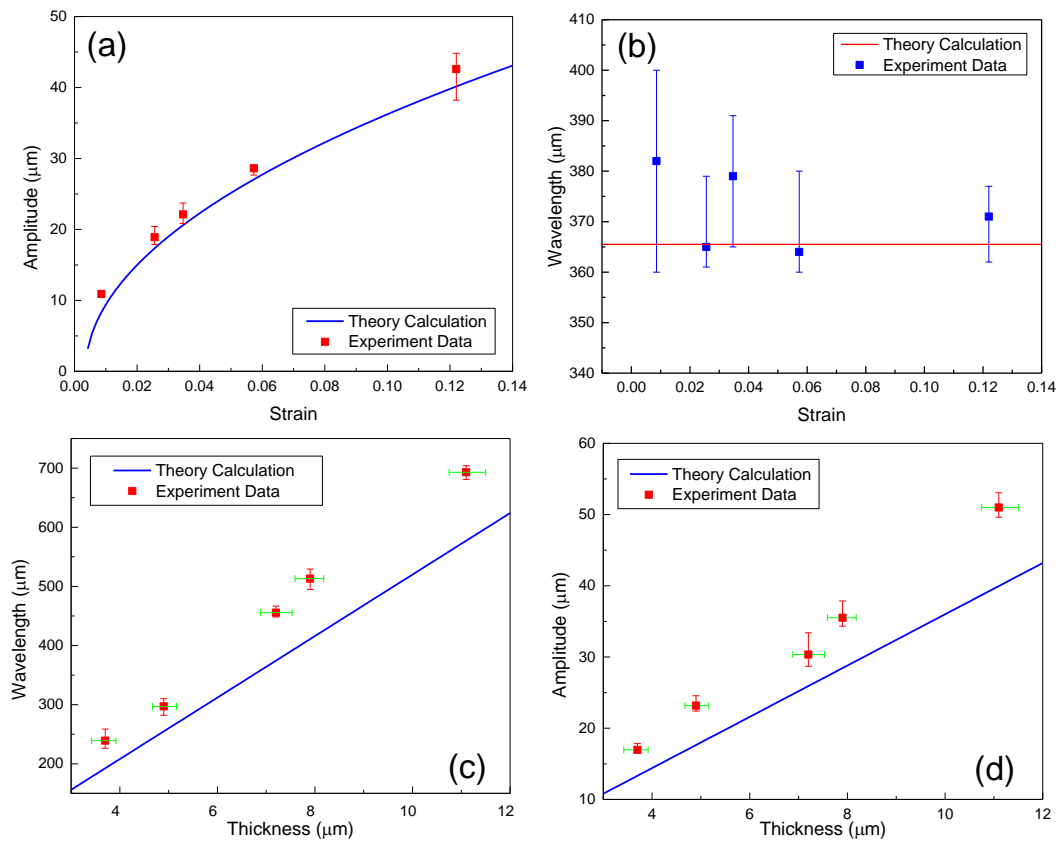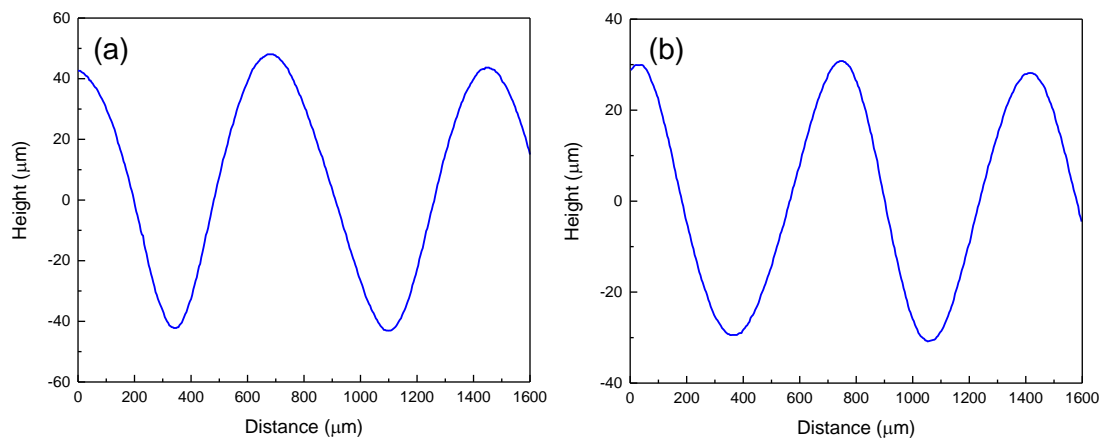
Figure 3.7: Profiles of surface wrinkling in wrinkling cycle II. (a) Profile of the wrinkling in step 1, (b) Profile of the wrinkling in step 2.

was recovered after the system was cooled. In room temperature, SMP shows glassy property and it was compressed by the substrate and wrinkled again. When the system was heated again, rubbery state SMP recovered and the surface became flat. At this time, there was no mechanical strain in the system and their length equal to the original ones and a new cycle was ready to be launched. In this cycle, prestrain was recovered in two steps, which made wrinkling formed and disappeared for two times. In fact, prestrain can be recovered in multiple steps to induce film wrinkle for multiple times. When the system is used as optical grating, the formation of period and amplitude can be tuned by strain recovery and system temperature.

Fig. 3.8a shows profile of the pattern after compressive strain was applied in room temperature in wrinkling cycle III and Fig. 3.8b shows profile after heating in this cycle. Here, film thickness is 6.7 μm. When prestrain (5.3%) in the substrate was recovered and compressive strain (0.02%) was applied in room temperature, strain mismatch between film and substrate is the summation of prestrain and compressive strain. After the system was heated, prestrain in SMP was recovered and it backed to the original length. However, the film was still compressed by PDMS due to the compression in the substrate. Amplitude decreased in heating process. But it did not decrease to zero due to the compression from the substrate. When the compression constraint was removed, the system was in the strain free state and wrinkling disappeared. The difference between the amplitude before and after heating is result from the strain difference in two stages. Before heating, wrinkling with amplitude A=31.2 μm was the result of prestrain and compressive strain combined action. After heating, the amplitude decreased to 1.7 μm, which was produced by compressive strain only. Wavelength of wrinkling before and after heating are close. It is 416.7 μm before heating and 415.7 μm after heating.

Wrinkling cycles discussed above are all programmable, controllable, and reversible. Controlling of appearance of wrinkling also gives an idea to tune surface properties in application of smart adhesion. Since surface pattern can affect adhesive properties of the interface significantly [61, 62]. Formation and disappearance of the wrinkling pattern leads to a total different adhesion state of the interface.
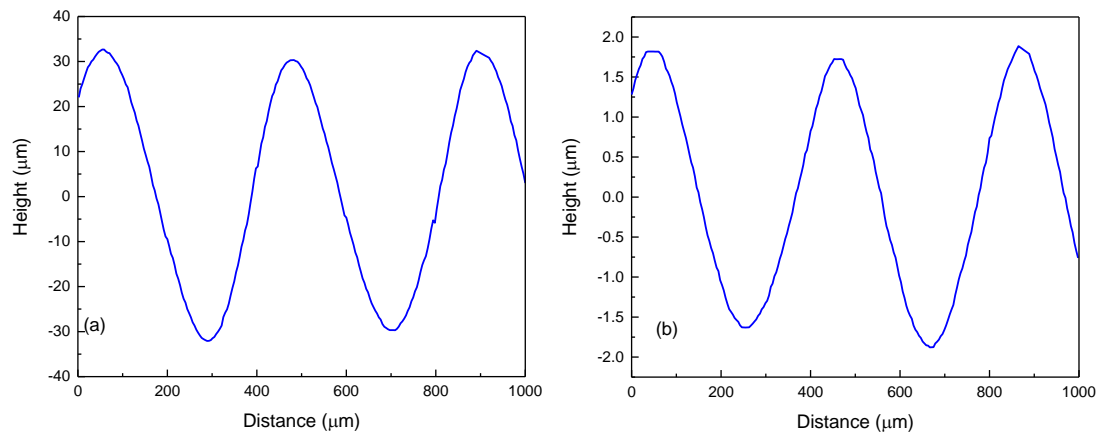
Figure 3.8: Profiles of surface wrinkling before and after heating in wrinkling cycle III. (a) Profile of the wrinkling when compression was applied (Before heating),(b) Profile of the wrinkling after the system was heated.

Ebata et al. found delamination in the wrinkling of bilayer system is preferred for the film with large thickness [103]. In the experiment we also observed delamination in the system when the film is thick. The reason for this phenomenon is the adhesion between film and substrate is not strong enough to support the wrinkling. To avoid this problem, one way is to use a type of SMP which has strong bonding with PDMS and the other way is to reduce the thickness of the film.

3.4 Conclusions

In this chapter, we built a film-substrate system with SMP as thin film and PDMS as substrate. Involving shape memory effect, three types of wrinkling cycle using such system were demonstrated. When the substrate was prestretched in temperature above T_g, SMP film was stretched simultaneously with same prestrain as the substrate. Wrinkling with good sinusoidal shape formed in the perpendicular direction of the programming strain when prestrain in the substrate was recovered in room temperature. Wavelength increases with film thickness linearly but has weak relationship with prestrain. Amplitude has a linear relationship with film thickness and increases nonlinearly with prestrain. Formation of wrinkling is controllable in all three types of wrinkling cycles by adjusting the prestrain recovery of the substrate and system temperature. When prestrain was recovered in multiple steps, with controlling the system temperature, wrinkling forms and disappears for multiple times (Fig. 3.2). These special features are significant in potential applications of surface wrinkling, such as optical grating, smart adhesion, and stretchable electronics. We expect this study can offer a simple method to fabricate unidirectional wavy pattern and control its formation and disappearance.

Chapter 4

Programmable localized wrinkling of thin film on shape memory polymer substrate

4.1   Research statement

In previous chapters, wrinkle forms all over the film surface. Here, SMP substrate will be heated locally to obtain localized wrinkling area. Different from wrinkling forms in the whole film in most literatures, some researchers have used some methods, such as focused ion beam or laser treatment to obtain surface wrinkling in desired areas [34,54]. Such form of wrinkling allow us to generate wrinkling pattern in a desired location and it has potential applications in programmable optical gratings, controlled patterning for tunable adhesion, tissue engineering and biology, and other demanding applications.

Using pre-programmed thermal responsive SMP as substrate, we demonstrate a new self-assembly fabrication method for localized surface wrinkling. Heating the thin film-substrate system locally leads to localized recovery of SMP substrate and thus induces localized thin film wrinkling. The wrinkle pattern shows good sinusoidal profile, with wavelength and amplitude decrease gradually with the distance from the heating source. The size of wrinkling area can be tuned by controlling heat input. In addition, the spectrum test was also performed, which shows peak shift of the spectrum with location due to the change of wavelength and amplitude. This study can offer a simple and programmable method to fabricate localized wrinkling pattern.

4.2   Methods and materials

Heating wire Heating wires were made from aluminum film on polyimide film (PI, thickness 25 μm, DuPont Kapton) by photolithography. A 150 nm layer of aluminum film was deposited on PI film by thermal evaporator. Then a thin layer of photoresist was spin coated on top of aluminum film. The next step is exposure with heating wire mask. Size of heating wire pattern is 30 $mm \times 200$ μm. After exposure, a photoresist layer of heating wire pattern array was defined on the structure. In order to make a good connection with the external circuit, 3×6 mm pad was designed in each end of the heating wire. To remove the exposed part of aluminum film, the structure was immerged into aluminum etchant type A at 50 ℃ for 15 seconds. The heating wire part was protected by photoresist from etching. Then sample was washed with de-ionized (DI) water for 2 minutes to clean the etchant. Next cleaning the sample with acetone to remove the resist layer and then the heating wire was cut from the PI film. According to the measurement, resistivity of such heating wire is $\sim 5 \times 10^{-8}$ $\Omega \cdot m$.

SMP substrate SMP solution is the same as that in chapter 2 and 3. Mixed solution was injected into a mold (30 mm in length and 8 mm in width), which was made by glass slides. Polymer solution was cured under UV lamp for 5 minutes followed by post-curing in the oven at 80 ℃ for 1 hour [101, 102]. After SMP sample was cured, it was demolded carefully. Heating wire was located in the center of the mode cavity and parallel to its upper and lower surface. The equal distance from heating wire to upper and lower surface made the sample was heated symmetrically. The mold determines the thickness of SMP substrate, which is about 2 mm. Uniaxial stretching of SMP samples were conducted at 60 ℃ ($>T_g$) using Dynamic Mechanical Analysis (DMA) tester (TA Instruments, DMA Q800). To fix the temporary shape, SMP samples were quenched to 25 ℃ with constraint in the furnace of DMA. And then a layer of aluminum with thickness of 150 nm was deposited on prestretched SMP sample using thermal evaporator. In the deposition process, the heating wire was covered to avoid the aluminum particles. Fabrication of the aluminum film-SMP substrate system was completed in this step. To avoid the recovery of the SMP due to the thermal

SMP

Heating Wire

SMP Prestrain 6%

Aluminum Deposition Thickness=150 nm

Turn on the Current

-

+
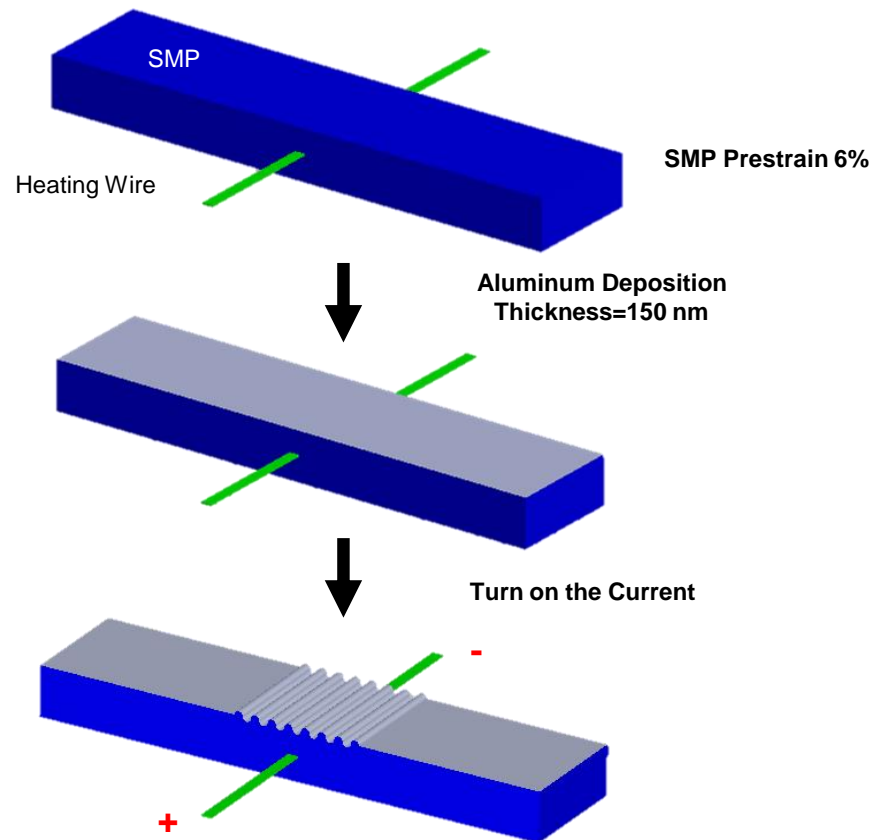
Figure 4.1: Method to produce localized wrinkling.

effect in the deposition process, SMP sample was clamped in both ends during deposition. After this process, SMP sample was cooled for 1 hour in the chamber and then removed from the clamp.

Anisotropic conductive films (ACF, Elform Heat Seal Connectors) were used to connect the heating wire with external circuit. DC power supply in current mode was used for supplying the power. This mode allows us to set output current to a desired value, which is very convenient in present study.

Fig. 4.1 shows the process to fabricate the localized surface wrinkling. SMP sample with heating wire in the center was programmed with 6% prestrain at 60 ℃, which is higher than its T_g. The second step is to deposited a 150 nm thick aluminum thin film on top of the SMP substrate. And then connecting the heating wire with DC power supply. After the current was turned on, SMP sample was heated locally by heating wire with desired current and time and recovered in this area to induce localized wrinkling. Wrinkling area can be tuned by changing input heating energy, for example, the input power or the heating time.

4.3   Results and discussions

Firstly, with current I=0.1 A, SMP sample was heated for 25 minutes. Results of this case is shown in Fig. 4.2. Fig. 4.2a is optical microscope image showing the wrinkling area just above the heating wire. Bright lines in this figure is peak or valley of the wavy shape. Fig. 4.2c and d are 2D and 3D AFM image, respectively. Profile of this wrinkling pattern is shown in Fig. 4.2b in blue line and red line in this figure is sinusoidal fitting. From Fig. 4.2b and d, we can see the typical profile shows good sinusoidal shape in perpendicular direction of the prestrain. Wrinkling pattern shown in this figure represent the typical morphology in current study. Width of wrinkling area is about 16 mm when the sample was heated for 25 minutes. We can also obtain a narrow wrinkling area by heating for a shorter time, for example 1 minute. Fig. 4.3 shows wrinkling area with $\sim$1 mm width after heating for 1 minute. The boundary of wrinkling is a transition area instead of a clear line. Wrinkling disappears gradually in the transition area. Beyond the transition area, the surface is still flat.

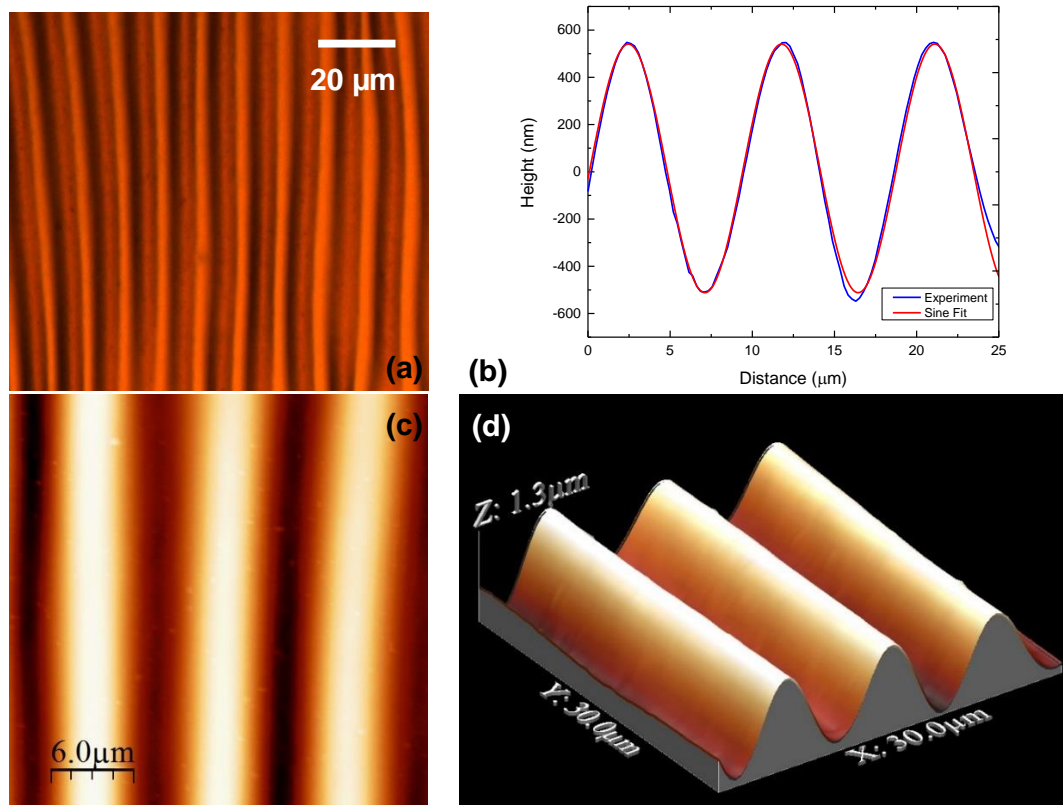Figure 4.2: Images of wrinkling pattern and the profiles in the center area. (a) Optical microscope image, (b) profile and sin fitting, (c) 2D AFM image, and (d) 3D AFM image.
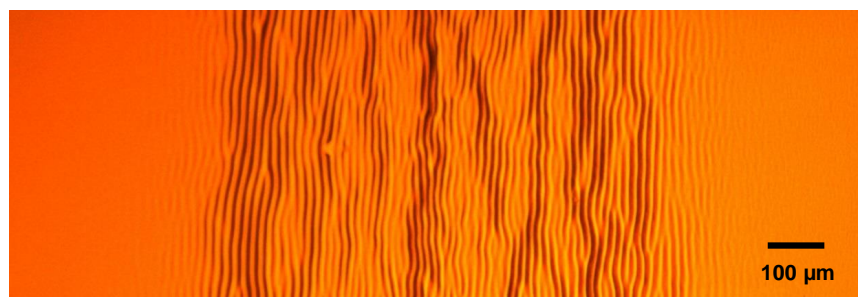
Figure 4.3: Optical image of localized wrinkling area and its boundary (Heating time 1 minute).

In the heating process, area near the heating wire was heated firstly. Prestrain of SMP in this local area was recovered due to shape memory effect. The metal film above this area is subjected to compression and introduces the wrinkling in the film once the strain beyond the critical value. According to the linear elastic buckling theory, the critical strain (ε_c), wavelength λ, and amplitude A of the wrinkling pattern are commonly derived as Eqs. 1.1, 1.2, and 1.3.

At 60 ℃, Young's modulus of SMP is $\sim$2 MPa and that of aluminum is $\sim$69 GPa. With ν_f=0.33 and ν_s=0.4, the critical strain of this system can be calculated to be 0.0005, which is very small compare to the prestrain in the experiment. The film wrinkles once compression strain beyond the critical value.

Unlike global wrinkling in most of the literature, localized heating by heating wire induced localized wrinkling in current study. Heating gradient from heating wire made wrinkling disappears gradually in the transition area. In the area without wrinkling, heating energy is not sufficient to make recovery of the prestrain beyond the critical value. In Fig. 4.3, wrinkling area with 1 mm width was obtained without affecting adjacent area. Therefore, we can control the formation of surface wrinkling by embedding heating wires in desired area and heating the sample selectively.

Surface wrinkling morphology due to localized heating in current study is the same as that in global heating using the same system in the literature [92]. Chen et al. used aluminum film-SMP substrate system with film thickness 30 nm to produce surface wrinkling [92]. Programmed SMP is recovered globally in the temperature above T_g leads to film wrinkling forms all over the surface. Besides the wavy shape pattern, they also observed cracks orthogonal to the wrinkling. They believed during shape recovery of SMP substrate, tensile stress in orthogonal direction of prestrain is developed in the thin film due to Poisson's effect. The tensile stress along the direction perpendicular to the prestrain resulting in cracks. In our experiment, there is no crack was found in samples with 150 nm aluminum thin film. We observed the cracks on the sample with aluminum film thickness 8 nm. The other possible reason for crack is the strain recovery rate, the higher the rate, the denser of the crack [25, 89]. However, it is not easy to measure the strain rate in the localized heating process.
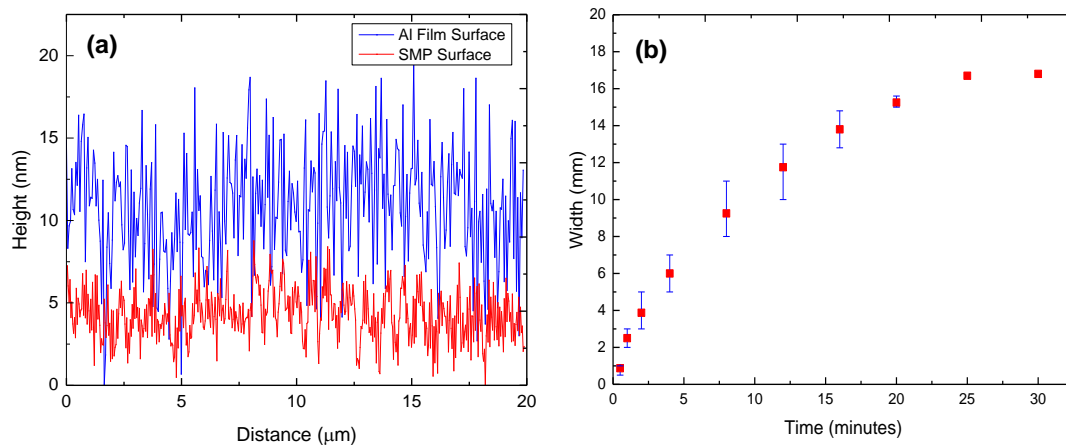
Figure 4.4: Relationship between width and time of wrinkling area. (a) Profiles of SMP and un-wrinkled Al film on SMP, (b) Relationship between width and time of wrinkling area, I=0.1 A.

Size of wrinkling area depends on the heating energy. In order to control the wrinkling size accurately, relationship between size of wrinkling area and input energy is studied. With this relationship, we may obtain desired width of the wrinkling area by adjusting the heating time. The boundary of the wrinkling is not a clear line. Therefore, we defined an area with certain roughness range to be boundary according to the roughness of un-wrinkled aluminum film. Profiles of SMP substrate before deposition and un-wrinkled aluminum film are shown in red and blue curve in Fig. 4.4a, respectively. From this figure, we can see that the roughness of the SMP substrate and film are about 9 nm and 20 nm, respectively. We define the area, roughness of which is two and half times of that of the un-wrinkled film, to be the boundary. According to the calculation, the roughness of the boundary is 50 nm. With this criterion, width of samples with same current and different heating time was measured and shown in Fig. 4.4b. In this figure, I=0.1 A. Width increases dramatically in the first 5 minutes. The width doesn't increase after 25 minutes. The possible reason for this phenomenon is that the system reaches a heating energy balance state. Under this condition, the energy input equals to the heat loss. This makes the heat cannot be delivered to the further area.

With a constant resistance, heating energy can be tuned by heating time and current. One can obtain the same heating energy by different combination of time and current. It is possible to achieve this goal by using higher current and shorter time. However, higher current ($>$0.2 A) in present study burns the heating wire (PI film with aluminum film). The heating wire that can bear higher current should be used in this case, which was not performed here. The advantage of this method is that it allows us to design heating wire patterns to produce corresponding wrinkling area. With specific heating wire pattern, wrinkling can be generated along the paths with desired width by controlling the heat input. In this research, we used the simplest heating wire pattern, which is the line shape. Different from the methods with surface treatment by ion beam or laser in desired path [34, 54], present study offers a new approach to produce localized surface wrinkling along desired path, which is easy and programmable.

Profiles of samples with 25 minutes heating in different location are shown in Fig. 4.5. We
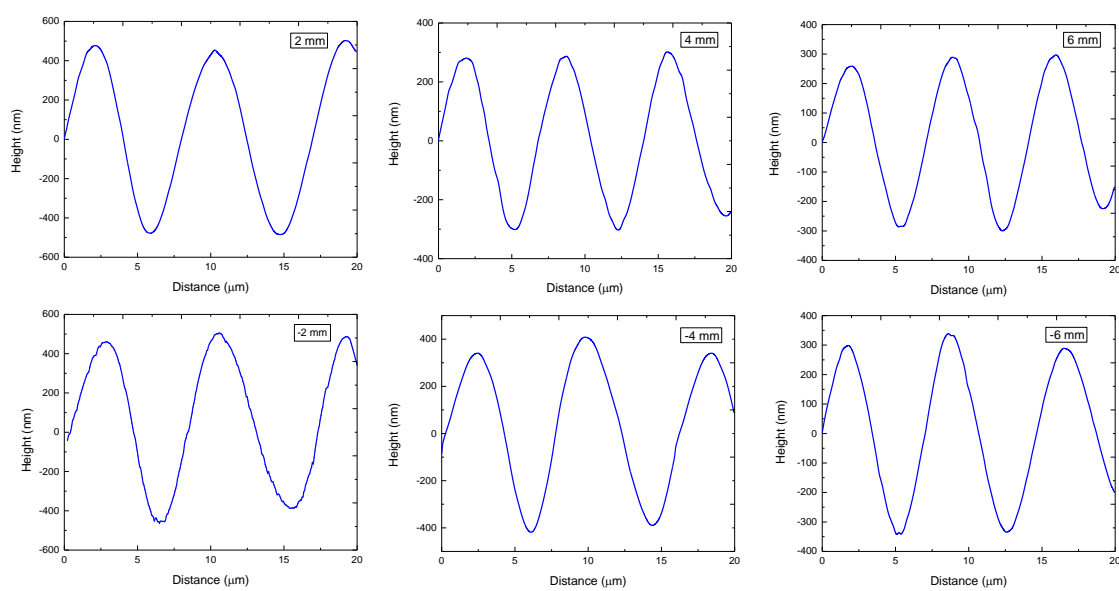
Figure 4.5: Profiles of wrinkling in different locations.

defined the area right above the heating wire is the center. Locations with 2 mm interval from the center were scanned. From this figure, we can see that wrinkling in range of 6 mm from the center show good sinusoidal shape. It is interesting that the wavelength and amplitude decrease with the distance from the center. Profiles in transition area were also obtained, which are shown in Fig. 4.6. At 8 mm, the profile still shows the wavy shape with amplitude $\sim$60 nm. The amplitude decreases with the distance and profile approach the roughness of the film surface without wrinkling. At 8.5 mm and 9 mm, the roughness are $\sim$50 nm and 40 nm, respectively. The area 8.5 mm away from the center can be treated as the boundary according to our criterion. Amplitude and wavelength in different locations are summarized in Fig. 4.7 in blue rhombus and red square, respectively. The schematic of corresponding positions is also shown in this figure. Both wavelength and amplitude show good symmetry about the center and decrease gradually from center to both sides.

The material property of SMP changes dramatically with the temperature. From room temperature to the temperature above its T_g, Young's modulus decreases three order of magnitude. In localized heating samples, the temperature decreases with the distance from heating source. The temperature in the center is the highest and decreases gradually to both sides. Therefore, the material in the center is the softest and become stiffer in both sides. According to the linear elastic buckling theory (Eq. 1.2), wavelength depends on the Young's moduli ratio of film and substrate when the film thickness is a constant. The higher the ratio, the larger the wavelength and amplitude, which leads to the largest wavelength and amplitude forms in the center and decrease in both sides and finally disappears. Similarly, higher temperature brings higher prestrain recovery percentage. Once the prestrain recovered beyond the critical value, wrinkling forms. In the wrinkling area, the prestrain recovered beyond the critical value and it is lower than that in the area without wrinkling. While in the transition area, the prestrain recovered is around the critical value. Although the assumption of linear elasticity may not be valid for the film-SMP substrate system due to SMP cannot be treated simply as elastic material, the temperature distribution does offer a qualitative explanation.

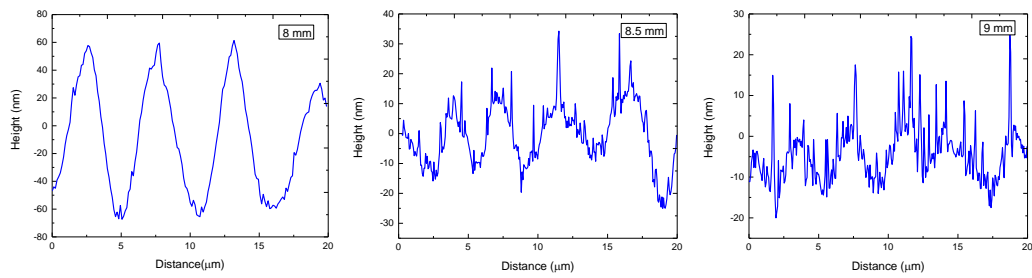Chirped grating with varies period is a common device used in optical communication sys-

Figure 4.6: Profiles in the boundary in the boundary of wrinkling area.
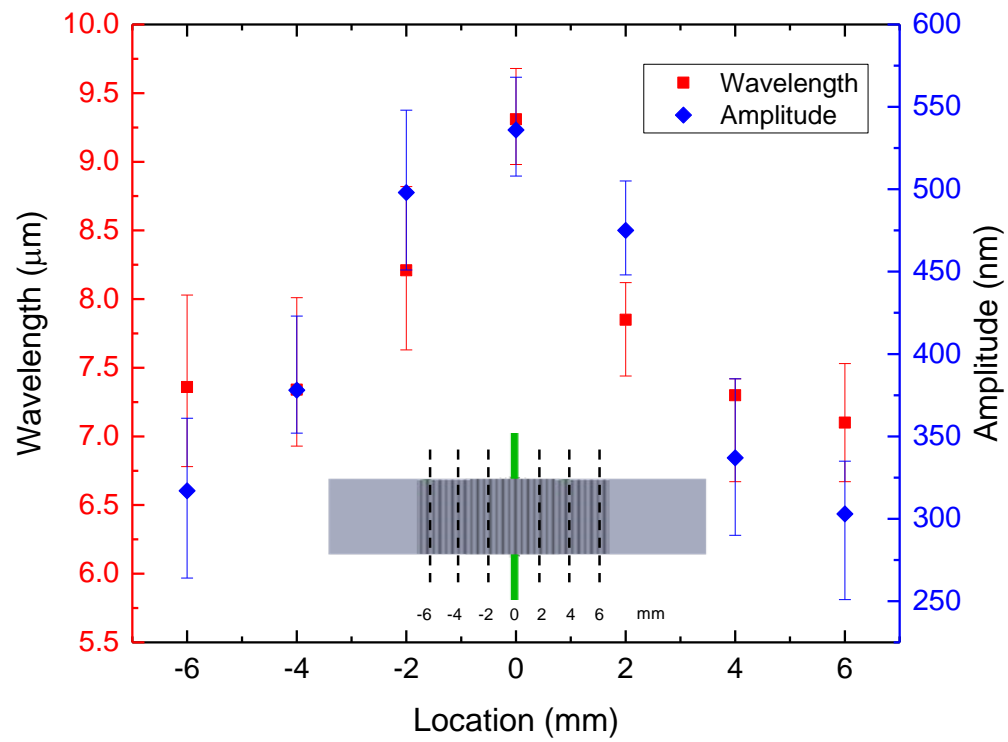
Figure 4.7: Wrinkling wavelength and amplitude in different locations.
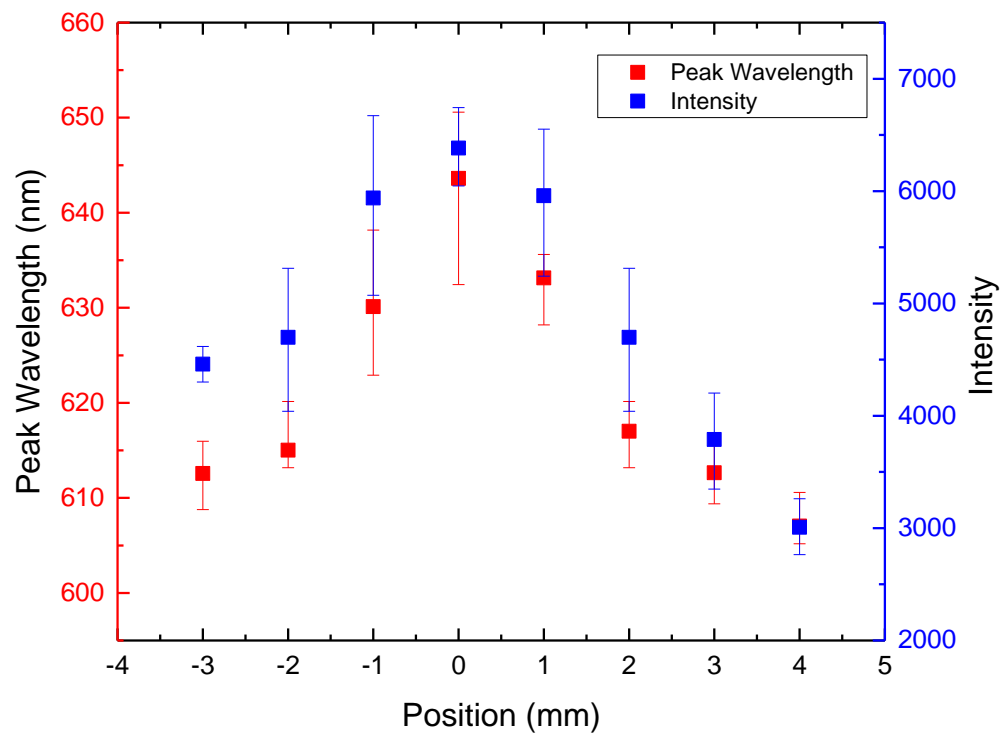
Figure 4.8: Peak wavelength and intensity of wrinkling surface in different locations (8 *nm* aluminum film).

tems [104]. Electron beam lithography is the conventional method to manufacture grating with non-uniform period. The low efficiency and high cost of this method makes the chirped grating fabrication is still a challenge [105]. Inspired by the localized wrinkling with non-uniform wavelength, one can use this simple and low cost method to fabricate the chirped grating. In order to obtain wrinkling wavelength comparable to that of visible light, 8 nm aluminum was deposited on SMP sample. Size of heating wire and prestrain are the same as those in the previous experiments. After the sample was heated for 10 minutes, reflection spectrum test was performed on the wrinkling surface. The diameter of incidence light spot is $92\pm2\mu m$, which is large enough compare with the wrinkling wavelength. The peak wavelength and intensity of reflective light in different locations is illustrated in Fig. 4.8. Location of center in this figure is the same as that in Fig. 4.7. Both peak wavelength and intensity are strongest in the center and decrease away the center. Reflective peak wavelength shift from the center to both sides due to the decrease of wrinkling wavelength with the distance from the center. From the center to both sides, the amplitude of the wrinkling profile also decreases, which leads to the decrease of the reflective intensity [9]. Chirped grating made in this way is simple, cheap, and programmable. It is a promising method to overcome the challenge of chirped grating fabrication.

4.4   Conclusions

In summary, we built a programmed metal film-SMP substrate system with heating wire. Upon the system was heated locally by the heating wire, localized wrinkling formed with good sinusoidal shape. The wrinkling area can be tuned by adjusting heating energy input. Both wavelength and amplitude decrease with the distance from the heating source. By decreasing the thickness of aluminum film, one can induce the localized wrinkling with non-uniform wavelength comparable to visible light, which can be used as chirped grating. This study support a method to produce wrinkling pattern along desired path. It has advantages of low cost and simple process for fabrication of wavy shape microstructures.

Chapter 5

Self-assembled formation of surface wrinkling with two distinct morphologies

5.1   Research statement

Using line heating in last chapter, localized 1D wrinkle was fabricated. In order to obtain 2D localized wrinkling, in this chapter, we use point heating source to heat the sample. System is built by deposit a thin layer of aluminum thin film on top of prestretched shape memory polymer (SMP) substrate. After the system is heated by a point heat source, two distinct wrinkling pattern formed in a circular area around the heat source. Two wrinkling morphologies are spoke and ring patterns, which distribute in the inner and outer of the circular area, respectively. Size of the wrinkling area can be tuned by the heat input. With 12 seconds heating, the wrinkling reaches to the width boundary of SMP sample. The formation of the wrinkling pattern with different heating time are captured by digital camera. This study can offer an easy and programmable method to fabricate spoke and ring patterns in micro-scale and support guidelines in potential applications, such as stretchable electronics, surface property control, and other demanding applications.

5.2   Methods and materials

Fig. 5.1 shows the process to make SMP sample. Here, a mold made of polydimethylsiloxane (PDMS) and glass slides was used to make SMP sample with a small hole. After SMP is unmolded, a piece of heating wire (FeCrAl Alloy, Diameter 127 μm, Resistance Range: 32.1 to 37.7 ohms/foot) is inserted in the hole. The bottom of the mold in this figure is PDMS with a needle inserted inside. PDMS was made from Sylgard 184 elastomer kit (Dow Corning) using a 10: 1 prepolymer-

crosslinker ratio by weight. After degassing and curing in the oven, PDMS slabs were cut with dimension $10\times10\times5$ mm. The needle was inserted in PDMS in direction perpendicular to the surface of PDMS. The length of the needle outside PDMS is 2 mm, which equals to the thickness of SMP sample. To control the thickness of SMP sample, two glass spacers with 2 mm thickness was put on the surface of PDMS. The distance between the spacers is about 8 mm, which equals to the width of SMP sample. The needle was located in the center of two spacers. A piece of glass slide was assembled on the top of spacers with a good contact with the tip of the needle. The size of SMP sample was defined by the cavity of the mold. The needle in the mold leads to a through hole in the center of SMP sample.

Next step is to inject SMP solution into the mold. SMP solution synthesis and curing process are the same as that used in the previous chapters. When SMP sample was fully cured, it was unmolded and a piece of heating wire about 20 mm long is injected through the hole on it.

Fig. 5.2 depicts the fabrication process of film-substrate system and the method to produce the wrinkling by point heat source. With heating wire, SMP sample was prestreched uniaxially with 6% strain at 60 ℃ using Dynamic Mechanical Analysis (DMA) tester (TA Instruments, DMA Q800). After the sample was quenched to 25 ℃ with constraint, the prestretched temporary shape was kept. Using thermal evaporator, a layer of aluminum thin film with thickness 150 nm was deposited on the surface of prestretched SMP sample. To heat the sample, heating wire was connected with DC power supply. In the heating process, heating wire kept in vertical direction, which is perpendicular to SMP sample. After the current was turned on, SMP sample was heated by a point heat source with desired power and time. Such point heat source induced two distinct wrinkling pattern in a circular area.

5.3   Results and discussions

The first group of film-SMP substrate samples was heated for 2 seconds with current 1 A. Fig. 5.3 is optical microscope image that shows the wrinkling area after heating. In this figure, prestrain was applied in horizontal direction. The hole in the center of the pattern is for inserting
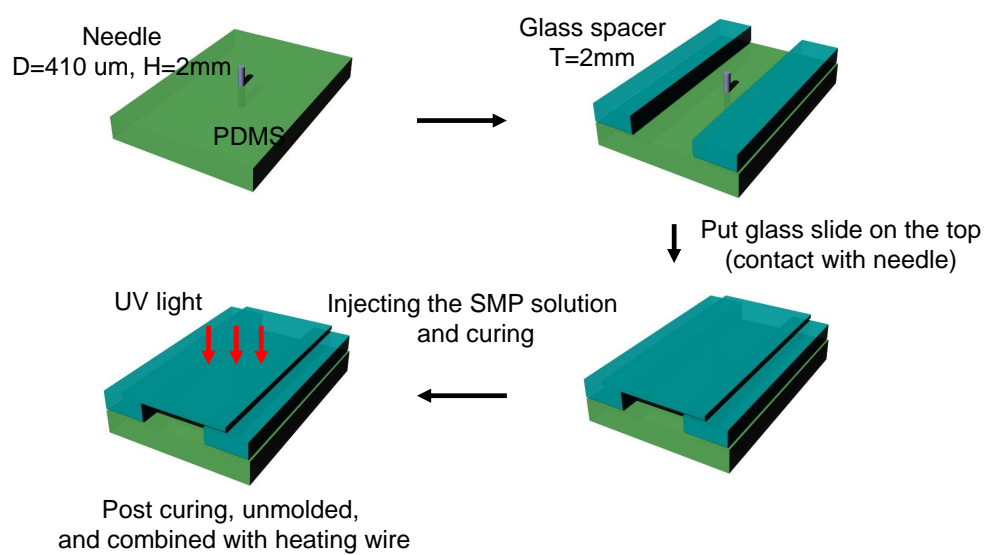
Figure 5.1: Process to make SMP sample for point heating.

SMP Prestrain 6%, at 60 ℃

Heating wire

SMP Substrate

Aluminum Deposition
Thickness=150 nm

Aluminum film

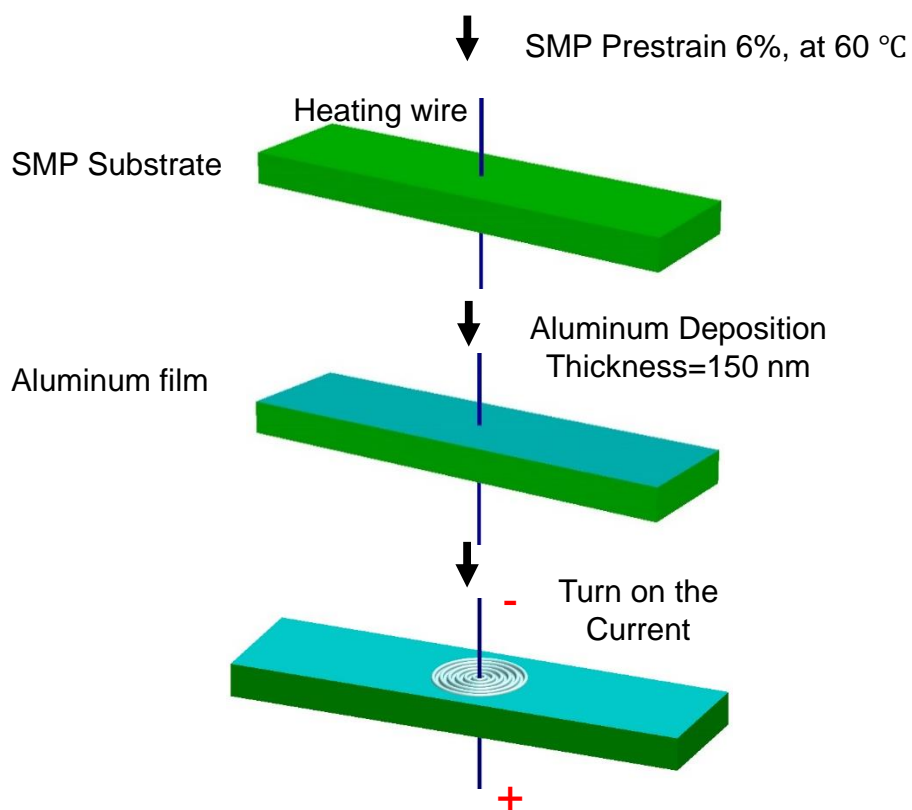Turn on the
Current

-

+

Figure 5.2: Schematic of the experimental set-up for fabrication of wrinkling pattern on SMP substrate by point heat source.

heating wire. In the heating process, heating wire kept straight and perpendicular to the upper and lower surface of SMP substrate. Such perpendicular position leads to uniform heat gradient distribution through the thickness direction. Wrinkling pattern in Fig. 5.3a shows two distinct wrinkling morphologies. Spoke pattern located in the inner of the circular area around the hole and ring pattern in the outer. Fig. 5.3b-e shows the top, bottom, left, and right boundary of the circular wrinkling area in Fig. 5.3a, respectively. These figures shows that outside of the ring wrinkling pattern, aluminum film is still flat, which implies the area outside of the wrinkling area is not affected by the point heat source.

Profiles from AFM of two wrinkling patterns is plotted in Fig. 5.4. With origin coincides with the center of the hole, 0°, 90°, 180°, and 270° in this figure represents right, top, left, and bottom of the circular wrinkling area, respectively. Hence, 0° and 180° are in prestrain direction, which is the horizontal direction. The distance from heat source to the scanned spots is 600 μm for the spoke wrinkling pattern and 1 mm for the ring pattern. Fig. 5.4a illustrates the profile of spoke wrinkling pattern in four directions. Blue curve in these figures are profiles obtained in the experiment and the red dot curve are sinusoidal fitting. It reveals that profiles of spoke pattern show good sinusoidal shape in four directions. The wavelength and amplitude of the wavy shape show good consistent in four directions. Fig. 5.4b shows the profiles of the ring pattern. From the figures, we can see the profiles show sawtooth shape. There is no significant different between the wavelength in four direction. However, the amplitude shows good consistent and symmetry in horizontal and vertical direction, respectively. It is ~100 nm in vertical direction, which is only half of that in horizontal direction. With the same distance from the heat source, these spot received the same heat energy. The only different between vertical and horizontal direction is the stress field, which due to the uniaxial prestrain in horizontal direction.

Fig. 5.5 and 5.6 plots the wavelength and amplitude of two types of wrinkling patterns in different locations. Definition of 0°, 90°, 180°, and 270° are the same as we discussed before. For the spoke wrinkling pattern, the wavelength increase with the distance from the center firstly and then decreases in the end. Wavelength in four directions reaches to the maximum value in the
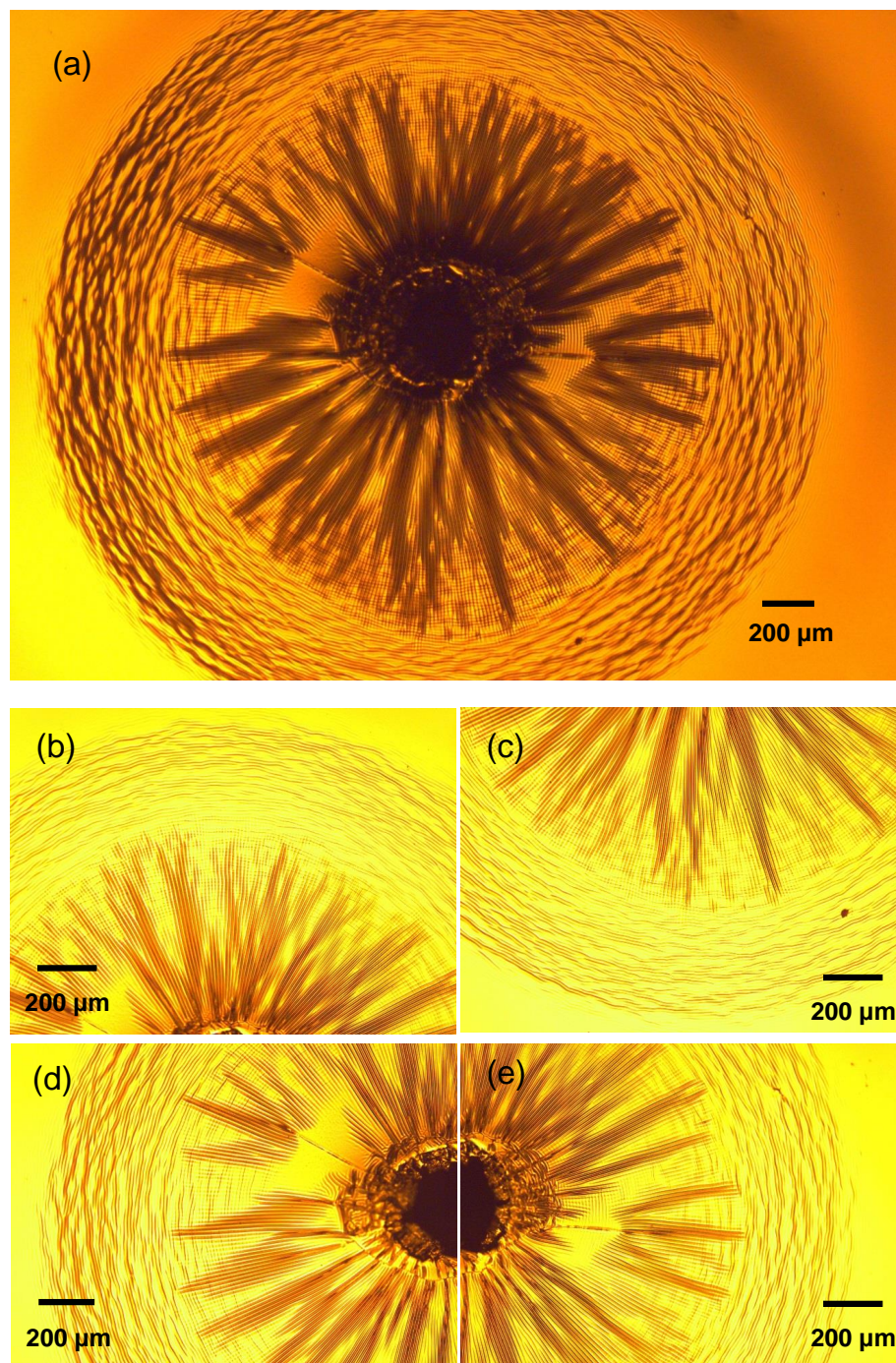
Figure 5.3: Wrinkling pattern and its boundary by point heating. (a) Overall view of the wrinkling pattern, (b) top, (c)bottom, (d)left, and (e)right boundary of the wrinkling pattern.
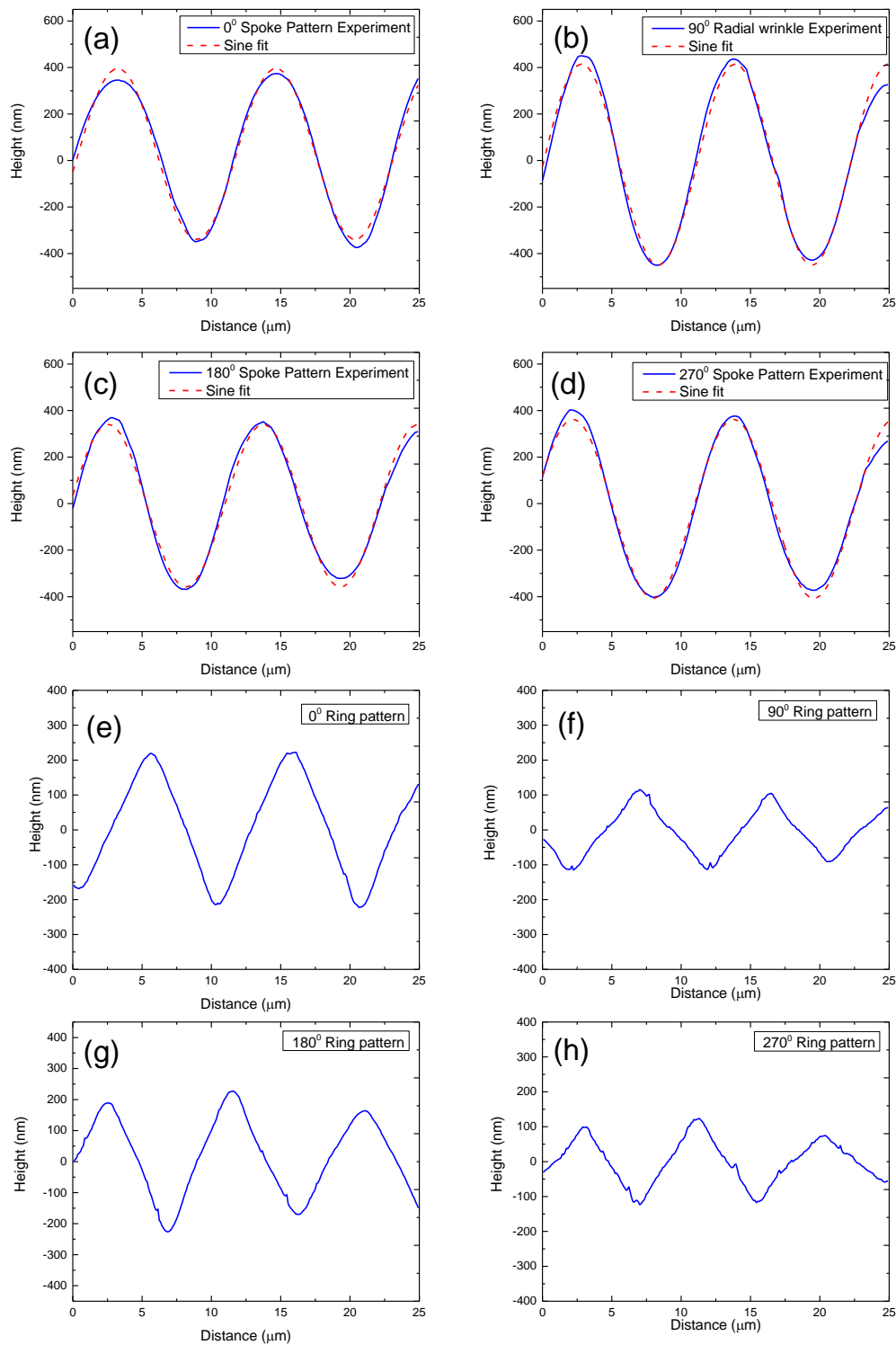
Figure 5.4: Profiles of wrinkling patterns in different locations (I=1 A, T=2 s). (a)-(d) Profile of spoke pattern, 0.6 mm away from the center, (e)-(h) Profile of ring pattern, 1 mm away from the center.
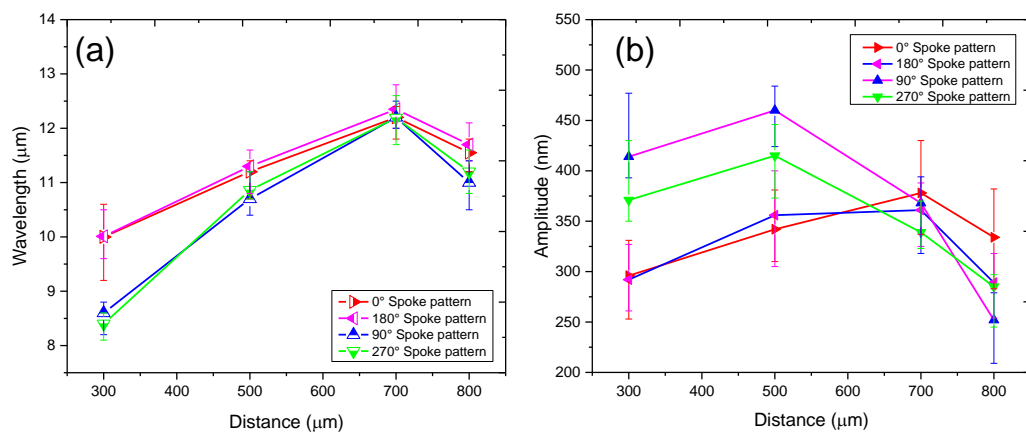
Figure 5.5: (a) Wavelength and (b) amplitude distribution of spoke wrinkling pattern (I=1 A, t=2s).
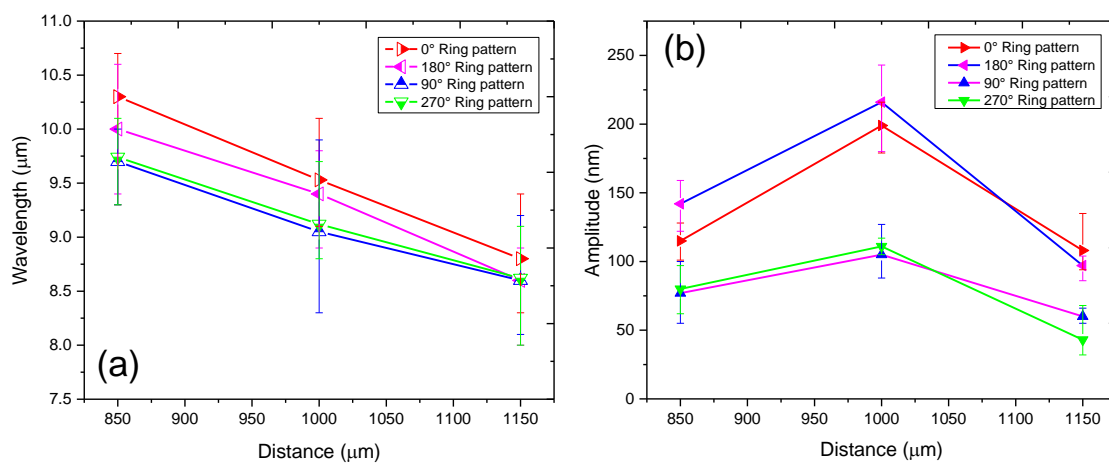
Figure 5.6: (a) Wavelength and (b) amplitude distribution of ring pattern (I=1 A, t=2 s).

position of 700 μm. Except for this position, wavelength of the pattern in horizontal direction (0°
and 180°) is larger than that in vertical direction (90° and 270°). In addition, due to the symmetry
of the structure and heat field, wavelength in both horizontal and vertical directions also show good
symmetry. Amplitude of this pattern increases from 300 to 500 μm and that in vertical direction
is larger than that in horizontal direction. There is no significant difference was found in the end
of the spoke pattern (700-800 μm). Area with distance from 850 to 1150 μm is the ring pattern
(Fig. 5.3b). Wavelength of this pattern decrease from the inner to the outer. While the amplitude
in the center of the ring pattern (1000 μm) is the largest. Both wavelength and amplitude in
horizontal direction is larger than that in vertical direction. Wavelength and amplitude also show
good symmetry in both horizontal and vertical direction.

The heating process was captured by the microscope with digital camera. Patterns in different
time are shown in Fig. 5.7. Figure 5.7a shows the surface with the hole before heating. After the
current is turned on, the ring pattern forms in a ring range. It propagates and looks like shock wave.
At 2 seconds, the current was turned off and the size changes little after heating. It is interesting
that there is no spoke pattern in the heating process. After the current was turned off, the spoke
pattern forms around the hole. It kept extending to the final wrinkling state with spoke inside and
ring outside at 6 seconds. In the heating process, the size of the wrinkling area increase with the
heating time. The radius of the whole circular wrinkling area, which equals to that of the outer
boundary of ring pattern is about 450 μm at 1 second and 1400 μm at 2 seconds. After heating
stops, the size of ring pattern increases little and the spoke pattern begins to form and extend.

In the prestretch step, SMP substrate was applied uniaxial prestrain in length direction, which
is identical with horizontal direction discussed above. The formation of the wrinkling pattern is
combined effect of thermal expansion and recovery of the prestrain. When the sample is heated by
the heating wire from the center, the heat energy spreads away from the center. Thermal effect
brings expansion of substrate in the radial direction and this is the reason for ring pattern. The
hole itself is traction free with circumferential strain only. Around the hole, only spoke pattern
forms. Recover of the substrate around the hole leads to compression strain in horizontal direction.
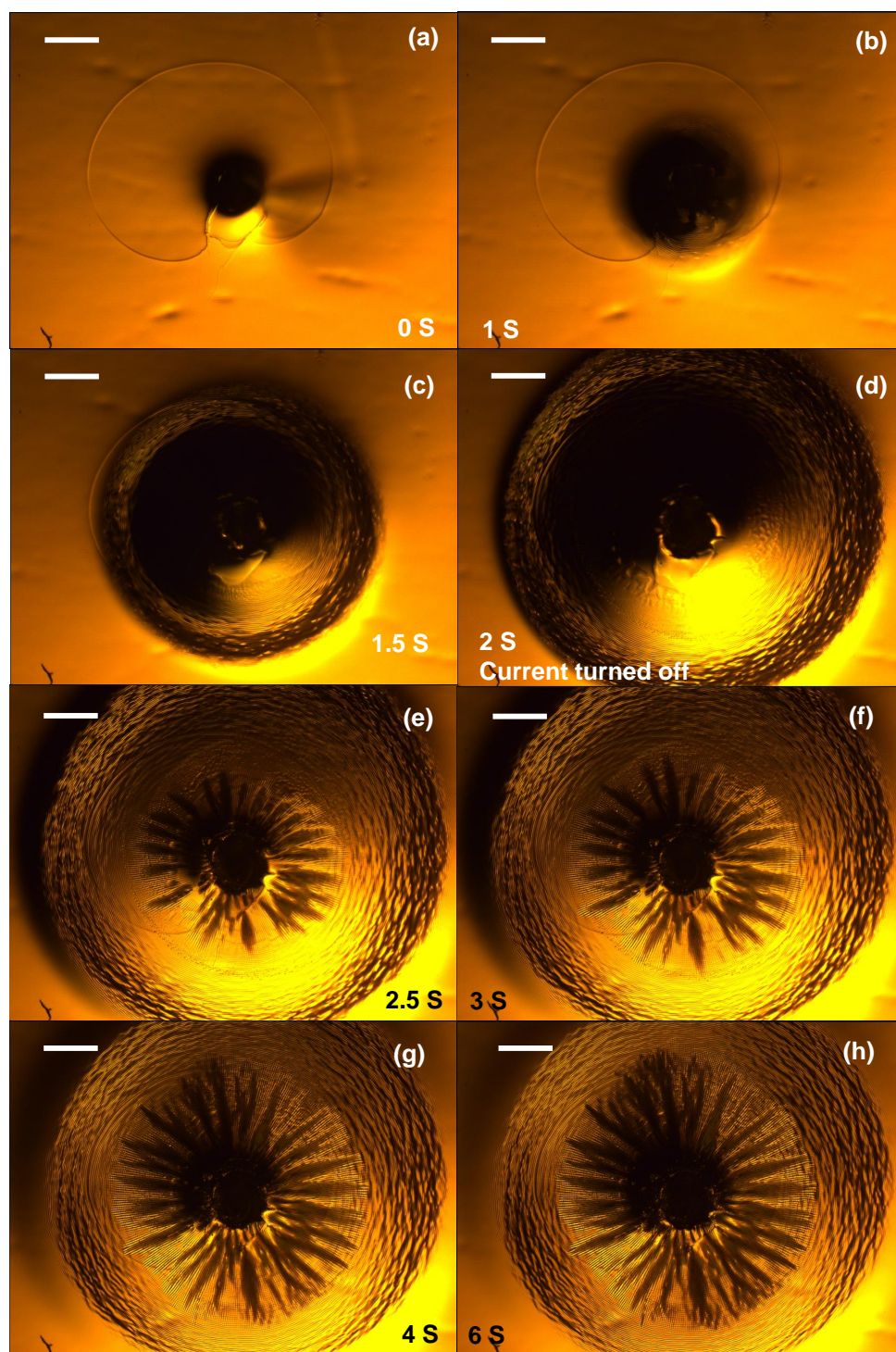
Figure 5.7: Time sequence of the wrinkling pattern (I=1A, t=2s, Scale bar 400 μm).

Such strain results in higher amplitude in horizontal direction for spoke pattern (Fig. 5.5). For ring pattern, amplitude is higher than that in vertical direction due to the strain recovery in the horizontal direction (Fig. 5.6).

Wrinkling area can be tuned by heat input. Fig. 5.7 are optical microscope images of the sample with heating time $t=12$ s and current $I=1$ A. Fig. 5.7a shows the wrinkling area round the hole and its boundary in four directions are shown in Fig. 5.7b-e. The whole wrinkling area shows oval shape with the hole as the center and minor axis along the horizontal direction, which is identical with the direction of prestrain. The wrinkling pattern extended to the boundary of SMP sample in vertical direction (Fig. 5.7b and c). Spoke wrinkling pattern dominates the center area in the vertical direction of SMP sample (Fig. 5.7a). Spoke wrinkling pattern in 90° and 270° changed their direction to approach to perpendicular to prestrain direction due to the strain recovery. In the horizontal direction, spoke wrinkling pattern forms around the hole in a narrow area (about 400 μm in width). However, it is not as clear as that on the sample with heating time $t=2$ s. Out of the spoke pattern in horizontal direction is ring wrinkling pattern. With the distance from the center, ring pattern approaches 1D wrinkling pattern in vertical direction (Fig. 5.7d and e). The film outside the wrinkling area is still flat.

Formation of wrinkling pattern with heating time $t=12$ s are demonstrated in Fig. 5.9. The pattern in the heating process is similar to that on the sample with 2 s heating time. Ring pattern forms firstly and was pushed away and the radius becomes larger and larger. Before the current was turned off, there is no spoke pattern formed (Fig. 5.9d). After the heating stopped, the spoke wrinkling pattern began to form and extended. In horizontal direction, the spoke pattern extended only ∼400 μm. While it extended to the width boundary of the SMP sample in vertical direction (Fig. 5.8b and c).

In the 12 s heating case, the wrinkling forms throughout the sample in vertical direction. Prestrain in horizontal direction is recovered and induced wrinkling in this area. Under this condition, the wrinkling area was not confined all around by the SMP sample. SMP sample shrunk locally in the vertical direction. This is different with the sample with 2 s heating, the wrinkling
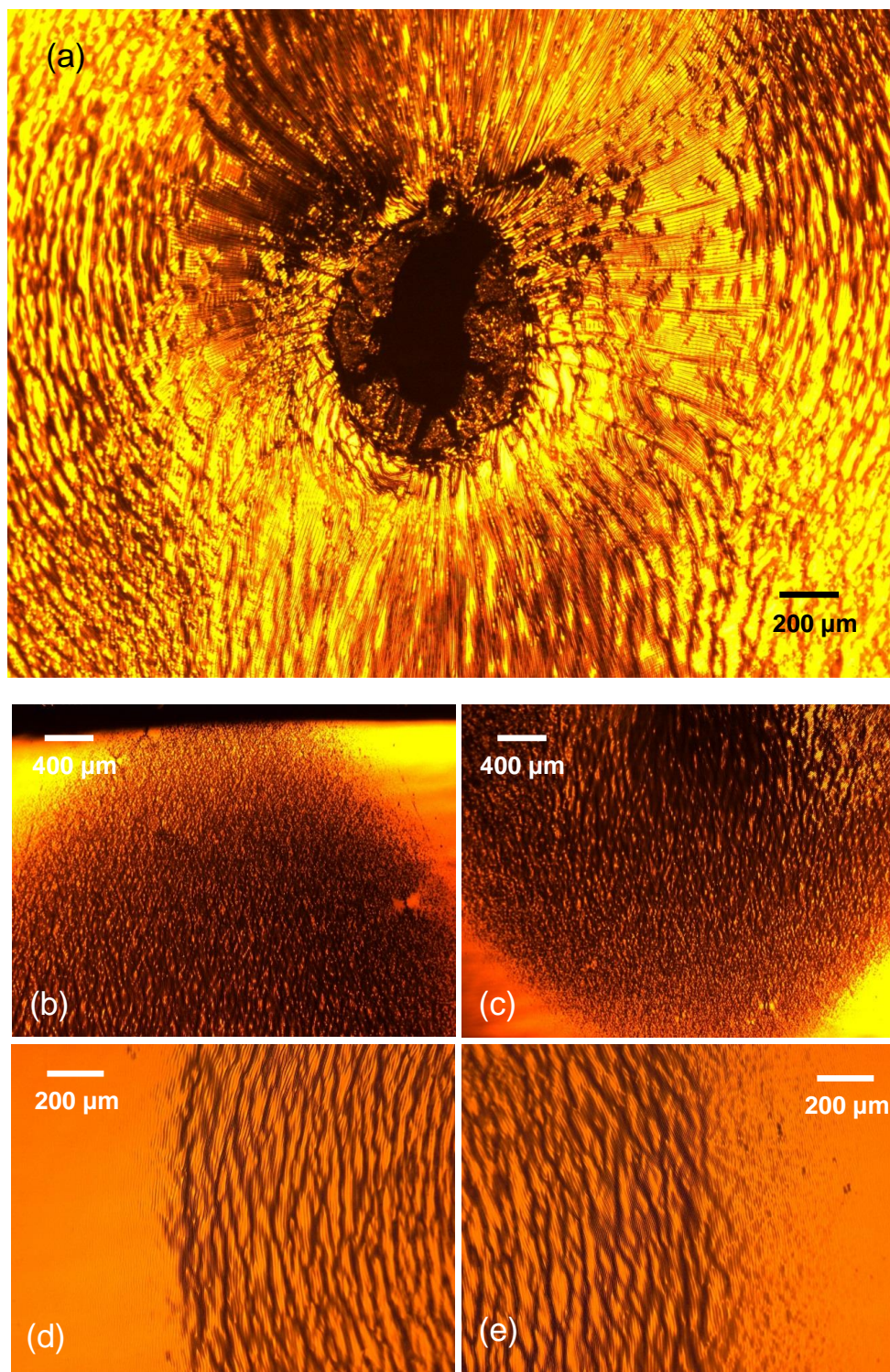
Figure 5.8: Wrinkling pattern and its boundary by point heating with 12 s heating. (a) Overall view of the wrinkling pattern, (b) top, (c)bottom, (d)left, and (e)right boundary of the wrinkling pattern.
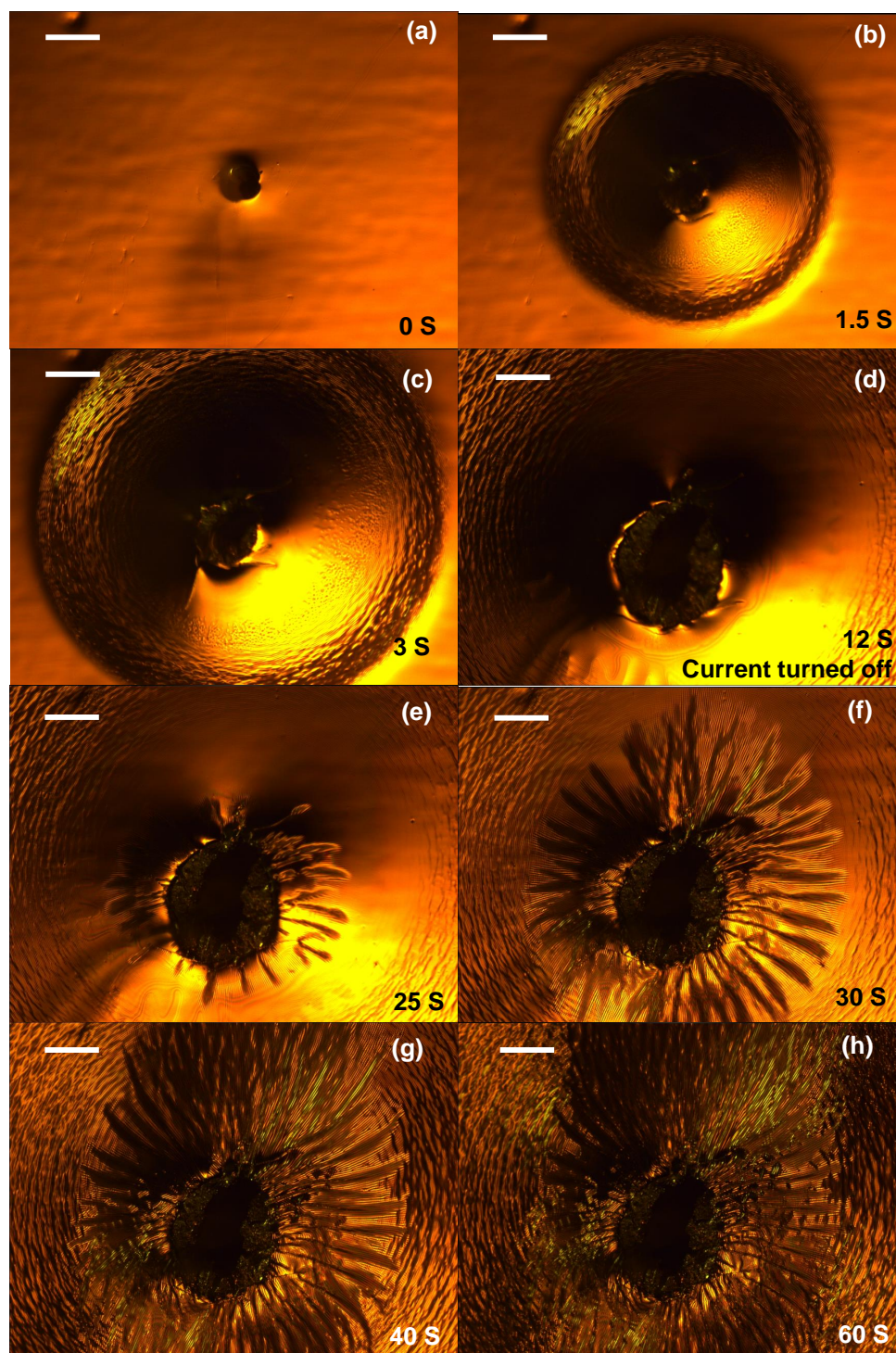
Figure 5.9: Formation of the wrinkling pattern (I=1 A, t=12 s, scale bar 400 μm).

area of which is confined by SMP sample all around. After uniaxial prestrain was applied on the sample, circumferential strain dominates the surface of the hole. It was recovered in the heating process and induced spoke wrinkling pattern around the hole. Far away from the center, effect of the hole vanishes gradually and leads to a horizontal strain state, which formed 1D wrinkling in direction perpendicular to that of the prestrain (Fig. 5.8b-e).

Profiles plotted in Fig. 5.10 represents the typical profile in 12 s heating case, which show good sinusoidal shape. The locations of these profiles are 1.5 mm away from the center. The distribution of wavelength and amplitude in horizontal and vertical direction are shown in Fig. 5.11a and b, respectively. Overall, distributions of wavelength and amplitude show good symmetry in both horizontal and vertical direction, respectively. And they decrease with the distance from the center. In Fig. 5.11a, rang from 1 to 2 mm away from the center represents the area of ring pattern in horizontal direction. Outside 2 mm the wrinkling disappears gradually. Wavelength and amplitude in Fig. 5.11b represents the spoke wrinkling pattern in vertical direction. The material property of SMP changes dramatically with the temperature. From room temperature to the temperature above its T_g, Young's modulus of SMP decreases three order of magnitude. In the heating process, Young's modulus decreases with the distance away from the heat source due to the heat gradient around the center. According to linear elastic buckling theory, with a constant film thickness, wavelength and amplitude increases with the Young's modulus ratio of film and substrate. Away from the center, increase of Young's modulus of SMP substrate induces the decrease of the wavelength and amplitude away from the center.

5.4   Conclusions

We construct a localized wrinkling pattern with two distinct morphologies, which are spoke and ring pattern on aluminum film-SMP substrate system. Involving shape memory effect, SMP sample with a small hole in the center was programmed with uniaxial strain. With I=1 A, the sample was heated by point heat source in the small hole. The wrinkling area can be tuned by heating time. With 2 seconds heating, the wrinkling area is circular and it reaches to the boundary
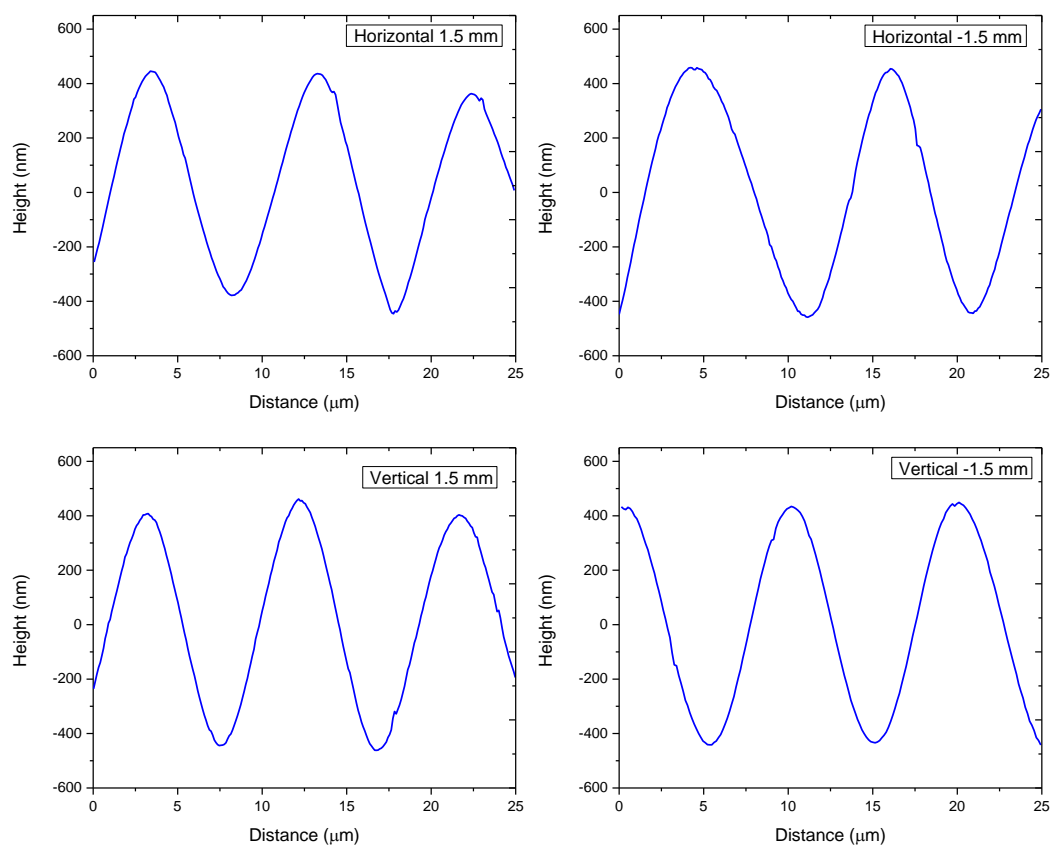
Figure 5.10: Profiles of wrinkling pattern in different locations (I=1 A, t=12 s).
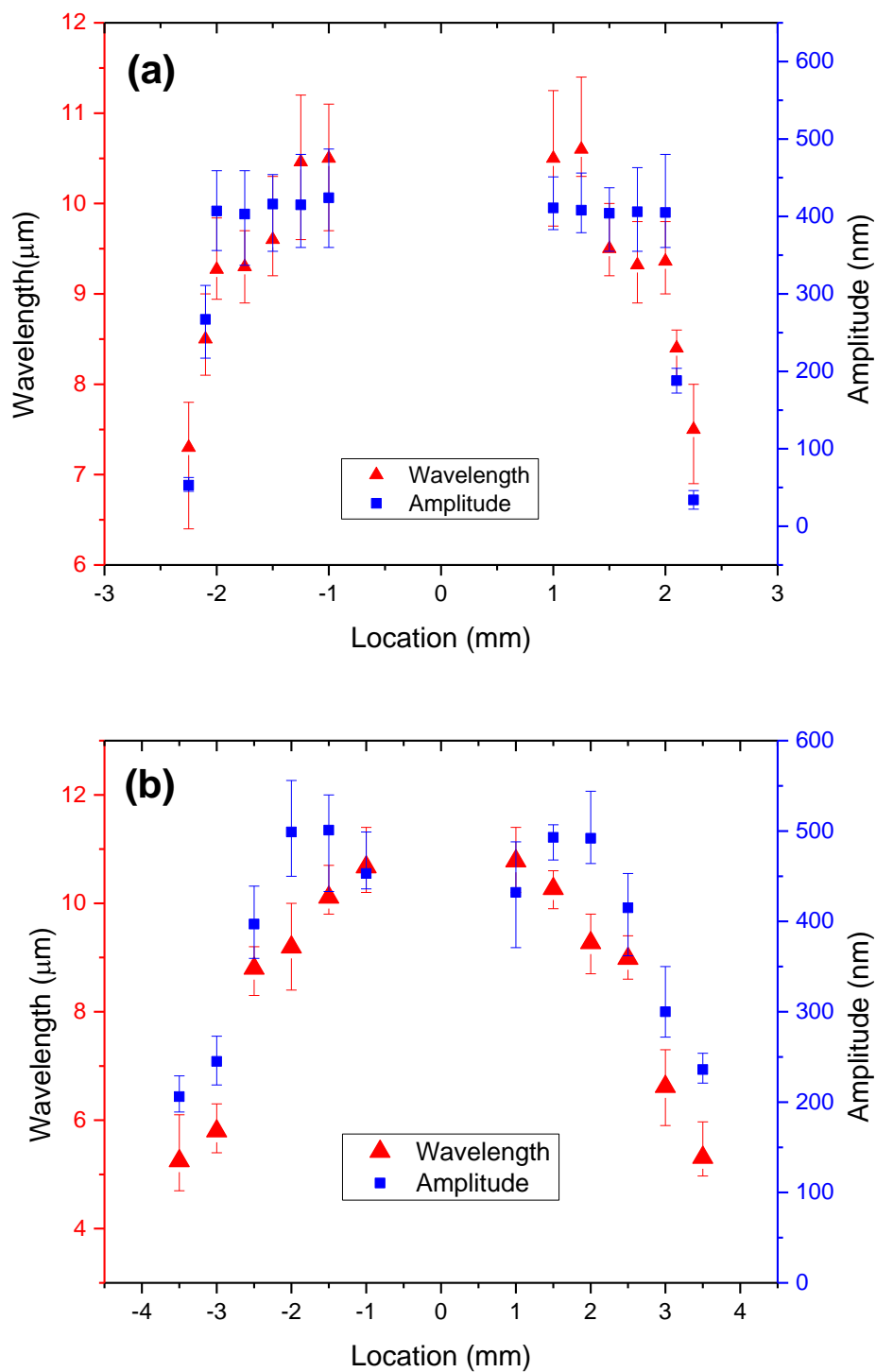
Figure 5.11: Distribution of wavelength and amplitude in (a) horizontal and (b) vertical direction (I=1 A, t=12 s).

of SMP sample after the sample was heated for 12 seconds. We observed the ring wrinkling pattern forms firstly and spoke wrinkling pattern around the hole begin to form after heating stops. The small hole in the center plays an important role in the formation of spoke and ring patterns. This study is expected to offer a simple method to fabricate micro-scale spoke and ring patterns, and provide guidelines in their potential applications.

Chapter 6

Fabrication of three-dimensional hierarchical structure through sequential wrinkling

6.1   Research statement

In previous chapters, methods to fabricate global and localized surface wrinkling were demonstrated. These structures are based on one layer thin film and substrate system. Using multilayer thin film-substrate system, hierarchical structure can be fabricated. Multiscale hierarchical structures hold great promise for important potential applications in reversible adhesion, controllable wetting, and selective filtration [106,107]. For example, in nature, gecko feet hair exhibits reversible adhesive property and lotus leaf with superhydrophobic surface shows the ability of self-cleaning. Inspired by these phenomena, numerous methods for creating hierarchical have been developed by researchers, such as lithography, plasma etching, and nanoimprint [106–108]. Recently, surface wrinkling is emerging as a powerful method to induce patterns over an entire surface. It is a simple and low cost approach for fabrication of surface patterns. Some researchers use combined methods, such as nanoimprint and mechanical strain induced surface wrinkling to fabricate the hierarchical structures. However, these approaches require multistep operations and making multiscale surface features over large area is not easy [108]. In 2015, Lee et al. [108] reported a multi-cycle plasma treatment method to generate hierarchical structure in large area. Multi-generation wrinkling pattern was obtained by this method. However, the thickness and mechanical properties of the skin layer are unknown, since plasma treatment bring depth-heterogeneous structure.

In this chapter, we demonstrate a facile fabrication method that combines surface wrinkling

induced by thermal expansion and mechanical strain. This is a three layers structure with aluminum film on top, stiff PDMS film in the center and prestretched soft PDMS substrate in the bottom. Deposition of aluminum film induce first order 2D wrinkling by thermal expansion and recovering the prestrain of the substrate leads to second and third order wrinkling. The hierarchical structure fabricated in this study can be tuned by changing the thickness of the film, mechanical strain, and material properties.

6.2   Methods and materials

PDMS substrate PDMS substrate was made from Sylgard 184 elastomer kit (Dow Corning), the same as that in previous chapters. Here, prepolymer-crosslinker ratio is 40: 1 in weight. Following degassing and curing process are the same as that discussed in previous chapters. Cured PDMS sheet was cut into slabs with dimension $30 \times 15 \times 5$ mm.

PDMS film PDMS film was made by spin coating of uncured degassed PDMS (prepolymer-crosslinker ratio is 5: 1) on glass slides. The thickness of the PDMS film depends on the speed and time of spin coating. The thickness will be measured before using. Glass slides with PDMS film was placed in oven at 80 ℃ for 2 hours for curing. Cured film was cut into sheet with dimension 20×5 mm.

To fabricate the hierarchical structure, three layers system was made, which includes PDMS substrate in the bottom, PDMS thin film in the center, and aluminum film on the top. Figure 6.1 illustrates the fabrication process. Soft PDMS substrate was prestretched with 20% or 30% strain by a homemade stretching system. In next step, stiff PDMS film was transferred on top of PDMS substrate. To build multiple layer structure, 20 nm aluminum film was deposited on PDMS film by DC sputter system. In this step, both PDMS film and substrate were heated by the thermal effect, which leads to volume expansion. Upon cooling of the system, shrinkage of PDMS film compress the aluminum film, which induced 2D surface wrinkling. The last step is to recover the prestrain in bottom PDMS layer. Middle layer PDMS film with aluminum was compressed by bottom layer PDMS and leads to 1D wrinkling.

PDMS substrate (40:1)
Prestretched

PDMS film (5:1) transfer

Aluminum film
deposition (20 nm)
(DC sputter, Ar)
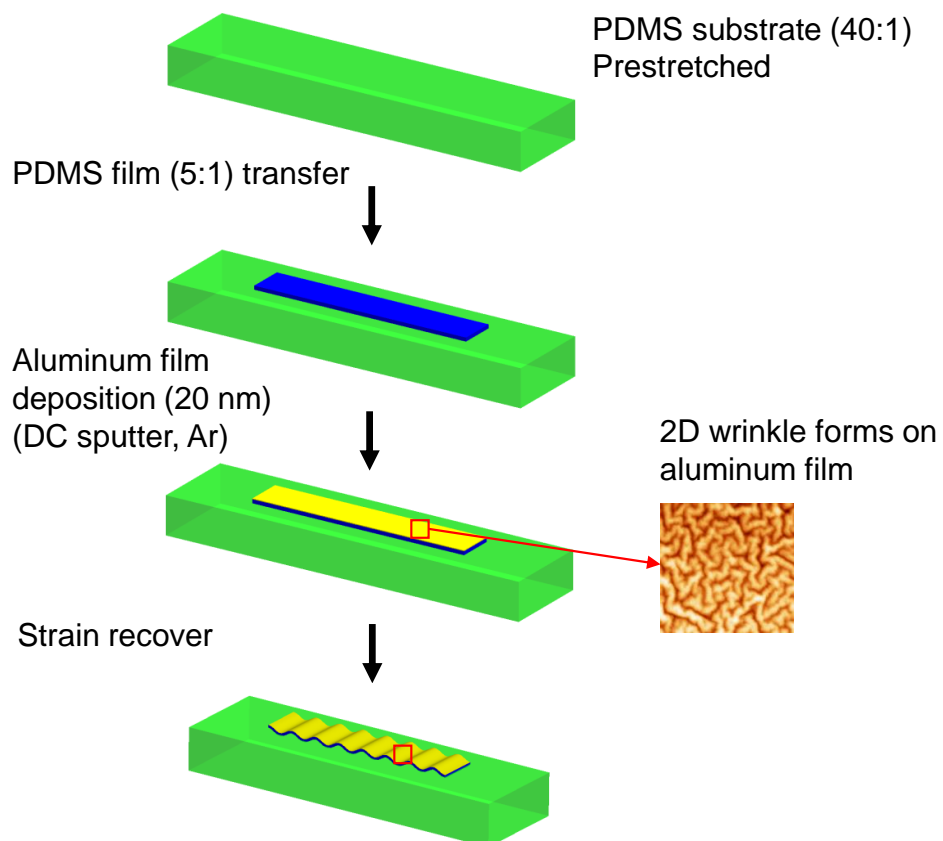
2D wrinkle forms on
aluminum film

Strain recover

Figure 6.1: Methods to fabricate three-dimensional hierarchical structure through sequential wrinkling.

The wrinkling morphology after strain recover is highly depends on the prestrain level. Low prestrain ($<30\%$) induces sinusoidal profile and higher one leads to folded structure.

Characterization Thickness of PDMS film and profile of large scale wrinkling were measured using BNC DEKATAK 3030 Stylus Profilemeter. Atomic Force Microscope (AFM) images were scanned using VEECO Dimension 3100 in tapping mode under ambient condition.

6.3   Results and discussions

Fig. 6.2 shows 2D wrinkling pattern on aluminum thin film after deposition. Figures 6.2a and b are 2D and 3D AFM images, respectively. The profiles in horizontal and vertical are depicted in Fig. 6.2c and d, respectively. From these images, we can see that the wrinkling in vertical and horizontal directions are uniform with wavelength $\sim$1.1 μm and amplitude $\sim$71 nm. Both wavelength and amplitude are dependent on the material properties and the thickness of the film. Therefore, both quantities can be tuned by changing material or film thickness.

In the film deposition step, thermal expansion induces 2D wrinkling. In next step, after the prestrain applied on the PDMS substrate was recovered, PDMS film with aluminum film on top wrinkles, which is shown in Fig. 6.3a. The bright lines in this figure are peaks of the wave pattern. Cracks on the peaks are due to the Poisson's effect. The profile of wrinkle is shown in Fig. 6.3b, which is uniform sinusoidal profile with amplitude 22 μm and wavelength 380 μm. Thickness of the PDMS film is 39 μm.

Figure 6.4a shows an enlarged microscope image of the wrinkled surface in Fig. 6.3. In this figure, center is a valley and areas beside it are peaks. Morphologies in different locations are scanned using AFM. Figures 6.4b-d are 3D AFM images of the peak, valley, and the area between peak and valley, respectively. It shows 2D wrinkling pattern in the peak, which is the first order 2D pattern formed by aluminum film. 2D patterns also appears in the area in between peak and valley. In the valley, we found 1D wrinkle, which is named as the second order wrinkle due to the size of the wavelength and amplitude. The wrinkle of PDMS thin film formed in strain recover step is named the third order wrinkle, which has the largest wavelength and amplitude. In addition, on
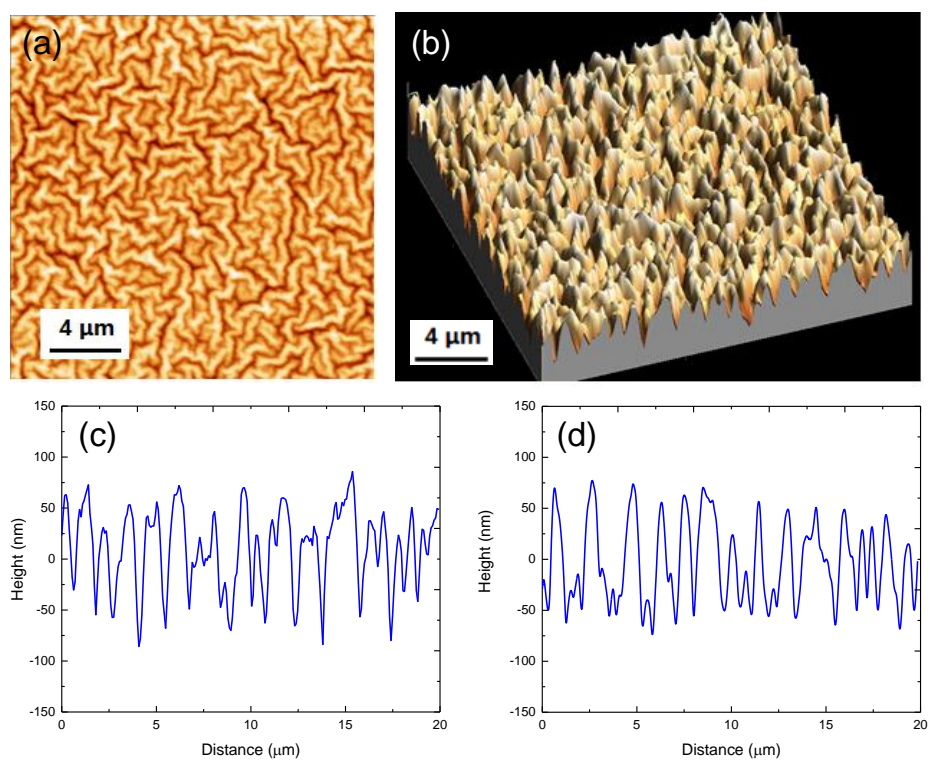
Figure 6.2: AFM images and profile of the wrinkled aluminum film after deposition (20% pretrain). (a) 2D and (b) 3D AFM image of wrinkled aluminum film surface after deposition, (c) Profiles of the wrinkled aluminum film surface in horizontal direction and (d) vertical direction.
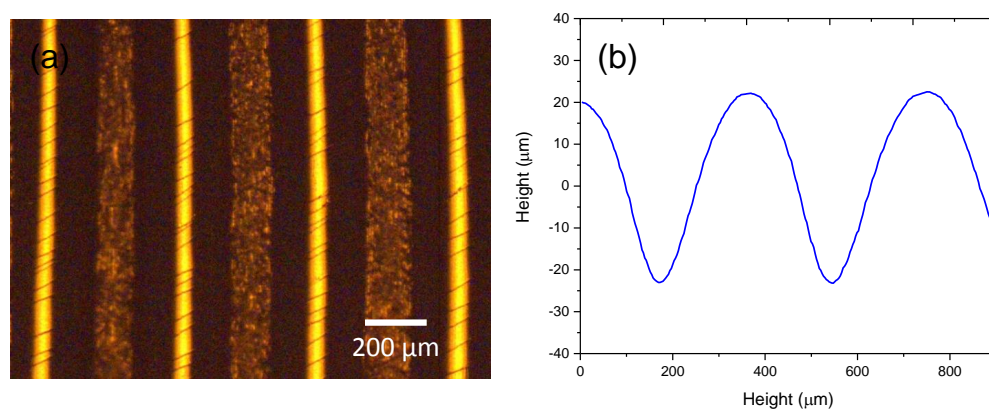
Figure 6.3: (a) Microscope image and (b) profile of the wrinkled PDMS film.

this 1D profile surface, the first order wrinkle is still there. The profiles in these positions are list in Fig. 6.5. Second row shows the profiles in horizontal direction and that in vertical direction is shown in the third row. The size of scanning is 15 μm, which is much smaller than the wavelength of the third order wrinkling pattern (380 μm). Wavelength and amplitude of 2D wrinkles in peak and in area in between are similar and no significant difference was found. In the valley, the second order wrinkle shows uniform pattern with wavelength $\sim$5 μm and amplitude $\sim$600 nm. In vertical direction, the profile shows similar pattern with that in other areas.

We have obtained three orders surface wrinkling with different wavelength and amplitude, which are the first order 2D aluminum film wrinkling, second order 1D wrinkling in the valley of the third order wrinkle, and third order 1D wrinkling of the PDMS film. It implies that a new layer of film is formed in the experiment and this layer is the requirement to form the second order wrinkle. Back to the process of deposition, argon plasma is used to deposit aluminum film in this step. In this process, the surface layer of PDMS was modified into a SiO_2 like material with nonuniform thickness by argon plasma [109]. This layer serves as rigid film in the formation of second order wrinkle.

The first order 2D aluminum film wrinkling is similar with that in previous research [21]. In the deposition process, substrate is heated up and induce thermal expansion of PDMS substrate. PDMS substrate shrinks upon cooling and brings compression on aluminum film in all directions, which forms the 2D wrinkling pattern on modified PDMS layer. The wavelength of the wave shape is about 1.1 μm. According to the relationship between wavelength and materials' properties (E_{Al}=69 GPa) [21], the effective modulus of the modified layer can be estimated to be 30 MPa, which is higher than that of PDMS (5:1) (3.6 MPa) and lower than that of SiO_2 (66 GPa). The thickness of the SiO_2 layer is not uniform. To estimate the thickness of this effective layer, effective modulus, wavelength of second order, and materials properties are substituted into Eq. 1.5, and yields the thickness to be 700 nm. For the third order wrinkle, with the amplitude and wavelength known, the maximum bending strain (maximum curvature$\times h_f/2$, $\varepsilon_{bending} = \frac{2\pi^2 hA}{\lambda^2}$) and membrane strain ($\varepsilon_{membrane} = \frac{\pi^2 A^2}{(1+\varepsilon_{pre})^2\lambda^2} - \frac{\varepsilon_{pre}}{1+\varepsilon_{pre}}$) in the wrinkled film are 0.12 and -0.14, respectively [74].
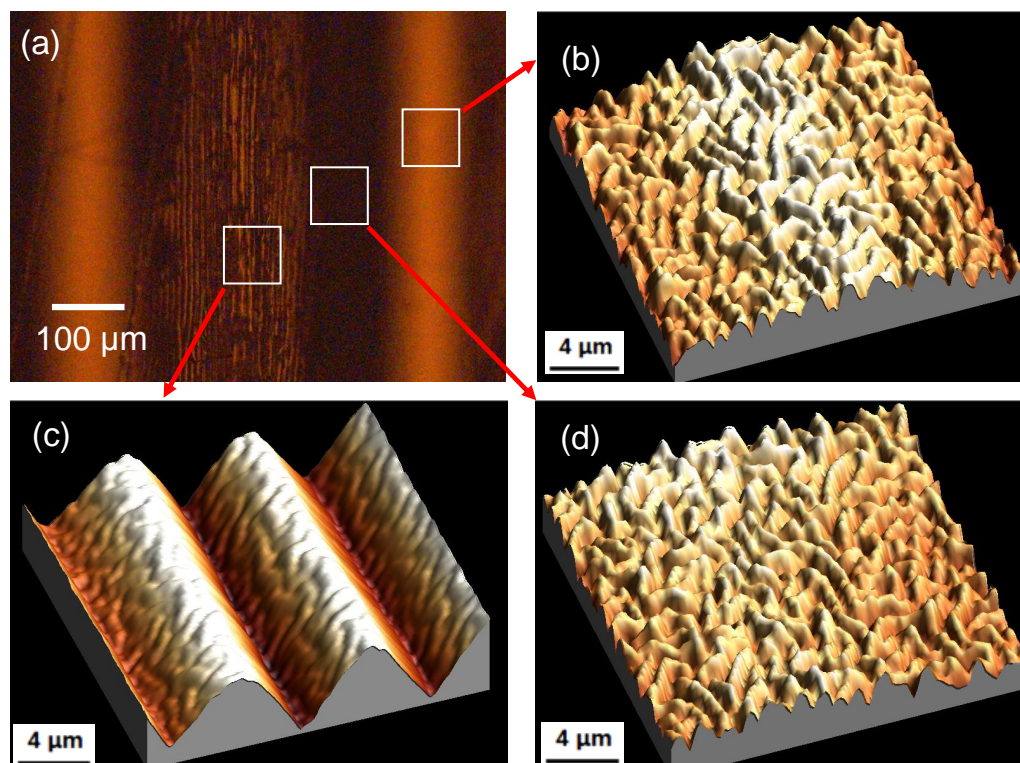
Figure 6.4: Patterns in different locations after strain recover. (a) Enlarged optical microscope image of Fig. 6.3a, (b) 3D AFM image of the pattern in the peak area of the third order wrinkle, (c) 3D AFM image of the pattern in the valley area, (d) 3D AFM image of the pattern in the area between peak and valley.
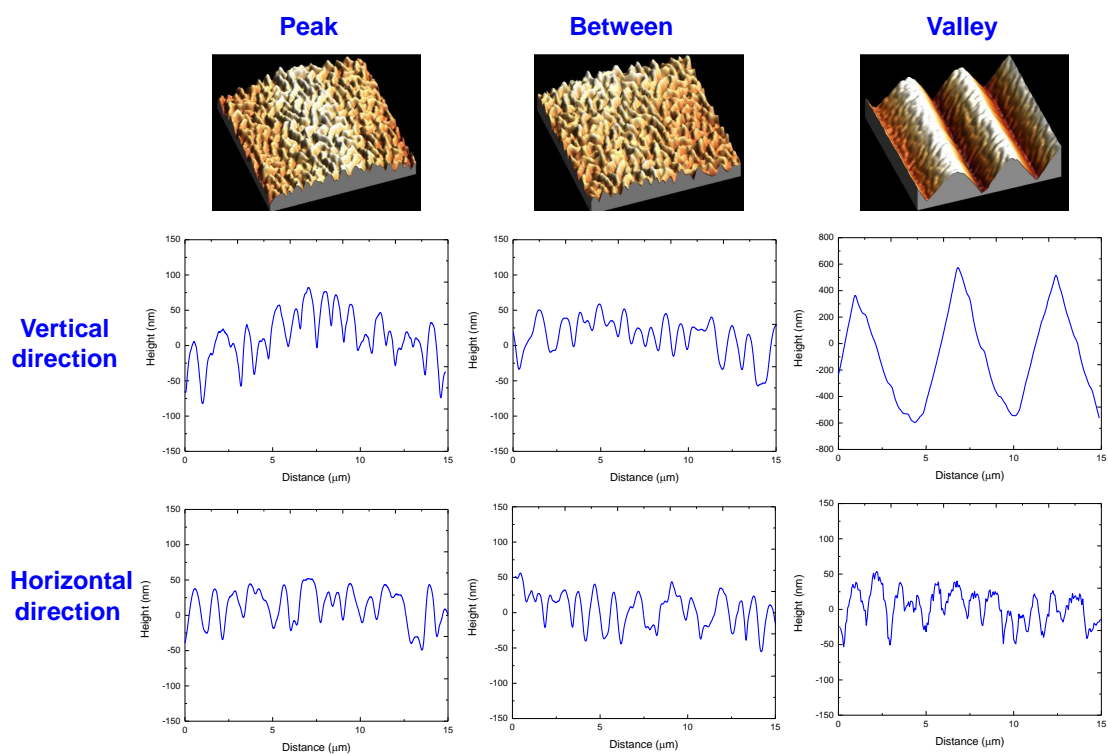
Figure 6.5: Profiles in different locations after strain recover.

thus, the strain in the peak of the third order wrinkle is -0.02 and that in the valley is -0.26. the compression strain in the valley is the reason to form the wrinkle of the second order.

The second and third order wrinkling forms simultaneously upon the recovery of the prestrain. The middle PDMS film serves as film and substrate. As thin film, it was compressed by PDMS substrate in the strain recovery step, and as substrate, its deformation affects the pattern on its surface. For formation of the second order wrinkle, deformation of the PDMS film offers strain mismatch in the valley.

As we discussed previously, a new SiO_2 layer forms in the deposition step and this layer serves as thin film in the second order wrinkle. To verify, 20 nm aluminum thin film is deposited on prestretched 5:1 PDMS (25% strain) substrate under the same parameters setting, as shown in Fig. 6.6a. After deposition, 2D wrinkling forms (Fig. 6.6b and c) and no significant difference was found comparing with the previous results. After prestrain was recovered, new order 1D wrinkling forms with first order 2D wrinkle on it, as shown in Fig. 6.6d. Fig. 6.6e shows the profile of such 1D wrinkle in horizontal and vertical direction. The wavelength in horizontal direction is about 5 μm and amplitude is about 600 nm, which are comparable with that of the wrinkling form in the valley in previous experiment.

Prestrain in the samples discussed above is 20%, which leads to wrinkle of the second and third order. In addition, we investigated the effect of higher level prestrain, such as 30%, on the morphology of the surface. The thickness of the PDMS here is 61 μm. Following the same procedure, 20 nm aluminum film was deposited on PDMS film-PDMS substrate system (Fig. 6.7a). Upon cooling, aluminum film wrinkles on PDMS film surface, as shown in Fig. 6.7b. Its profile is shown in Fig. 6.7c. From the figure, we can see that 2D wrinkling pattern formed on the surface. Comparing with previous samples (Fig. 6.2), no significant difference was found. This pattern can be considered as uniform, which implies that effect of prestrain on the first order wrinkling is negligible. After 30% prestrain was recovered, PDMS film folds instead of forming wavy shape. Fig. 6.7d is optical microscope image of the folded film surface. There are two narrow valleys that located in the left and right side of the image, which are marked as fold. Center in this figure is
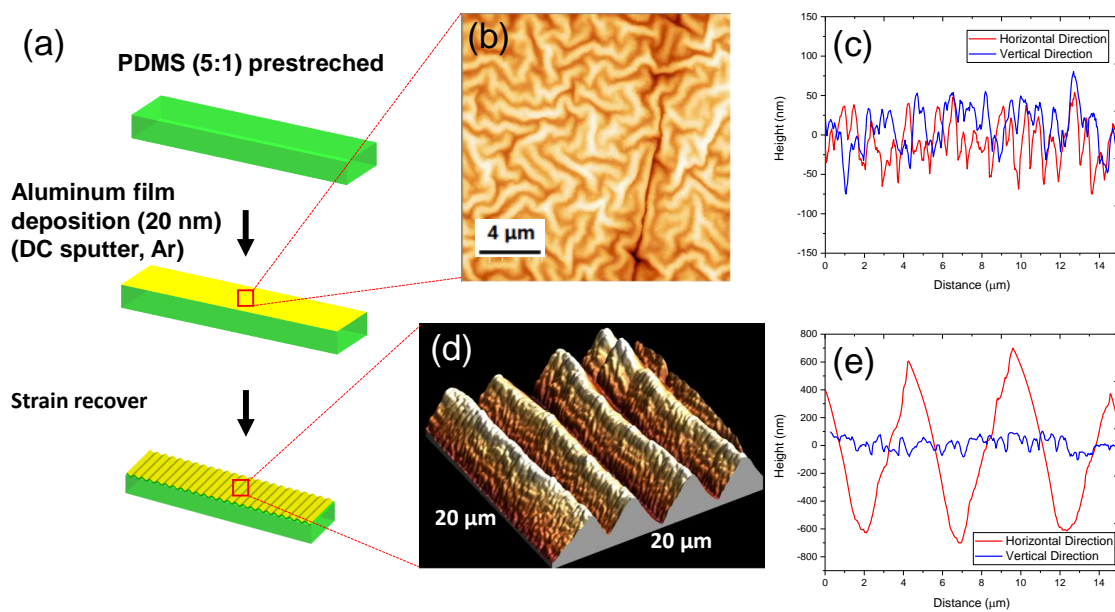
Figure 6.6: Validation of the new order wrinkle. (a) Method to validate the new order wrinkle, (b) 2D AFM image of wrinkling of aluminum thin film in deposition step, (c) Profiles of the wrinkling pattern in horizontal and vertical direction, (d) 3D AFM image of the pattern after strain recover, (e) Profile of the wrinkling pattern in (d) in horizontal and vertical direction.
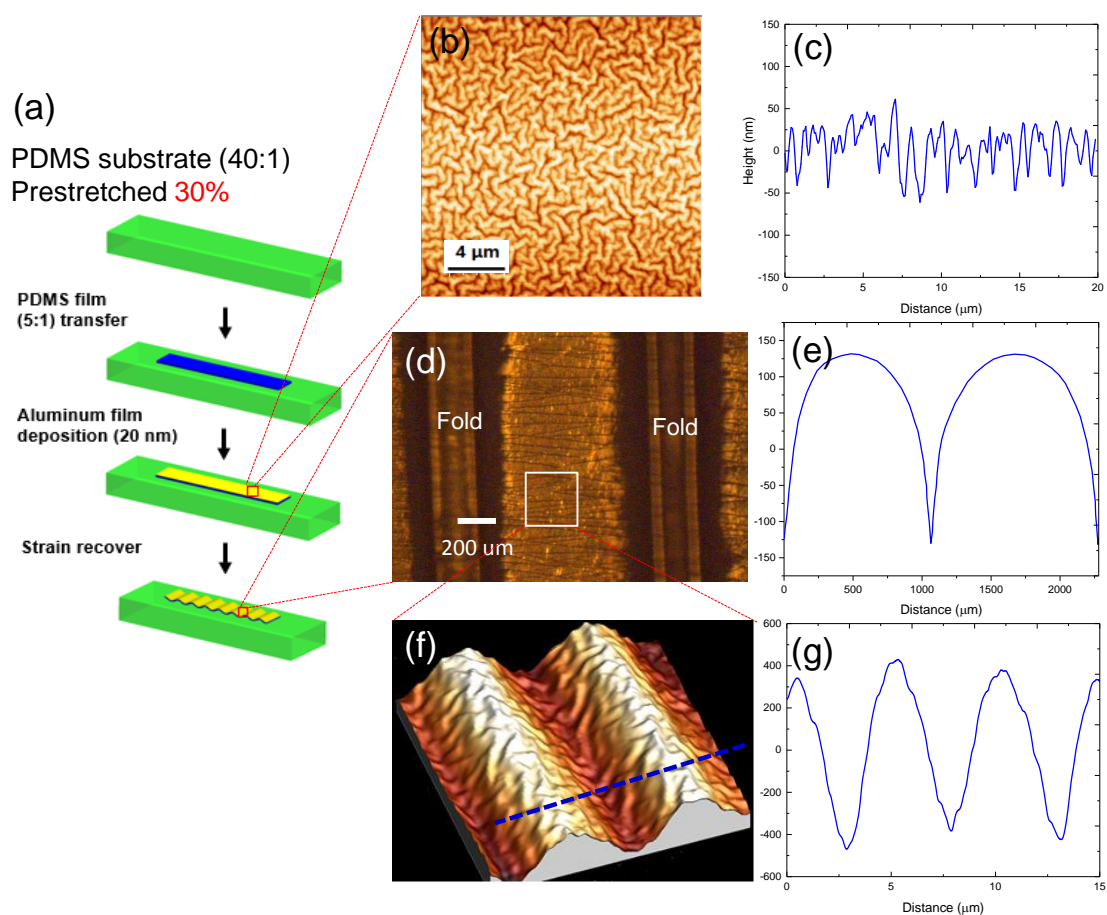
Figure 6.7: Fold structure induced by 30% prestrain. (a) Fabrication of hierarchical structure with 30% strain, (b) Wrinkling of aluminum thin film in deposition step, (c) Profiles of the wrinkling of aluminum thin film, (d) Optical microscope image of fold structure and (e) its profile, (f) 3D AFM image of the area between folds, (g) Profile of the 1D wrinkle in (f).

peak region. Horizontal lines in this region are cracks due to Poisson's effect. The profile of the surface is shown in Fig. 6.7e, which has period about 1250 μm and distance from valley to peak about 290 μm. For the thin film-substrate system, folding is a type of strain localization, which occurs when compressive strain applied increases beyond a critical value [103]. The reason behind this phenomenon is the instability associated with a geometric non-linearity [110]. Figure 6.7f is 3D AFM images showing the surface of the peak region. Similarly, 1D wrinkle forms with 2D wrinkle on top of it. The profile of 1D wrinkle is shown in Fig. 6.7g. The wavy shape of the 1D wrinkle has wavelength $\sim$4.7 μm and amplitude $\sim$420 nm, which are in the same level with that in the first sample.

6.4   Conclusions

In this chapter, a simple and low cost two steps method to fabricate three-dimensional hierarchical structure was presented. PDMS substrate with different prestrain were studied. The results show that low prestrain induces wrinkling pattern with sinusoidal profile, while higher prestrain leads to folding structure after strain recover. The hierarchical structure can be tuned by changing the prestrain level. In both cases, no significant difference was found in the first order 2D wrinkling induced by thermal expansion. Such structure has promising potential in tunable surface property, optical gratings, and cell alignment.

Chapter 7

Summary

In summary, we demonstrate the process to fabricate smart surface wrinkling based on thin film-substrate bilayer and multiple layer system. Wrinkling on the whole film surface and localized area are investigated and three-dimensional hierarchical structure is also studied.

Si ribbon-SMP substrates system is used for studying the evolution of wrinkling pattern with the recovery of the substrate under different temperature. We observed Si ribbon wrinkles with uniform sinusoidal wavy profile. With the recovery of SMP substrate, wavelengths and amplitudes of the wrinkled Si ribbon increase with time. The higher the recovery temperature, the shorter time it uses to achieve equilibrium state. Results reveal that the wrinkling of stiff thin films on thermal triggered SMP substrate is time and temperature dependent. This study is helpful for the design of such structure and its applications.

Based on SMP thin film-PDMS substrate system, we built a controllable, programmable, and reversible form of wrinkling. Totally three types of wrinkling cycles were investigated. By adjusting the prestrain recovery of the substrate and system temperature, formation and disappearance of the wrinkling pattern can be controlled in all of the cycles. Such system has potential application in tunable optical gratings, surface engineering, and stretchable electronics. This study is expected to offer a simple way to fabricate unidirectional wavy pattern and control its formation and disappearance.

Using aluminum thin film-SMP substrate system, we demonstrate a self-assembly fabrication method for programmable localized surface wrinkling by heat the sample locally, such as line

heating and point heating. By controlling heat input, the size of surface wrinkling area can be tuned. In line heating case, the localized wrinkle pattern shows good sinusoidal profile, with wavelength and amplitude decreasing gradually away the heating source. For the point heating case, two distinct wrinkling pattern formed in a circular area around the heat source with spoke in the inner area and ring patterns in the outer of the circular area. This study provide an easy and programmable approach to fabricate micro-scale localized wrinkling pattern and support guidelines in potential applications, such as stretchable electronics, surface property control, and other demanding applications.

We also developed a facile fabrication method that combines surface wrinkling induced by thermal expansion and mechanical strain. The system used in this approach is a three layers structure with aluminum film on top, stiff PDMS film in the center and pre-stretched soft PDMS substrate in the bottom. Deposition of aluminum film induce first order 2D wrinkling by thermal expansion. Recover of the prestrain of the substrate leads to second and third order wrinkling. Interestingly, 1D wrinkle forms in the valley area of the second order wrinkle. Changing the thickness of the film, mechanical strain, and materials can tune the size of the feature in the hierarchical structure.

These results in this dissertation offer simple methods to fabricate different types of programmable surface wrinkling pattern, with potential applications in stretchable electronics, optical gratings, surface engineering, advanced manufacturing, and other demanding applications.

Bibliography

[1] D. H. Kim, J. L. Xiao, J. Z. Song, Y. G. Huang, and J. A. Rogers, "Stretchable, curvilinear electronics based on inorganic materials," Advanced Materials, vol. 22, no. 19, pp. 2108–2124, 2010.

[2] A. J. Baca, J. H. Ahn, Y. G. Sun, M. A. Meitl, E. Menard, H. S. Kim, W. M. Choi, D. H. Kim, Y. Huang, and J. A. Rogers, "Semiconductor wires and ribbons for high-performance flexible electronics," Angewandte Chemie-International Edition, vol. 47, no. 30, pp. 5524–5542, 2008.

[3] J. A. Rogers, "Materials for semiconductor devices that can bend, fold, twist, and stretch," Mrs Bulletin, vol. 39, no. 6, pp. 549–556, 2014.

[4] S. Wagner and S. Bauer, "Materials for stretchable electronics," MRS Bulletin, vol. 37, no. 03, pp. 207–213, 2012.

[5] J. A. Rogers and Y. Huang, "A curvy, stretchy future for electronics," Proc Natl Acad Sci U S A, vol. 106, no. 27, pp. 10875–6, 2009.

[6] H. C. Ko, M. P. Stoykovich, J. Song, V. Malyarchuk, W. M. Choi, C. J. Yu, r. Geddes, J. B., J. Xiao, S. Wang, Y. Huang, and J. A. Rogers, "A hemispherical electronic eye camera based on compressible silicon optoelectronics," Nature, vol. 454, no. 7205, pp. 748–53, 2008.

[7] T. Someya, T. Sekitani, S. Iba, Y. Kato, H. Kawaguchi, and T. Sakurai, "A large-area, flexible pressure sensor matrix with organic field-effect transistors for artificial skin applications," Proceedings of the National Academy of Sciences of the United States of America, vol. 101, no. 27, pp. 9966–9970, 2004.

[8] S. P. Lacour, S. Wagner, Z. Huang, and Z. Suo, "Stretchable gold conductors on elastomeric substrates," Applied Physics Letters, vol. 82, no. 15, p. 2404, 2003.

[9] C. Yu, K. OBrien, Y.-H. Zhang, H. Yu, and H. Jiang, "Tunable optical gratings based on buckled nanoscale thin films on transparent elastomeric substrates," Applied Physics Letters, vol. 96, no. 4, p. 041111, 2010.

[10] C. Harrison, C. M. Stafford, W. Zhang, and A. Karim, "Sinusoidal phase grating created by a tunably buckled surface," Applied Physics Letters, vol. 85, no. 18, p. 4016, 2004.

[11] D. H. Kim, N. Lu, R. Ma, Y. S. Kim, R. H. Kim, S. Wang, J. Wu, S. M. Won, H. Tao, A. Islam, K. J. Yu, T. I. Kim, R. Chowdhury, M. Ying, L. Xu, M. Li, H. J. Chung, H. Keum, M. McCormick, P. Liu, Y. W. Zhang, F. G. Omenetto, Y. Huang, T. Coleman, and J. A. Rogers, "Epidermal electronics," Science, vol. 333, no. 6044, pp. 838–43, 2011.

[12] H. J. Chung, M. S. Sulkin, J. S. Kim, C. Goudeseune, H. Y. Chao, J. W. Song, S. Y. Yang, Y. Y. Hsu, R. Ghaffari, I. R. Efimov, and J. A. Rogers, "Stretchable, multiplexed ph sensors with demonstrations on rabbit and human hearts undergoing ischemia," Advanced Healthcare Materials, vol. 3, no. 1, pp. 59–68, 2014.

[13] S. Xu, Y. Zhang, J. Cho, J. Lee, X. Huang, L. Jia, J. A. Fan, Y. Su, J. Su, H. Zhang, H. Cheng, B. Lu, C. Yu, C. Chuang, T. I. Kim, T. Song, K. Shigeta, S. Kang, C. Dagdeviren, I. Petrov, P. V. Braun, Y. Huang, U. Paik, and J. A. Rogers, "Stretchable batteries with self-similar serpentine interconnects and integrated wireless recharging systems," Nat Commun, vol. 4, p. 1543, 2013.

[14] D.-H. Kim and J. A. Rogers, "Stretchable electronics: Materials strategies and devices," Advanced Materials, vol. 20, no. 24, pp. 4887–4892, 2008.

[15] D. H. Kim, J. Song, W. M. Choi, H. S. Kim, R. H. Kim, Z. Liu, Y. Y. Huang, K. C. Hwang, Y. W. Zhang, and J. A. Rogers, "Materials and noncoplanar mesh designs for integrated circuits with linear elastic responses to extreme mechanical deformations," Proc Natl Acad Sci U S A, vol. 105, no. 48, pp. 18675–80, 2008.

[16] D. H. Kim, J. H. Ahn, W. M. Choi, H. S. Kim, T. H. Kim, J. Song, Y. Y. Huang, Z. Liu, C. Lu, and J. A. Rogers, "Stretchable and foldable silicon integrated circuits," Science, vol. 320, no. 5875, pp. 507–11, 2008.

[17] D.-H. Kim, W. M. Choi, J.-H. Ahn, H.-S. Kim, J. Song, Y. Huang, Z. Liu, C. Lu, C. G. Koh, and J. A. Rogers, "Complementary metal oxide silicon integrated circuits incorporating monolithically integrated stretchable wavy interconnects," Applied Physics Letters, vol. 93, no. 4, p. 044102, 2008.

[18] Y. Sun, W. M. Choi, H. Jiang, Y. Y. Huang, and J. A. Rogers, "Controlled buckling of semiconductor nanoribbons for stretchable electronics," Nat Nanotechnol, vol. 1, no. 3, pp. 201–7, 2006.

[19] D.-Y. Khang, H. Jiang, Y. Huang, and R. J. A., "A stretchable form of single-crystal silicon for high-performance electronics on rubber substrates," Science, vol. 311, p. 5, 2006.

[20] E. Cerda and L. Mahadevan, "Geometry and physics of wrinkling," Physical Review Letters, vol. 90, no. 7, 2003.

[21] N. Bowden, S. Brittain, A. G. Evans2, J. W. Hutchinson, and G. M. Whitesides, "Spontaneous formation of ordered structures in thin films of metals supported on an elastomeric polymer," nature, vol. 393, p. 4, 1998.

[22] Y. Sun, V. Kumar, I. Adesida, and J. . Rogers, "Buckled and wavy ribbons of gaas for high-performance electronics on elastomeric substrates," Advanced Materials, vol. 18, no. 21, pp. 2857–2862, 2006.

[23] C. M. Stafford, C. Harrison, K. L. Beers, A. Karim, E. J. Amis, M. R. VanLandingham, H. C. Kim, W. Volksen, R. D. Miller, and E. E. Simonyi, "A buckling-based metrology for measuring the elastic moduli of polymeric thin films," Nat Mater, vol. 3, no. 8, pp. 545–50, 2004.

[24] J. Y. Chung, A. J. Nolte, and C. M. Stafford, "Diffusion-controlled, self-organized growth of symmetric wrinkling patterns," Advanced Materials, vol. 21, no. 13, pp. 1358–1362, 2009.

[25] K. Efimenko, M. Rackaitis, E. Manias, A. Vaziri, L. Mahadevan, and J. Genzer, "Nested self-similar wrinkling patterns in skins," Nat Mater, vol. 4, no. 4, pp. 293–7, 2005.

[26] D. Breid and A. J. Crosby, "Surface wrinkling behavior of finite circular plates," Soft Matter, vol. 5, no. 2, p. 425, 2009.

[27] S. Yang, K. Khare, and P.-C. Lin, "Harnessing surface wrinkle patterns in soft matter," Advanced Functional Materials, vol. 20, no. 16, pp. 2550–2564, 2010.

[28] Y. Yang, X. Han, W. Ding, S. Jiang, Y. Cao, and C. Lu, "Controlled free edge effects in surface wrinkling via combination of external straining and selective o2 plasma exposure," Langmuir, vol. 29, no. 23, pp. 7170–7, 2013.

[29] D. B. H. Chua, H. T. Ng, and S. F. Y. Li, "Spontaneous formation of complex and ordered structures on oxygen-plasma-treated elastomeric polydimethylsiloxane," Applied Physics Letters, vol. 76, no. 6, p. 721, 2000.

[30] N. Bowden, W. T. S. Huck, K. E. Paul, and G. M. Whitesides, "The controlled formation of ordered, sinusoidal structures by plasma oxidation of an elastomeric polymer," Applied Physics Letters, vol. 75, no. 17, p. 2557, 1999.

[31] W. T. S. Huck, N. Bowden, P. Onck, T. Pardoen, J. W. Hutchinson, and G. M. Whitesides, "Ordering of spontaneously formed buckles on planar surfaces," Langmuir, vol. 16, p. 5, 2000.

[32] P.-C. Lin and S. Yang, "Spontaneous formation of one-dimensional ripples in transit to highly ordered two-dimensional herringbone structures through sequential and unequal biaxial mechanical stretching," Applied Physics Letters, vol. 90, no. 24, p. 241903, 2007.

[33] P.-C. Lin, S. Vajpayee, A. Jagota, C.-Y. Huid, and S. Yang, "Mechanically tunable dry adhesive from wrinkled elastomers," Soft Matter, vol. 2007, no. 4, pp. 1830–1835, 2008.

[34] M. W. Moon, S. H. Lee, J. Y. Sun, K. H. Oh, A. Vaziri, and J. W. Hutchinson, "Wrinkled hard skins on polymers created by focused ion beam," Proc Natl Acad Sci U S A, vol. 104, no. 4, pp. 1130–3, 2007.

[35] J. Xiao, A. Carlson, Z. J. Liu, Y. Huang, H. Jiang, and J. A. Rogers, "Stretchable and compressible thin films of stiff materials on compliant wavy substrates," Applied Physics Letters, vol. 93, no. 1, p. 013109, 2008.

[36] J. Song, Y. Huang, J. Xiao, S. Wang, K. C. Hwang, H. C. Ko, D. H. Kim, M. P. Stoykovich, and J. A. Rogers, "Mechanics of noncoplanar mesh design for stretchable electronic circuits," Journal of Applied Physics, vol. 105, no. 12, p. 123516, 2009.

[37] S. D. Wang, J. L. Xiao, J. Z. Song, H. C. Ko, K. C. Hwang, Y. G. Huang, and J. A. Rogers, "Mechanics of curvilinear electronics," Soft Matter, vol. 6, no. 22, pp. 5757–5763, 2010.

[38] I. Jung, J. Xiao, V. Malyarchuk, C. Lu, M. Li, Z. Liu, J. Yoon, Y. Huang, and J. A. Rogers, "Dynamically tunable hemispherical electronic eye camera system with adjustable zoom capability," Proc Natl Acad Sci U S A, vol. 108, no. 5, pp. 1788–93, 2011.

[39] Y. M. Song, Y. Xie, V. Malyarchuk, J. Xiao, I. Jung, K. J. Choi, Z. Liu, H. Park, C. Lu, R. H. Kim, R. Li, K. B. Crozier, Y. Huang, and J. A. Rogers, "Digital cameras with designs inspired by the arthropod eye," Nature, vol. 497, no. 7447, pp. 95–9, 2013.

[40] S. Xu, Z. Yan, K. I. Jang, W. Huang, H. R. Fu, J. Kim, Z. Wei, M. Flavin, J. McCracken, R. Wang, A. Badea, Y. Liu, D. Q. Xiao, G. Y. Zhou, J. Lee, H. U. Chung, H. Y. Cheng, W. Ren, A. Banks, X. L. Li, U. Paik, R. G. Nuzzo, Y. G. Huang, Y. H. Zhang, and J. A. Rogers, "Assembly of micro/nanomaterials into complex, three-dimensional architectures by compressive buckling," Science, vol. 347, no. 6218, pp. 154–159, 2015.

[41] H. C. Ko, G. Shin, S. Wang, M. P. Stoykovich, J. W. Lee, D. H. Kim, J. S. Ha, Y. Huang, K. C. Hwang, and J. A. Rogers, "Curvilinear electronics formed using silicon membrane circuits and elastomeric transfer elements," Small, vol. 5, no. 23, pp. 2703–9, 2009.

[42] D. Gray, J. Tien, and C. Chen, "High-conductivity elastomeric electronics," Advanced Materials, vol. 16, no. 5, p. 393397, 2004.

[43] X. L. Hu, P. Krull, B. de Graff, K. Dowling, J. A. Rogers, and W. J. Arora, "Stretchable inorganic-semiconductor electronic systems," Advanced Materials, vol. 23, no. 26, pp. 2933–2936, 2011.

[44] X. Huang, Y. H. Liu, K. L. Chen, W. J. Shin, C. J. Lu, G. W. Kong, D. Patnaik, S. H. Lee, J. F. Cortes, and J. A. Rogers, "Stretchable, wireless sensors and functional substrates for epidermal characterization of sweat," Small, vol. 10, no. 15, pp. 3083–3090, 2014.

[45] R. H. Kim, D. H. Kim, J. L. Xiao, B. H. Kim, S. I. Park, B. Panilaitis, R. Ghaffari, J. M. Yao, M. Li, Z. J. Liu, V. Malyarchuk, D. G. Kim, A. P. Le, R. G. Nuzzo, D. L. Kaplan, F. G. Omenetto, Y. G. Huang, Z. Kang, and J. A. Rogers, "Waterproof alingap optoelectronics on stretchable substrates with applications in biomedicine and robotics," Nature Materials, vol. 9, no. 11, pp. 929–937, 2010.

[46] Y. H. Zhang, Y. G. Huang, and J. A. Rogers, "Mechanics of stretchable batteries and super-capacitors," Current Opinion in Solid State & Materials Science, vol. 19, no. 3, pp. 190–199, 2015.

[47] K. Efimenko, W. E. Wallace, and J. Genzer, "Surface modification of sylgard-184 poly(dimethyl siloxane) networks by ultraviolet and ultraviolet/ozone treatment," Journal of Colloid and Interface Science, vol. 254, no. 2, pp. 306–315, 2002.

[48] H. Jiang, D.-Y. Khang, H. Fei, H. Kim, Y. Huang, J. Xiao, and J. A. Rogers, "Finite width effect of thin-films buckling on compliant substrate: Experimental and theoretical studies," Journal of the Mechanics and Physics of Solids, vol. 56, no. 8, pp. 2585–2598, 2008.

[49] J. Song, H. Jiang, W. M. Choi, D. Y. Khang, Y. Huang, and J. A. Rogers, "An analytical study of two-dimensional buckling of thin films on compliant substrates," Journal of Applied Physics, vol. 103, no. 1, p. 014303, 2008.

[50] T. Ohzono and M. Shimomura, "Ordering of microwrinkle patterns by compressive strain," Physical Review B, vol. 69, no. 13, 2004.

[51] S. Wang, J. Song, D.-H. Kim, Y. Huang, and J. A. Rogers, "Local versus global buckling of thin films on elastomeric substrates," Applied Physics Letters, vol. 93, no. 2, p. 023126, 2008.

[52] C. Yu, Z. Duan, P. Yuan, Y. Li, Y. Su, X. Zhang, Y. Pan, L. L. Dai, R. G. Nuzzo, Y. Huang, H. Jiang, and J. A. Rogers, "Electronically programmable, reversible shape change in two- and three-dimensional hydrogel structures," Adv Mater, vol. 25, no. 11, pp. 1541–6, 2013.

[53] W. M. Choi, J. Song, D.-Y. Khang, H. Jiang, Y. Huang, and J. A. Rogers, "Biaxially stretchable wavy silicon nanomembranes," Nano Lett, vol. 7, pp. 1655–1663, 2007.

[54] C. F. Guo, V. Nayyar, Z. Zhang, Y. Chen, J. Miao, R. Huang, and Q. Liu, "Path-guided wrinkling of nanoscale metal films," Adv Mater, vol. 24, no. 22, pp. 3010–4, 3076, 2012.

[55] T. Ohzono, S. I. Matsushita, and M. Shimomura, "Coupling of wrinkle patterns to microsphere-array lithographic patterns," Soft Matter, vol. 1, no. 3, p. 227, 2005.

[56] H. S. Kim and A. J. Crosby, "Solvent-responsive surface via wrinkling instability," Adv Mater, vol. 23, no. 36, pp. 4188–92, 2011.

[57] J. A. Fan, W. H. Yeo, Y. Su, Y. Hattori, W. Lee, S. Y. Jung, Y. Zhang, Z. Liu, H. Cheng, L. Falgout, M. Bajema, T. Coleman, D. Gregoire, R. J. Larsen, Y. Huang, and J. A. Rogers, "Fractal design concepts for stretchable electronics," Nat Commun, vol. 5, p. 3266, 2014.

[58] T. Ma, H. Liang, G. Chen, B. Poon, H. Jiang, and H. Yu, "Micro-strain sensing using wrinkled stiff thin films on soft substrates as tunable optical grating," Opt Express, vol. 21, no. 10, pp. 11994–2001, 2013.

[59] J. Y. Chung, A. J. Nolte, and C. M. Stafford, "Surface wrinkling: a versatile platform for measuring thin-film properties," Adv Mater, vol. 23, no. 3, pp. 349–68, 2011.

[60] T. Xie and X. Xiao, "Self-peeling reversible dry adhesive system," Chem. Mater., vol. 20, no. 9, p. 3, 2008.

[61] Y. Rahmawan, C. M. Chen, and S. Yang, "Recent advances in wrinkle-based dry adhesion," Soft Matter, vol. 10, no. 28, pp. 5028–39, 2014.

[62] E. . Chan, E. . Smith, R. . Hayward, and A. . Crosby, "Surface wrinkles for smart adhesion," Advanced Materials, vol. 20, no. 4, pp. 711–716, 2008.

[63] L. Xu, S. R. Gutbrod, Y. Ma, A. Petrossians, Y. Liu, R. C. Webb, J. A. Fan, Z. Yang, R. Xu, r. Whalen, J. J., J. D. Weiland, Y. Huang, I. R. Efimov, and J. A. Rogers, "Materials and fractal designs for 3d multifunctional integumentary membranes with capabilities in cardiac electrotherapy," Adv Mater, vol. 27, no. 10, pp. 1731–7, 2015.

[64] D. H. Kim, N. S. Lu, R. Ghaffari, Y. S. Kim, S. P. Lee, L. Z. Xu, J. A. Wu, R. H. Kim, J. Z. Song, Z. J. Liu, J. Viventi, B. de Graff, B. Elolampi, M. Mansour, M. J. Slepian, S. Hwang, J. D. Moss, S. M. Won, Y. G. Huang, B. Litt, and J. A. Rogers, "Materials for multifunctional balloon catheters with capabilities in cardiac electrophysiological mapping and ablation therapy," Nature Materials, vol. 10, no. 4, pp. 316–323, 2011.

[65] J. Kim, A. Banks, H. Cheng, Z. Xie, S. Xu, K. I. Jang, J. W. Lee, Z. Liu, P. Gutruf, X. Huang, P. Wei, F. Liu, K. Li, M. Dalal, R. Ghaffari, X. Feng, Y. Huang, S. Gupta, U. Paik, and J. A. Rogers, "Epidermal electronics with advanced capabilities in near-field communication," Small, vol. 11, no. 8, pp. 906–12, 2015.

[66] Z. Li and J. Xiao, "Mechanics and optics of stretchable elastomeric microlens array for artificial compound eye camera," Journal of Applied Physics, vol. 117, no. 1, p. 014904, 2015.

[67] D. H. Kim, N. S. Lu, Y. G. Huang, and J. A. Rogers, "Materials for stretchable electronics in bioinspired and biointegrated devices," Mrs Bulletin, vol. 37, no. 3, pp. 226–235, 2012.

[68] K. I. Jang, S. Y. Han, S. Xu, K. E. Mathewson, Y. Zhang, J. W. Jeong, G. T. Kim, R. C. Webb, J. W. Lee, T. J. Dawidczyk, R. H. Kim, Y. M. Song, W. H. Yeo, S. Kim, H. Cheng, S. I. Rhee, J. Chung, B. Kim, H. U. Chung, D. Lee, Y. Yang, M. Cho, J. G. Gaspar, R. Carbonari, M. Fabiani, G. Gratton, Y. Huang, and J. A. Rogers, "Rugged and breathable forms of stretchable electronics with adherent composite substrates for transcutaneous monitoring," Nat Commun, vol. 5, p. 4779, 2014.

[69] X. Huang, Y. H. Liu, H. Y. Cheng, W. J. Shin, J. A. Fan, Z. J. Liu, C. J. Lu, G. W. Kong, K. Chen, D. Patnaik, S. H. Lee, S. Hage-Ali, Y. G. Huang, and J. A. Rogers, "Materials and designs for wireless epidermal sensors of hydration and strain," Advanced Functional Materials, vol. 24, no. 25, pp. 3846–3854, 2014.

[70] D. H. Kim, J. Viventi, J. J. Amsden, J. L. Xiao, L. Vigeland, Y. S. Kim, J. A. Blanco, B. Panilaitis, E. S. Frechette, D. Contreras, D. L. Kaplan, F. G. Omenetto, Y. G. Huang, K. C. Hwang, M. R. Zakin, B. Litt, and J. A. Rogers, "Dissolvable films of silk fibroin for ultrathin conformal bio-integrated electronics," Nature Materials, vol. 9, no. 6, pp. 511–517, 2010.

[71] J. Genzer and J. Groenewold, "Soft matter with hard skin: From skin wrinkles to templating and material characterization," Soft Matter, vol. 2, no. 4, p. 310, 2006.

[72] Z. Y. Huang, W. Hong, and Z. Suo, "Nonlinear analyses of wrinkles in a film bonded to a compliant substrate," Journal of the Mechanics and Physics of Solids, vol. 53, no. 9, pp. 2101–2118, 2005.

[73] E. A. Wilder, S. Guo, S. Lin-Gibson, M. J. Fasolka, and C. M. Stafford, "Measuring the modulus of soft polymer networks via a buckling-based metrology," Macromolecules, vol. 39, pp. 4138–4143, 2006.

[74] J. Song, H. Jiang, Y. Huang, and J. A. Rogers, "Mechanics of stretchable inorganic electronic materials," Journal of Vacuum Science & Technology A: Vacuum, Surfaces, and Films, vol. 27, no. 5, p. 1107, 2009.

[75] J. Xiao, S. Y. Ryu, Y. Huang, K. C. Hwang, U. Paik, and J. A. Rogers, "Mechanics of nanowire/nanotube in-surface buckling on elastomeric substrates," Nanotechnology, vol. 21, no. 8, p. 85708, 2010.

[76] J. Xiao, H. Jiang, D. . Khang, J. Wu, Y. Huang, and J. A. Rogers, "Mechanics of buckled carbon nanotubes on elastomeric substrates," Journal of Applied Physics, vol. 104, no. 3, p. 033543, 2008.

[77] S. Y. Ryu, J. Xiao, W. I. Park, K. S. Son, Y. Y. Huang, U. Paik, and J. A. Rogers, "Lateral buckling mechanics in silicon nanowires on elastomeric substrates," Nano Lett, vol. 9, no. 9, pp. 3214–9, 2009.

[78] Y. Wang, J. Song, and J. Xiao, "Surface effects on in-plane buckling of nanowires on elastomeric substrates," Journal of Physics D: Applied Physics, vol. 46, no. 12, p. 125309, 2013.

[79] R. Huang, "Kinetic wrinkling of an elastic film on a viscoelastic substrate," Journal of the Mechanics and Physics of Solids, vol. 53, no. 1, pp. 63–89, 2005.

[80] R. Huang and Z. Suo, "Wrinkling of a compressed elastic film on a viscous layer," Journal of Applied Physics, vol. 91, no. 3, p. 1135, 2002.

[81] R. Huang and Z. Suo, "Instability of a compressed elastic film on a viscous layer," International Journal of Solids and Structures, 2002.

[82] S. Im and R. Huang, "Wrinkle patterns of anisotropic crystal films on viscoelastic substrates," Journal of the Mechanics and Physics of Solids, vol. 56, no. 12, pp. 3315–3330, 2008.

[83] H. Jiang, D. Y. Khang, J. Song, Y. Sun, Y. Huang, and J. A. Rogers, "Finite deformation mechanics in buckled thin films on compliant supports," Proc Natl Acad Sci U S A, vol. 104, no. 40, pp. 15607–12, 2007.

[84] J. Song, H. Jiang, Z. J. Liu, D. Y. Khang, Y. Huang, J. A. Rogers, C. Lu, and C. G. Koh, "Buckling of a stiff thin film on a compliant substrate in large deformation," International Journal of Solids and Structures, vol. 45, no. 10, pp. 3107–3121, 2008.

[85] Z. Huang, W. Hong, and Z. Suo, "Evolution of wrinkles in hard films on soft substrates," Physical Review E, vol. 70, no. 3, 2004.

[86] X. Chen and J. W. Hutchinson, "Herringbone buckling patterns of compressed thin films on compliant substrates," Journal of Applied Mechanics, vol. 71, no. 5, p. 597, 2004.

[87] X. Chen and J. W. Hutchinson, "A family of herringbone patterns in thin films," Scripta Materialia, vol. 50, no. 6, pp. 797–801, 2004.

[88] T. Xie, X. Xiao, J. Li, and R. Wang, "Encoding localized strain history through wrinkle based structural colors," Adv Mater, vol. 22, no. 39, pp. 4390–4, 2010.

[89] J. Li, Y. An, R. Huang, H. Jiang, and T. Xie, "Unique aspects of a shape memory polymer as the substrate for surface wrinkling," ACS Appl Mater Interfaces, vol. 4, no. 2, pp. 598–603, 2012.

[90] Y. Zhao, W. M. Huang, and Y. Q. Fu, "Formation of micro/nano-scale wrinkling patterns atop shape memory polymers," Journal of Micromechanics and Microengineering, vol. 21, no. 6, p. 067007, 2011.

[91] C.-C. Fu, A. Grimes, M. Long, C. G. L. Ferri, B. D. Rich, S. Ghosh, S. Ghosh, L. P. Lee, A. Gopinathan, and M. Khine, "Tunable nanowrinkles on shape memory polymer sheets," Advanced Materials, vol. 21, no. 44, pp. 4472–4476, 2009.

[92] Z. Chen, Y. Young Kim, and S. Krishnaswamy, "Anisotropic wrinkle formation on shape memory polymer substrates," Journal of Applied Physics, vol. 112, no. 12, p. 124319, 2012.

[93] H. W.M., D. Z., W. C.C., W. J., Z. Y., and P. H., "Shape memory materials," Materials Today, vol. 13, pp. 54–61, 2010.

[94] T. Chung, A. Romo-Uribe, and P. T. Mather, "Two-way reversible shape memory in a semicrystalline network," Macromolecules, vol. 41, no. 1, p. 9, 2008.

[95] P. T. Mather, X. Luo, and I. A. Rousseau, "Shape memory polymer research," Annual Review of Materials Research, vol. 39, no. 1, pp. 445–471, 2009.

[96] L. A., J. HY., J. O., and L. R., "Light-induced shapememory polymers," Nature, vol. 434, pp. 879–882, 2005.

[97] A. M. Schmidt, "Electromagnetic activation of shape memory polymer networks containing magnetic nanoparticles," Macromolecular Rapid Communications, vol. 27, no. 14, pp. 1168–1172, 2006.

[98] W. M. Huang, B. Yang, L. An, C. Li, and Y. S. Chan, "Water-driven programmable polyurethane shape memory polymer: Demonstration and mechanism," Applied Physics Letters, vol. 86, no. 11, p. 114105, 2005.

[99] B. Yang, W. M. Huang, C. Li, and L. Li, "Effects of moisture on the thermomechanical properties of a polyurethane shape memory polymer," Polymer, vol. 47, no. 4, pp. 1348–1356, 2006.

[100] K. K. Westbrook, P. H. Kao, F. Castro, Y. Ding, and H. Jerry Qi, "A 3d finite deformation constitutive model for amorphous shape memory polymers: A multi-branch modeling approach for nonequilibrium relaxation processes," Mechanics of Materials, vol. 43, no. 12, pp. 853–869, 2011.

[101] Q. Ge, K. Yu, Y. Ding, and H. Jerry Qi, "Prediction of temperature-dependent free recovery behaviors of amorphous shape memory polymers," Soft Matter, vol. 8, no. 43, p. 11098, 2012.

[102] C. M. Yakacki, R. Shandas, C. Lanning, B. Rech, A. Eckstein, and K. Gall, "Unconstrained recovery characterization of shape-memory polymer networks for cardiovascular applications," Biomaterials, vol. 28, no. 14, pp. 2255–63, 2007.

[103] Y. Ebata, A. B. Croll, and A. J. Crosby, "Wrinkling and strain localizations in polymer thin films," Soft Matter, vol. 8, no. 35, p. 9086, 2012.

[104] N. Chen, K. Okamoto, K. Tada, G. Morthier, and R. Baets, "Analysis, fabrication, and characterization of tunable dfb lasers with chirped gratings," IEEE JOURNAL OF SELECTED TOPICS IN QUANTUM ELECTRONICS, vol. 3, pp. 541–546, 1997.

[105] L. Li, L. Lu, S. Li, R. Guo, Y. Shi, and X. Chen, "Phase-shifted distributed feedback laser with linearly chirped grating fabricated by reconstruction equivalent chirp technique," Optics & Laser Technology, vol. 61, pp. 57–61, 2014.

[106] J. H. Lee, H. W. Ro, R. Huang, P. Lemaillet, T. A. Germer, C. L. Soles, and C. M. Stafford, "Anisotropic, hierarchical surface patterns via surface wrinkling of nanopatterned polymer films," Nano Lett, vol. 12, no. 11, pp. 5995–9, 2012.

[107] Y. Li, S. Dai, J. John, and K. R. Carter, "Superhydrophobic surfaces from hierarchically structured wrinkled polymers," ACS Appl Mater Interfaces, vol. 5, no. 21, pp. 11066–73, 2013.

[108] W. K. Lee, C. J. Engel, M. D. Huntington, J. Hu, and T. W. Odom, "Controlled three-dimensional hierarchical structuring by memory-based, sequential wrinkling," <u>Nano Lett</u>, vol. 15, no. 8, pp. 5624–9, 2015.

[109] D. Fuard, T. Tzvetkova-Chevolleau, S. Decossas, P. Tracqui, and P. Schiavone, "Optimization of poly-di-methyl-siloxane (pdms) substrates for studying cellular adhesion and motility," <u>Microelectronic Engineering</u>, vol. 85, no. 5-6, pp. 1289–1293, 2008.